

FRICION IDENTIFICATINON AND COMPENSATION IN STABILIZED
PLATFORMS

A THESIS SUBMITTED TO
THE GRADUATE SCHOOL OF NATURAL AND APPLIED SCIENCES
OF
MIDDLE EAST TECHNICAL UNIVERSITY

BY

EYYUP SINCAR

IN PARTIAL FULFILLMENT OF THE REQUIREMENTS
FOR
THE DEGREE OF MASTER OF SCIENCE
IN
MECHANICAL ENGINEERING

SEPTEMBER 2013

Approval of the thesis:

**FRICITION IDENTIFICATINON AND COMPENSATION IN STABILIZED
PLATFORMS**

submitted by **EYYÜP SİNCAR** in partial fulfillment of the requirements for the degree of
**Master of Science in Mechanical Engineering Department, Middle East Technical
University** by,

Prof. Dr. Canan Özgen
Dean, Graduate School of **Natural and Applied Sciences**

Prof. Dr. Suha Oral
Head of Department, **Mechanical Engineering**

Prof. Dr. Tuna Balkan
Supervisor, **Mechanical Engineering Dept., METU**

Prof. Dr. Bülent E. Platin
Co-supervisor, **Mechanical Engineering Dept., METU**

Examining Committee Members:

Prof. Dr. Kemal Özgören
Mechanical Engineering Dept., METU

Prof. Dr. Tuna Balkan
Mechanical Engineering Dept., METU

Prof. Dr. Bülent E. Platin
Mechanical Engineering Dept., METU

Assist. Prof. Dr. Yiğit Yazıcıoğlu
Electrical and Electronics Engineering Dept., METU

M.Sc. Burak Gürcan
Technical Leader of Unmanned Systems Department, ASELSAN Inc.

Date: 10/09/2013

I hereby declare that all information in this document has been obtained and presented in accordance with academic rules and ethical conduct. I also declare that, as required by these rules and conduct, I have fully cited and referenced all material and results that are not original to this work.

Name, Last name : Eyyüp SİNCAR

Signature :

ABSTRACT

FRICTION IDENTIFICATION AND COMPENSATION OF ITS EFFECTS IN STABILIZED PLATFORMS

Sincar, Eyyüp

M.Sc., Department of Mechanical Engineering

Supervisor : Prof. Dr. Tuna Balkan

Co-Supervisor : Prof. Dr. Bülent E. Platin

September 2013, 101 pages

A frequent problem encountered in the stabilization of a dynamic system supported by a moving base is the disturbance rejection associated with moving components. Due to relative motion of adjacent components, the friction induces a destabilizing force from base motion to the stabilized object, which degrades the motion accuracy. Therefore, the compensation of frictional effects is necessary in order to obtain a highly precise stabilization performance, especially, when the stabilized system undergoes low-velocity or reversal motions at which the friction is the dominant destabilizing factor. Since the friction has quite complex and nonlinear behaviors, classical industrial control techniques such as PI and PID are insufficient to compensate frictional effects.

In this thesis, the frictional behaviors observed by different researchers and notable friction compensation techniques proposed in literature are presented. The compensation methods are compared in terms of their capability to capture frictional effects and their simplicity to be applicable. Various types of friction identification experiments are performed on a test setup in order to observe frictional behaviors and to estimate friction model parameters.

System performance is analyzed on an experimental level by applying two different compensations methods which are model-based and model-free. The improvement in stabilization performance is determined and compared for these compensations techniques.

Keywords: Disturbance, disturbance observer, friction, friction compensation, friction identification, friction models, gimbal, line of fire (LOF), stabilization

ÖZ

STABİLİZE PLATFORMLARDA SÜRTÜNMENİN TANILANMASI VE ETKİLERİNİN GİDERİLMESİ

Sincar, Eyyüp

Yüksek Lisans, Makina Mühendisliği Bölümü

Tez Yöneticisi : Prof. Dr. Tuna Balkan

Ortak Tez Yöneticisi : Prof. Dr. Bülent E. Platin

Eylül 2013, 101 sayfa

Hareketli tabanlar üzerinde bulunan dinamik sistem stabilizasyonunda hareketli parçalara bağlı bozucu etki sık görülen bir sorundur. Parçaların bağlı hareketlerinden dolayı oluşan sürtünme, sistemin stabilize olmasını engellemekte ve hareketin doğruluğunu düşürmektedir. Bundan dolayı, özellikle eğer stabilize olan sistem düşük ya da yö değiştirme hareketlere maruz kalıyorsa, hassas bir stabilizasyon sürtünmeye bağlı etkilerin giderilmesi gerektirmektedir. Sürtünmenin son derece karmaşık ve doğrusal olmayan davranışa sahip olmasından dolayı, PI ve PID gibi klasik endüstriyel kontrol yöntemleri sürtünmenin etkilerini gidermede yetersiz kalmaktadır.

Bu tezde, farklı araştırmacılar tarafından gözlemlenen sürtünme davranışları ve literatürki önemli sürtünme giderme teknikleri incelenmiştir. Giderme teknikleri sürtünmenin etkilerini yakalamadaki kapasitesi ve uygulanabilirliği açısından karşılaştırılmıştır. Test düzeneği üzerinde farklı sürtünme davranışlarını gözlemlenmek ve sürtün modelinin parametrelerini tahmin etmek için birçok farklı sürtünme tanımlama deneyleri gerçekleştirilmiştir.

Sürtünme modeli tabanlı ve model tabanlı olmayan sürtünme giderme teknikleri sisteme uygulanarak sistemin performansı deneysel olarak analiz edilmiştir. Stabilizasyon performansındaki iyileşme bu farklı sürtünme teknikleri açısından saptanmış ve karşılaştırılmıştır

Anahtar kelimler: Bozucu etki, bozucu etki gözlemci, sürtünme, sürtünme giderme, sürtünme tanımlama, sürtünme modelleri, cimbal, ateşleme çizgisi, stabilizasyon

To my parents, Naile and Yahya,

ACKNOWLEDGEMENTS

I would first like thank to my advisor, Prof. Dr. Tuna BALKAN and my co-advisor, Prof. Dr. Bülent Emre PLATIN for their guidance, advices and helpful criticism. It is a great honor to be able to work with them and to meet with their experience, knowledge and ideas.

I would like to express my special gratitude to Mr. Burak GÜRCAN. I appreciate his taking the time to talk to me about my work, giving me support and encouragement and sharing his technical and physical insight that really helped me.

I would also like to extend my appreciation to my colleagues Erva ULU and Onur Cem ERDOĞAN for their technical support and helping me during my experimental studies. Their support and patience are sincerely appreciated. Furthermore, I am thankful to all my colleagues of Aselsan Unmanned System Group. I feel fortunate in getting the opportunity to work with these distinguished people.

Finally and most importantly, I wish to express my deepest gratitude to my parents Yahya, and Naile for their unconditional love, prayers and unshaken belief in me throughout my life.

TABLE OF CONTENTS

ABSTRACT.....	v
ÖZ	vi
ACKNOWLEDGEMENTS	viii
TABLE OF CONTENTS.....	ix
LIST OF TABLES	xii
LIST OF FIGURES	xiv
LIST OF SYMBOLS AND ABBREVIATIONS	xvii
CHAPTERS	
1. INTRODUCTION	1
1.1 Background.....	1
1.2 Goal of the Study.....	3
1.3 Scope of the Study	3
2. FRICTION: MECHANISM AND BASIC BEHAVIORS	5
2.1 Introduction	5
2.2 Friction at Asperity Scale	7
2.2.1 The Bristle Model.....	8
2.2.2 The Generic Friction Model.....	9
2.3 Basic Appearing Types of Friction Behavior	11
2.3.1 Pre-sliding Versus Gross Sliding	11
2.3.2 Dry Versus Lubricated friction.....	12
2.3.3 Static Versus Kinetic Friction, Break-away Force.....	13
2.3.4 The Stribeck Effect.....	14
2.3.5 Friction Lag and Hysteresis.....	15

2.3.6	Stick-Slip Motion	16
2.3.7	Position Dependent Friction	17
2.3.8	Time Dependence of Friction	18
3.	FRICITION COMPENSATION METHODS	19
3.1	Friction Problem Avoidance	19
3.2	Non-model-based Friction Compensation	20
3.2.1	Linear Feedback Controller	20
3.2.2	Dither	21
3.2.3	Joint Torque Control.....	22
3.2.4	Dual Mode Control.....	22
3.2.5	Disturbance Observer	23
3.3	Non-model-based Friction Compensation	24
3.3.1	Adaptive Controller	26
3.3.2	Static Friction Models.....	26
3.3.3	Karnopp Friction Model	28
3.3.4	Armstrong Friction Model.....	29
3.3.5	Dynamic Friction Models	30
3.4	Conclusions.....	37
4.	FRICITION IDENTIFICATION.....	39
4.1	Experimental Setup.....	39
4.2	The System Analysis: Non-collocated Friction and the Flexibility	41
4.3	The Identification of the Friction Model Parameters.....	44
4.3.2	Presliding Phase Experiments and Estimation of Dynamic Friction Parameters	52
4.4	Identified Friction Model.....	55
5.	FRICITION COMPENSATION	57
5.1	Gyro Stabilized Motion Platform.....	57

5.2 Model-based Friction Compensation.....	59
5.2.1 Simulation Results.....	61
5.2.2 Experimental Studies.....	63
5.3 Model-free Friction Compensation.....	75
5.3.1 Single-State Disturbance Observer	77
5.3.2 Single-State Disturbance Observer Characteristics.....	79
5.3.3 Simulation Results.....	80
5.3.4 Experimental Studies.....	82
5.4 Conclusion	90
6. CONCLUSION.....	91
6.1 Summary.....	91
6.2 Conclusions	92
6.3 Future Works	93
REFERENCES	95
APPENDIX A BLOCK DIAGRAM OF SIMULINK MODEL FOR SIMULATION	99

LIST OF TABLES

TABLES

Table 3.1 Comparison of friction behaviors for different friction models.....	38
Table 4.1 Friction test results of the load side.....	42
Table 4.2 Definition of parameters of LuGre model.....	50
Table 4.3 Estimated static parameters of LuGre model	50
Table 4.4 Comparison of estimated static parameters of LuGre model for different experiments.....	52
Table 4.5 Estimated dynamic friction parameters.....	55
Table 5.1 Definitions of parameters and symbols used in the block diagram shown in Figure 5.3.....	61
Table 5.2 Simulation analysis of stabilization performance for different compensation techniques.....	63
Table 5.3 System servo characteristics with and without friction model.....	65
Table 5.4 Stabilization performance of friction compensation methods.....	68
Table 5.5 Stabilization performance of friction compensation methods for different disturbance frequencies	70
Table 5.6 Stabilization performance of friction compensation methods in case of increasing the average friction torque	71
Table 5.7 Stabilization performance of friction compensation methods with an increased normal force at different disturbance frequencies	72
Table 5.8 Simulation analysis of stabilization performance for compensation techniques	81
Table 5.9 System servo characteristics with and without adding the disturbance observer	84
Table 5.10 Stabilization performance at different compensation methods.....	87
Table 5.11 Stabilization performance at different disturbance frequencies.....	89
Table 5.12 Stabilization performance for variations in normal force	89

Table 5.13 Stabilization performance for variations in normal force at different disturbance frequencies	89
Table 6.1 Simulation and experiment results of improvement in stabilization performance for different compensation methods.....	92

LIST OF FIGURES

FIGURES

Figure 1.1 A gyro stabilized motion platform (Photo Courtesy of ASELSAN Inc.)..	2
Figure 1.2 Some application of gyro stabilized motion platforms (Photo Courtesy of ASELSAN Inc.).....	2
Figure 2.1. Basic friction configuration [5].....	7
Figure 2.2 Surfaces in contact at asperities [6]	8
Figure 2.3 The bristle model	8
Figure 2.4 A generic representation of the sliding contact of rough bodies [9].....	9
Figure 2.5 Life cycle of one asperity contact [9]	10
Figure 2.6 Dynamic friction regimes for lubricated friction.....	12
Figure 2.7 Visualization of break-away force, a) no applied force, b) small applied force, c) large enough applied force to overcome breakaway	13
Figure 2.8 Break-away force as a function of force rate	14
Figure 2.9 The Stribeck effect.....	15
Figure 2.10 The Friction lag around the Stribeck curve in sliding regime	16
Figure 2.11 The friction as a function of the displacement in presliding regime.....	16
Figure 2.12 Observing stick-slip phenomena.....	17
Figure 2.13 Friction as a function of dwell-time.....	18
Figure 3.1 Representation of dither method.....	21
Figure 3.2 Representation of the joint torque control	22
Figure 3.3 Representation of dual mode control	23
Figure 3.4 Representation of the disturbance observer structure	24
Figure 3.5 Representation of model-based friction compensation.....	25
Figure 3.6 Various combinations of static friction model [17].	28
Figure 3.7 Karnopp friction model.....	29
Figure 3.8 Dahl curve.....	31

Figure 3.9 Physical explanation of LuGre model	33
Figure 3.10 Representation of Maxwell-slip friction model using N elementary models	35
Figure 3.11 The characteristics of one element Maxwell-slip model	35
Figure 4.1 The gyro-stabilized test system (Photo Courtesy of ASELSAN Inc.)....	40
Figure 4.2 Subcomponents of the gyro-stabilized test system 3D wireframe.....	40
Figure 4.3 Representation of collocated and non-collocated friction	41
Figure 4.4 Friction measurement of the motor and gearbox	42
Figure 4.5 Open loop frequency response of the system	44
Figure 4.6 Schematic representation of rigid body assumption.....	44
Figure 4.7 Step response of the linear system with a tuned controller	45
Figure 4.8 Determining of one point on friction-velocity map.....	47
Figure 4.9 Friction-velocity map for two different set of experiments.....	48
Figure 4.10 A typical representation of static LuGre model.....	49
Figure 4.11 Friction torque-velocity map and fitted static LuGre friction model	51
Figure 4.12 Representation of modeling of contact surfaces in LuGre	52
Figure 4.13 Estimation of bristle damping constant in presliding regime	54
Figure 4.14 Identified friction model curves.....	56
Figure 5.1 A typical gyro stabilized motion platform application.....	58
Figure 5.2 Gyro stabilized platform mounted on a Stewart platform (Photo Courtesy of ASELSAN Inc.)	58
Figure 5.3 Block diagram of one axis stabilization loop and friction compensation scheme using friction model-based feedback.....	60
Figure 5.4 The velocity of the system relative to hull for application compensation methods	62
Figure 5.5 Experimental closed loop frequency response of system with and without friction compensation.....	64
Figure 5.6 Experimental open loop frequency response of system with and without friction compensation.....	65

Figure 5.7 The Gimbal velocity relative to the base and corresponding compensation output.....	66
Figure 5.8 The system velocity relative to hull for application of different friction compensation methods	67
Figure 5.9 Position error for application of compensation methods	68
Figure 5.10 Position error for 2 Hz disturbance frequency	69
Figure 5.11 Spring preloaded anti-backlash mechanism 3D wireframe	71
Figure 5.12 LuGre friction model output as a response to variations in its dynamic parameters.....	73
Figure 5.13 LuGre friction model output as a response to variations in its static parameters.....	73
Figure 5.14 Stabilization accuracy as a response to LuGre model parameters variations	75
Figure 5.15 Disturbance observer architecture.....	76
Figure 5.16 Block diagram of the application of disturbance observer on the system stabilization loop.....	78
Figure 5.17 Block diagram view of adding some noise on the gyro output.....	80
Figure 5.18 The system's velocity relative to hull for application compensation techniques.....	81
Figure 5.19 Experimental closed loop frequency response with and without DOB	83
Figure 5.20 Experimental open loop frequency response with and without DOB....	84
Figure 5.21 (a) the rate output and (b) the output of the disturbance observer	84
Figure 5.22 The system velocity relative to hull for application of compensation methods.....	85
Figure 5.23 Position error for application of compensation methods	86
Figure 5.24 Position error for 2 Hz disturbance frequency for compensation techniques	88

LIST OF SYMBOLS AND ABBREVIATIONS

DOB	:	Disturbance observer
LOS	:	Line of sight
LOF	:	Line of fire
GMS	:	Generalized Maxwell-slip
PD	:	Proportional with derivative control action
PI	:	Proportional with integral control action
PID	:	Proportional with integral and derivative control actions
PWM	:	Pulse width modulation
C	:	Attraction parameter of the GMS friction model
DV	:	Velocity threshold for Karnopp friction model
e	:	Error
F_a	:	Applied external force
F_C	:	Coulomb friction force / torque
F_f	:	Friction force
F_{ss}	:	Steady-state friction force
$F_h(z)$:	Hysteresis function of Leuven friction model
F_i	:	Individual force of an element in GMS friction model
F_n	:	Normal force
F_s	:	Static friction or breakaway force
F_t	:	Static friction or breakaway torque
F_μ	:	Adhesion force
G_{cv}	:	Velocity controller transfer function
G_{cc}	:	Current controller transfer function
J	:	Effective mass moment of inertia of the system
k_n	:	Normal stiffness of asperity
k_t	:	Tangential stiffness of asperity
K_0	:	Single-state disturbance observer gain
K_a	:	Current feedback scale factor
K_e	:	Motor back EMF constant
K_g	:	Gyro scale factor
K_r	:	Resolver scale factor
K_t	:	Motor torque constant
L	:	Motor winding inductance
n	:	Noise on the gyro
N	:	Gearbox reduction ratio
q	:	Angular displacement variable
\dot{q}	:	Angular velocity variable
\dot{q}_s	:	Stribeck velocity
R	:	Motor winding resistance
s	:	Laplace operator
$s(\cdot)$:	Stribeck curve
$sgn(\cdot)$:	Signum function

t	:	Time variable
T_C	:	Coulomb torque
T_f	:	Actual friction torque
T'_f	:	Estimated friction torque
T_m	:	Motor torque
T_s	:	Static friction or breakaway torque
u	:	Input signal
V_b	:	Motor back EMF voltage
V_m	:	Voltage across motor windings
v	:	Velocity variable
W_i	:	Maximum force of an element in GMS friction model
x	:	Displacement variable
x_d	:	Desired position input
z	:	Internal state variables of bristles
α_i	:	Constant fractional parameter of an element in the GMS model
δ	:	Stribeck curve shape factor
ξ	:	Tangential deformation of the asperity
ζ	:	Normal deformation of the asperity
μ	:	Local friction coefficient
μ_s	:	Static friction coefficient
μ_C	:	Coulomb friction coefficient
ω	:	Output rate of LOF
ω_b	:	Base velocity
ω_i	:	Input rate command
σ_0	:	Stiffness of bristles
σ_1	:	Micro-viscous damping coefficient
σ_2	:	Linear viscous friction coefficient

CHAPTER 1

INTRODUCTION

1.1 Background

Stabilized motion systems have been widely used in different engineering fields on varied applications such as cameras, telescopes, array of sensors and weapons [10]. Though the requirements change depending on the applications, the main control aim of the stabilized systems is to maintain a chosen direction or so called the line of sight (LOS) of a stabilized object relative to the another object or target despite the disturbances.

This study is focused on a gyro stabilized motion platform consisting of two orthogonal stabilized axes which are azimuth and elevation as shown in Figure 1.1. In practical applications, the platform is mounted on a land or naval vehicle as seen in Figure 1.2. The vehicle is subjected to some movements originating from land or sea waves during its voyage. The main goal for this system is to segregate the stabilized platform from the disturbances resulted from base's swinging and to track the appointed position by utilizing a gyro or gyroscope that measures the angular rate of the stabilized object, which is also called as the rate of the line of the fire (LOF). Errors in this angular rate error drive a stabilization loop controller which drives servomotor to generate a correction torque to counter the disturbance torques and stabilize the system. The stabilization loop consists of a PI controller, motor drive circuits, current sensor, rate gyro and actuator.

The platform is demanded to have high tracking accuracy and low stabilization error-deviation between chosen direction and LOF. To do so, the system feedback loop is to be able to oppose the disturbances and maintain the aim point. The disturbance rejection capability depends generally on the loop bandwidth which is directly affected by the dynamic of the gyroscope, actuator and electromechanical design of the system. The stabilized motion platform is adopted a geared transmission in order to produce high torques at load side. However, the geared servo systems have some undesirable characteristics such as elasticity and backlash which cause the effective stiffness of gear structure to reduce and eventually decrease the bandwidth of the system limited its the resonance frequency. An anti-backlash mechanism is used in order to decrease that drawback by amplifying the effective stiffness of transmission line and moving the resonance frequency to higher ones. However, this mechanism causes the gear train to have more friction due to initial preloading torque of the anti-backlash spring, which induces a destabilizing torque and makes difficult to obtain a high performance stabilization control of the system.



Figure 1.1 A gyro stabilized motion platform (Photo Courtesy of ASELSAN Inc.)



Figure 1.2 Some application of gyro stabilized motion platforms (Photo Courtesy of ASELSAN Inc.)

During the stabilization, due to the carrier's movements, the system experiences high number of velocity reversals or low speed motions in which the friction is the most dominant destabilizing factor. At low velocities, the friction may mostly affect the control signal (torque) and this generates some undesirable stick-slip motions and tracking errors. Hence, the stabilization applications with high precision and low speed demands mostly show unacceptable performance due to frictional effects. Taking the friction into account during the design of controller and modifying the controller reducing the frictional effects may improve the stabilization performance.

The increasing demands for quality and precision have made many research works and large number of publication related to the friction compensation. The main aim of these studies is to eliminate or minimize frictional effects so that discontinuous motions due to friction are reduced. Although many compensation methods have been proposed in literature, they may basically divided in two groups which are friction model based and non-model based friction compensation methods. Model-based friction compensation methods attempt to

capture the nonlinear friction behavior by modeling friction with reasonable complexity. The basic idea is that if a well-modeled nonlinear friction model is available, it is possible to compensate the actual (real) friction by applying a torque command signal equal and opposite to the real friction. On the other side, model-free compensation methods refer to the approaches that do not require a structured non-linear friction model. These approaches are suitable for control applications with friction in presence of varying and uncontrollable factors such as wear, temperature, humidity, and lubricants conditions. These techniques can prevent not only frictional but other nonlinear disturbances. Yet, these techniques are leaning to have additional drawbacks such as extra power consumption in steady state since they are indirect compensation scheme.

1.2 Goal of the Study

An effective friction compensation of frictional effects is a prerequisite for high performance gyro stabilized systems applications where the systems pass their time mostly around zero velocity motions and hence the friction is the dominant disturbance factor.

The objective of this thesis may be summarized as: *“To improve the stabilization performance of a system controlled by classical cascaded PI control scheme by adding a simple but effective friction compensation mechanism into the system stabilization loop control structure”*.

In order to reduce the frictional effects on the stabilization performance, both friction model based and model-free friction compensation techniques are applied. Two different model based friction compensation methods are applied and compared: a general classical static model and more advanced LuGre dynamic friction model [27]. As a friction model-free friction compensation technique, the single-state disturbance observer [47, [48] is selected and applied since it is robust, simple and effective. With applied three compensations methods, the stabilization performance tests are carried out on real system under various disturbance characteristics. Also, the stability of the system with adding compensation mechanisms is examined by conducting frequency response tests.

In literature, many of compensation techniques are applied on simple servo mechanisms which generally consist of a servomotor, inertia disk, and a friction pad [3], [22], [25], and [36]. In this study, the compensation techniques will be validated on a rather complex geared gyro stabilized system.

1.3 Scope of the Study

The remainder of the thesis may be outlined as below:

In Chapter 2, the friction mechanism and basic appearing types of friction characteristics stated in various research reports are given. Since the friction phenomena is related to the interface between mechanical parts, analyzing the behavior of contacting surfaces is

necessary to get insight about the friction effects. For this purpose, some generic methods to model the friction at asperity scale are stated.

In Chapter 3, some notable friction compensation techniques dealing with control problems such as steady state errors, limit cycles and instabilities are analyzed and summarized. These methods are compared in terms of their capacity to capture frictional behaviors and simplicity to be applicable. After comparisons, the chosen friction model to be applied on real system is given with reasons.

In Chapter 4, the friction behaviors given in Chapter 2 are observed in a real system. Then, a identification procedure to identify the chosen friction model parameters is presented. In this identification procedure, some test results on the real system to identify both static and dynamic friction parameters are presented.

Chapter 5 focuses on the friction compensation design in a gyro stabilized platform. The application of friction compensations techniques which are static, dynamic friction models and disturbance observer as model free compensation method are given. Stabilization performances are determined and compared when these techniques for various disturbances on the real system are applied. The system servo characteristic with adding these compensation mechanisms are examined experimentally.

Chapter 6 presents conclusions and future suggestions regarding to the performance of the friction compensation techniques for applications of stabilization purposes.

CHAPTER 2

FRICITION: MECHANISM AND BASIC BEHAVIORS

2.1 Introduction

The friction is defined as the resistance to sliding of one solid body over or along another one as ordinarily understood in the macroscopic world [1]. During this sliding motion between two bodies, there is a manifestation of energy consumption due to frictional resistance at the interface. Physically, this resistance between two interacting surfaces depends on many different mechanisms. In Tribophysics by Suh [7], the basic mechanisms for this resistance and so friction at dry sliding interface are defined as:

- Removal of asperities by asperity interaction at the interface
- Adhesion of sliding interface
- Plowing of the surface by wear debris and other particles

Experimental results showed that of these three mechanisms, the most significant mechanism for the friction at the interface metals and most plastic surfaces is the plastic deformation of the surface by wear particles, which plow the surface. The wear mechanism will not be detailed here, but in order to get an insight in mechanism of the friction, some basics of tribology in terms of friction will be given in this work.

Friction is one of the main topics of tribology, which is defined as the science and technology between two interacting surfaces in relative motion and of related subjects and practices. Besides the field of tribology, there are several other domains where friction plays a crucial role since most engineering mechanisms are composed of a certain number of interfaces between the machine parts. Some of these domains are control, geomechanics, structural dynamics and design and life-cycle engineering. Each of these fields approaches friction in a different manner since the required degree of complexity of friction models changes within these fields. In cases where frictional effects to the system performance are small, the friction models are considered in simple form. On the other hand, for high performance applications much more sophisticated frictional models are needed.

Generally, the goal of modeling friction is to minimize uncertainties about the behavior of a system. To figure out the principles behind the friction phenomena, modeling and identification of the friction are essential. However, though friction has been studied for centuries by scientists and engineers, there is no general frictional model available. This reason was stated simply by Tabor [2] as "We do not have a way of seeing what is actually taking place at the interface while sliding is taking place". The interacting surfaces can be examined only before and after sliding has occurred but what take place at the interface during sliding is not accessible. Moreover, the sliding mechanism between two interacting

surfaces is very complex and interwoven because residual stress, micro cracks are observed in contacting surfaces, which cause the contacting points likely to be chemically and structurally different from main body. Also, during the sliding process, the heat is generated which results in a non-uniform temperature distribution near the sliding surfaces and this is significant in terms of oxidation, diffusion, and adsorption processes [9]. Hence, the friction is a collection complex mechanical, chemical, and thermal mechanism, therefore making a general friction model is almost impossible.

The increasing demands for quality and precision have made many research studies and large number of publication on the subject of friction. The main aim of these studies was to eliminate or minimize frictional effects so that intermittent motions due to friction are reduced if not eliminated completely. The results of these studies showed that although the friction is defined as the resistance for sliding one body in reference to another, it depends on many parameters [[6], [22]] such as:

- Real contact area (Mechanical)
- Normal force on body (Mechanical)
- Relative motion between bodies (Mechanical)
- Local temperature at contact spots (Thermal)
- Wear of material (Mechanical & Chemical)
- Stiffness of contacting surfaces (Mechanical)
- Adhesion of contacting surfaces (Mechanical & Chemical)
- Lubricant (Mechanical)
- Welding of contacting points (Chemical)
- History of friction contact (Mechanical)
- Surface geometry (microscopic and macroscopic) (Mechanical)
- Elastic and plastic deformation of junction at interface (Mechanical)
- Dynamic friction forces on bodies (Mechanical)

This list gives an idea of the complexity of friction phenomena.

Since the friction phenomena related to the interface between mechanical parts, at the first step an analysis of the behavior of contacting surfaces is necessary. At the microscopic level, the surfaces of machine parts have a complicated, largely random profile as seen in Figure 2.1. When analyzing this figure, one can observe that when two surfaces are squeezed together, they contact each other only at some points. Therefore, the apparent area of contact is much higher than the real area of contact. This implies that the friction is a collective behavior of these all contacting points (asperities) between surfaces.

In order to investigate frictional behavior at these contacting points, various physically motivated friction models were developed in literature. According to the scale of approach, these proposed physical friction models can be grouped under three scales or domains [22]:

- Atomic / molecular scale (in nanotechnology domain)
- Asperity scale (in control domain)
- Tectonic plate scale (in the geophysics domain)

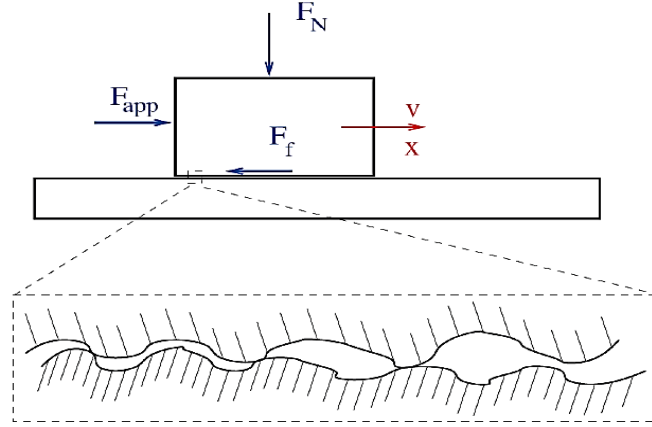


Figure 2.1. Basic friction configuration [5]

In this work, to observe frictional characteristics behind physical of interface behaviors for control purposes, friction models at only asperity scale will be investigated.

2.2 Friction at Asperity Scale

At asperity scale, generic or physically based friction models are described. Generic models focus on the physical friction properties. These models are required a lot of dense computation because individual measurements are conducted for each asperities separately. The main aim of these models is to gain deep insight in frictional phenomena in terms of physical behavior at microscopic level. These models will not be given here in detail since they are not practical.

From microscopic point of view, the frictional phenomenon does not continuously cover all the surface, but it is made up the number of asperities resented at the interface (Figure 2.2). The friction is as a result of the interaction of these surface asperities. The asperities interact with each other when two surfaces are in contact. The force value to deform these asperities and to overcome the interfacial adhesion is equal to the friction force. The friction is proportional to the shear strength of the asperity junction or the weaker of the bulk materials [6]. The static friction force F_s can be expressed as:

$$F_s = \mu_s P = \tau_m A \quad (2.1)$$

$$\mu_s = \frac{\tau_m}{P} A \quad (2.2)$$

where μ_s is the static friction coefficient, A is the real contact area, τ_m is shear stress, and P is the normal force comprised of both the normal component due to adhesion forces at the interface and the applied load. From Equation 2.2, it can be observed that friction force is dependent of real contact area (effective area) although this fact is not apparent from macroscopic perspective. Moreover, since the asperities and so the real area of contact changes with the load on the body (the weight of body and/or the external normal force acting on the body), the friction force depends on the load.

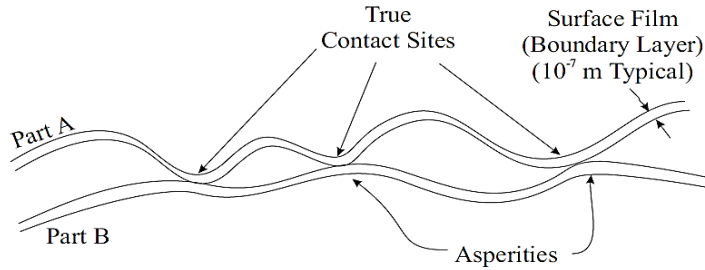


Figure 2.2 Surfaces in contact at asperities [6]

2.2.1 The Bristle Model

Based on the behaviors of asperities, Haessing and Friendland developed a bristle model [8]. In the bristle model, the friction is represented by a set of bristles. Bristles are extending from one surface with the rigid bristles and to the other surface with flexible bristles (Figure 2.3). There is a bond between the bristles. When surfaces move relative to each other, bristles deflect and then the strain in each bond between bristles increases. As the strain of any particular flexible bristle exceeds a certain level, the bond is broken and it attaches itself to a new bristle and then a new bond with a smaller strain is established.

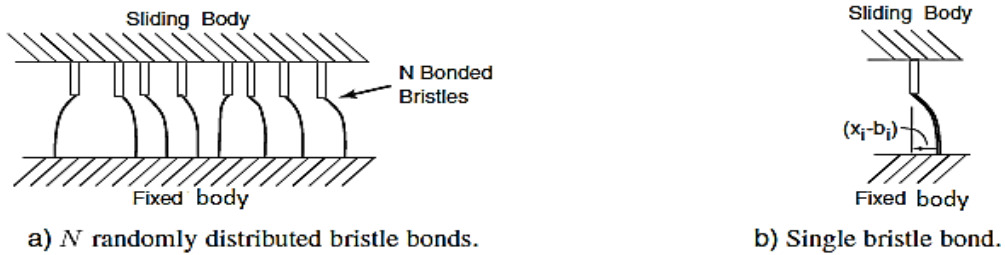


Figure 2.3 The bristle model

The space changes randomly between bristles. The force F developed between the rigid and flexible bristle is given by

$$F = \sigma_0(x_i - b_i) \quad (2.3)$$

where σ_0 is the stiffness of flexible bristle, x_i is the location of rigid bristle and b_i is the location of flexible bristle. The total friction force at the interface is the sum of all bonding force for each of bristle pair, which is given by

$$F_{\text{sum}} = \sum \sigma_0(x_i - b_i) \quad (2.4)$$

In the bristle model, the cause behind frictional behavior at macroscopic level is the physical interaction of the asperities. However, the possibility of microslip before the bond breaks is not represented in the bristle model. The number of bristles and bonds to be used in this model is not constant but they are function of the velocity, which makes model somehow unrealistic [9]. Still, most empirical friction models, especially for control area are developed based on the asperity scenario of the bristle model.

2.2.2 The Generic Friction Model

A novel generic friction model at asperity scale was developed by Lampaert et al [9]. This model is based on some well-established phenomenological mechanisms which are creep, adhesion, and deformation. Creep is a tendency of a solid material to slowly move or deform permanently under the influence of stress. Adhesion is a molecular attraction exerted between to surfaces of bodies in contact.

As in the bristle model, this generic model is based on the asperity contact of two surfaces. During the motion of two surfaces relative to each other, some asperity contacts will be broken and others will be established. Despite its simplicity, this model is able to represent most of the frictional characteristics observed experimentally. The schematic representation of the friction contacts for the novel generic friction model is shown in Figure 2.4.

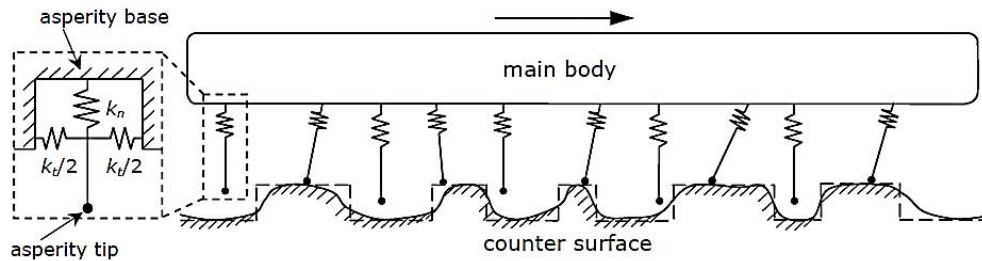


Figure 2.4 A generic representation of the sliding contact of rough bodies [9]

In this model, one body (main body) is assumed to be in motion and other one (counter surface) is assumed to be rigid. The moving body has asperities, each with its own stiffness, mass, and length. The asperities can deform in vertical and horizontal direction due to

normal and tangential forces, respectively. The counter surface has some spots since the surfaces are not smooth and so contacts will occur only at some discrete points. The surface roughness and mechanical properties of the contacting bodies determine the size of spots for a given load. The shape of spots even for an isotropic surface can be quite irregular that is why the spots are shown in different size in the schematic view (Figure 2.4). The contact spots are interconnected to each other at the interface so they do not behave independently and they can sustain some elastic or plastic deformation. Hence, the asperity junctions deform elasto-plastically, thus behaving as nonlinear hysteretic springs whose spring constants are related to the properties of contacting materials.

The life cycle of one equivalent asperity junction is represented schematically in Figure 2.5, which is based on the physical behavior of junction at interface during relative movement. The life of one asperity depends on the characteristics of two interlocking asperities at the interface.

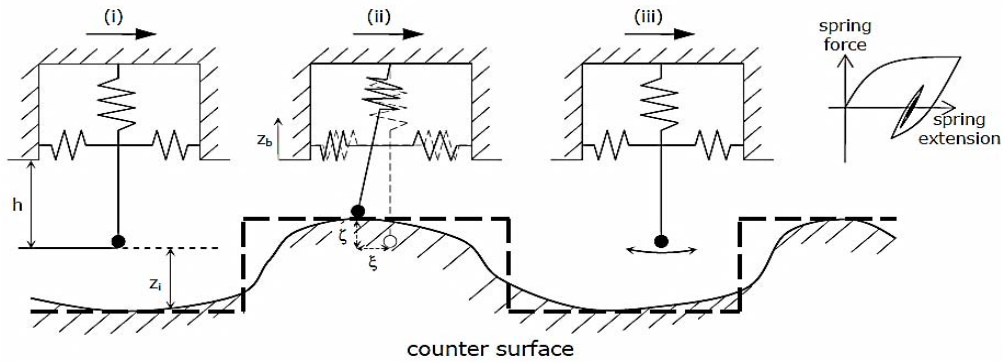


Figure 2.5 Life cycle of one asperity contact [9]

In Figure 2.5, it is assumed that upper body moves from left to right over or along the lower body which is assumed to be fixed. Also, the relative displacement between two surfaces is assumed to be corresponding to the displacement of asperity base. In this model-contact scenario, three main phenomenological friction mechanisms are incorporated: By introducing the normal stiffness k_n , the asperity can deform normally which shows that the friction increases with increase of normal force. Also, the asperity can deform tangentially by introducing the tangential stiffness k_t . During sliding, the asperity can stick on the lower spot profile because of adhesion and the adhesion force increases with contact time because of the creep.

The stiffness, adhesion, compression, and mass characteristics of two interacting asperities are lumped in to the asperity tip shown by a mark (\bullet). Initially, this point is moving freely (i) until it touches the lower rigid surface at spot (ii). Here, the asperity tip sticks on the lower profile and during sticking time the adhesion force increases until the applied force overcomes this adhesion force. Then, the asperity tip slips over the lower profile. After sticking and slipping, it breaks completely loose from the lower profile (iii). In case (iii), the

asperity is said to be in an inactive state while for case (ii), the asperity is said to be in an active state.

During sticking (active state of the asperity), some normal ζ and tangential ξ deformations occur, which result in normal and tangential forces, respectively. The normal force and tangential force are represented by following equations [9]:

$$F_n(t) = k_n \zeta(t) \quad (2.5)$$

$$F_t(t) = k_t \xi(t) \quad (2.6)$$

The maximal tangential force developed at onset of slipping is equal to the adhesion force:

$$F_\mu(t) = \mu(t)F_t = k_t \xi(t) \quad (2.6)$$

where the local friction coefficient $\mu(t)$ is the function of contact time due to creep. This is a very important result because it states that the friction increases with the dwell or rest time, indicating the time dependence of the friction.

2.3 Basic Types of Friction Behavior

Various types of frictional characteristics observed by different researchers are described in this section. In order to obtain a well-established friction model, it is necessary to understand these friction behaviors. As it is stated in previous section, two surfaces are in contact at asperity junctions and the complexity of the friction comes from these junctions behavior. Different types of friction behaviors are all related with each other by the friction mechanism at asperity scale.

2.3.1 Pre-sliding Versus Gross Sliding

In literature, two different frictional regimes are distinguished for friction: (i) pre-sliding regime and (ii) sliding (or gross sliding) regime.

The classical friction law states that the friction force depends on only the velocity and normal load. However, this law is valid only for the sliding regime, i.e., for large displacements. Before any sliding occurs, some preliminary displacements are observed at the lower force level [11]. This preliminary displacement at microscopic level is called as pre-sliding displacement. In the pre-sliding regime, due to asperity-junctions contacts, the adhesive forces are dominant. When a tangential force is applied, these junctions deform elastically or plastically. When the applied load is brought to zero value, a portion of the displacement will be recovered but the rest will not. Hence, the asperities behave as nonlinear hysteretic springs. So, the friction in the pre-sliding regime is a function of

displacement and a hysteresis behavior is observed between the friction force and displacement.

The transition from the pre-sliding to sliding regime is critical and depends on many factors such as the relative velocity and acceleration of the sliding objects [4].

When the applied force gets a certain threshold, the asperity-junctions are continuously formed and broken, resulting eventually in a sliding (or gross sliding) regime. In the sliding regime, the friction will depend mostly on the relative velocity [11].

2.3.2 Dry Versus Lubricated Friction

In most mechanical systems, the surfaces are lubricated in order to prevent wear and reduce the friction. Many studies were conducted to investigate the effect of lubricants and certain additives on the friction and wear. Suh in Tribophysics [7] stated the role of lubricants between surfaces as follows:

- o Lower shear stress
- o Transport particles
- o Prevent particle agglomeration
- o Prevent adhesion

For a lubricated friction, the friction has four different dynamic regimes [11] (Figure 2.6).

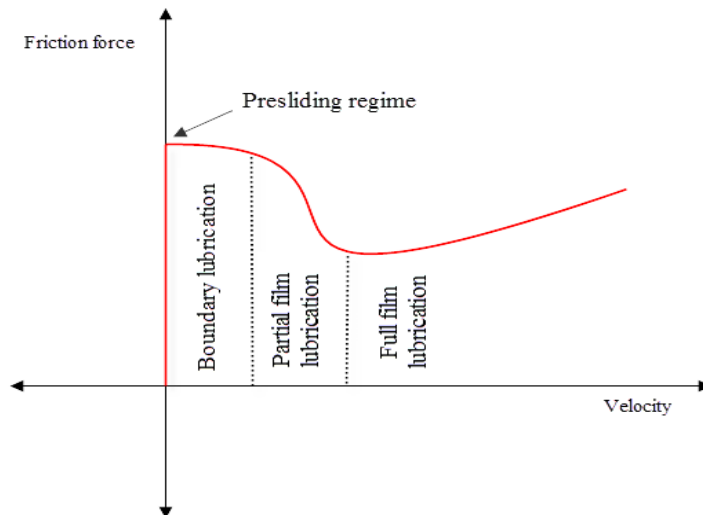


Figure 2.6 Dynamic friction regimes for lubricated friction

Pre-sliding regime: In this regime, the asperity-junctions contact is dominant. The asperities deform elastically, giving rise to pre-sliding displacement. Also, both boundary layer and asperities deform plastically, giving rise to static friction.

Boundary lubrication: In this regime, a very low velocity is observed and this velocity is not adequate to build up a fluid film between the solids so there is still a solid-solid contact, giving rise to a shear stresses.

Partial fluid lubrication: In this regime, a fluid film is formed between the surfaces through rolling or sliding relative motion. When this film is not thicker than the height of the asperities, some solid-solid contact is observed so the surfaces are lubricated only partially. The shear strength of solid lubricant at low velocities is generally higher than the shear strength of the solid lubricant at high velocities. Hence, the friction forces decrease with increasing relative velocity.

Full fluid lubrication: In this regime, there is no asperity contact between surfaces anymore. The friction force increases with increasing relative velocity due to the viscosity of the lubricant between surfaces.

The friction may be dry or lubricated but the qualitative behavior of its dynamics appears to be similar [9]. As in case of dry friction, the lubricated friction has two regimes where the asperity-junctions play a significant role, which are the pre-sliding regime and boundary lubricated regime.

2.3.3 Static Versus Kinetic Friction, Break-away Force

The break-away force is the maximum friction force at the onset of sliding. Yet, the starting point of motion is not well defined because the motion is already observed before sliding begins. As stated earlier, at pre-sliding regime, the friction is a function of displacement and the asperity behavior can be represented by springs. The friction force increases with the elongation of the springs. But after the friction force reaches its maximum point, which is the break-away force, the body starts to slide and the friction force decreases. This idea can be visualized as shown in Figure 2.7.

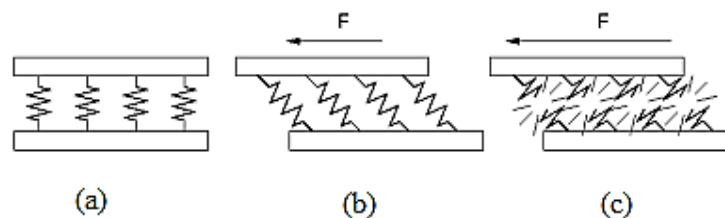


Figure 2.7 Visualization of break-away force, a) no applied force, b) small applied force, c) large enough applied force to overcome breakaway

The experiments, performed by Johannes et al [6] showed that the break-away force changes with the rate of increase of applied force (Figure 2.8). They concluded that the

break-away force increases with decreasing the rate of increase of applied load and vice versa.

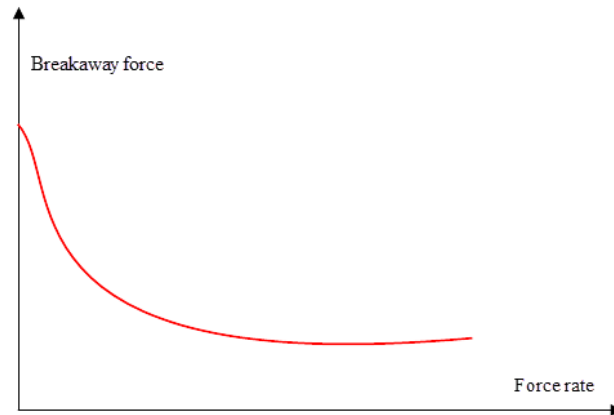


Figure 2.8 Break-away force as a function of force rate

The static friction is defined as the maximum break-away force that can be observed whereas the kinetic friction is used for the friction force in sliding regime since the friction force depends only on the velocity for sliding regime. When the friction force does not depend on the velocity, the kinetic friction is called the Coulomb friction. Also, some authors call the kinetic friction as dynamic friction (Figure 2.9).

2.3.4 The Stribeck Effect

It was discovered that for lubricated surfaces the drop from static friction to dynamic friction is not discontinuous but it is a function of velocity [6]. At very low velocities, the surfaces are not layered completely by the fluid film so there are some the asperity-junctions contacts between the surfaces. As the velocity increases, the effect of these junctions become less effective and so the friction force decreases with increasing velocity. As the velocity increases more, the fluid film builds up and there will be no asperity contacts anymore, but the hydrodynamic effect becomes more dominant and the friction force increases with increasing velocity due to viscous effect of lubricant, see Figure 2.9.

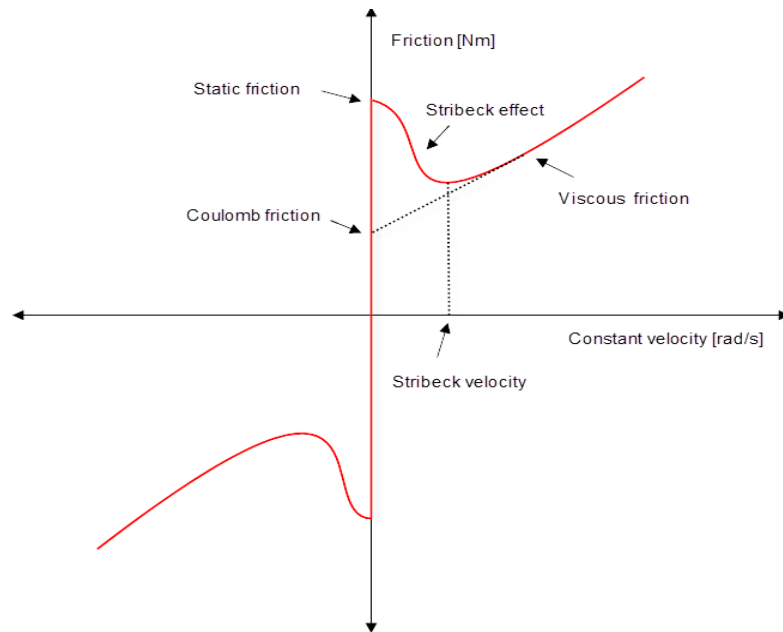


Figure 2.9 The Stribeck effect

In later studies [6], it was observed experimentally that the Stribeck effect is not valid only for lubricated friction between lubricated surfaces but also for dry friction between dry surfaces (Figure 2.9). As the velocity increases, the friction force decreases and goes through a minimum point and then increases with increasing velocity. The nonlinear but continuous transition from static friction to dynamic friction is located at Stribeck effect (or Stribeck curve) and the dip point of this curve is called Stribeck velocity, where the friction force reaches its minimum value. The decreasing part of the friction-velocity curve is called the velocity weakening and the increasing part of the friction-velocity curve is called velocity strengthening.

2.3.5 Friction Lag and Hysteresis

Around the Stribeck curve of the friction force, there is a delay or lag between friction force and the sliding velocity. The friction force for increasing velocities is larger than the friction force for decreasing velocities (Figure 2.10). This difference between accelerating and decelerating branches of friction-velocity curve is called friction lag or frictional memory.

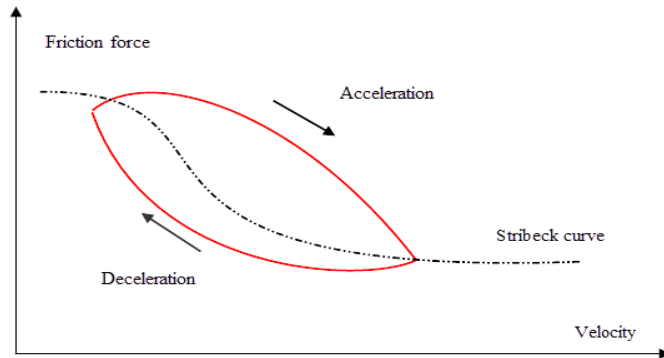


Figure 2.10 The Friction lag around the Stribeck curve in sliding regime

The size of the loop depends on the normal load, viscosity, and frequency of velocity variations [22]. This phenomenon is the reason of the time lag for breaking the asperities and building up the fluid film between the surfaces. But the friction lag is observed in both lubricated and dry surfaces.

In presliding regime, the friction lag is a hysteresis behavior as observed between friction force and displacements (Figure 2.11). In case of pre-sliding regime, the hysteresis loop between the friction force and displacement indicates the dissipation of the energy. But, for the friction lag, the enclosed curve does not show the energy dissipation but it is just a delay phenomenon between friction force and the velocity [4].

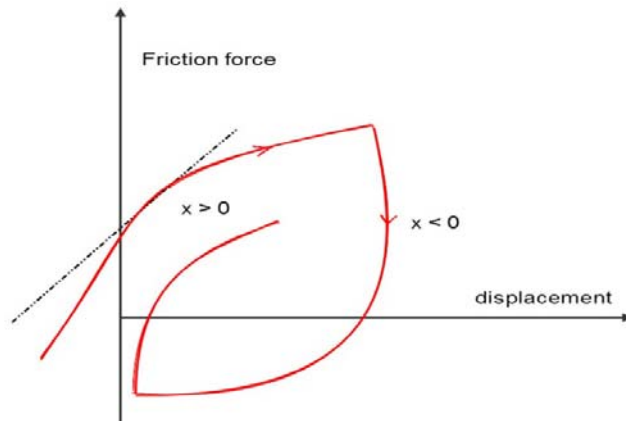


Figure 2.11 The friction as a function of the displacement in presliding regime

2.3.6 Stick-Slip Motion

When one body moves with respect to other at certain low velocity conditions it stops and ‘sticks’ for a certain time and then suddenly ‘slip’ and this behavior is observed

periodically. This behavior is similar to life cycle of one asperity junction as described in the generic friction model. In controlled mechanical systems applications, this behavior of the friction can arise at some low velocities where the motion alternates between the stick and slip conditions. Stick-slip is an undesirable phenomenon in servo systems because of its oscillatory and intermittent behavior. The stick-slip behavior may also result in surface damage and failure of the machine components due to generated oscillatory and vibratory motions.

A stick-slip motion occurs whenever there are stiction and instability [14]. In a controlled servo system, the integral action used in PID controller is instability mechanism or drive flexibility [14]. The stiction is observed due to the fact that the static friction force is higher than the kinetic friction or Coulomb friction force. This behavior can be observed well by a test apparatus consisting of a mass and spring over a surface (Figure 2.12). Here, the instability mechanism or drive flexibility is the spring but the stick-slip oscillation is also influenced by the nature of the surfaces and dynamic of the system (inertia, stiffness, damping...). As the external force on the block increases, the friction also increases to balance this force transmitted to the block through the spring. In this condition, the mass is in stick and external force causes only small displacements (pre-sliding). As the external force increase to the break-away force value, the imbalance between the friction force and spring force is occurred, resulting sudden slip of the mass.

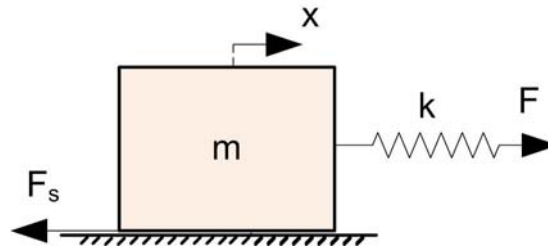


Figure 2.12 Observing stick-slip phenomena

2.3.7 Position Dependent Friction

In the pre-sliding regime, it is observed that the friction depends on the displacement due to the asperity-junctions behavior. Besides that, the friction depends on the position in sliding regime as a result of surface finish of device or geometry-induced preload. For example, for a gear-pinion driven system, the imperfections in the gear mesh can cause a friction which changes with the teeth positions of the gear mesh. Also, in motor drives, any misalignment in the shaft and the gearbox center may cause a position-dependent friction.

2.3.8 Time Dependence of Friction

Rabinowics [15] observed experimentally that the static friction force increases with time that the body is at rest. Hence, it is easier to initiate the motion of the object after it stops if the surface between the objects did not have enough time to glue together. Hence, the friction is a function of the dwell-time (rest time passed in stick position), (Figure 2.13)

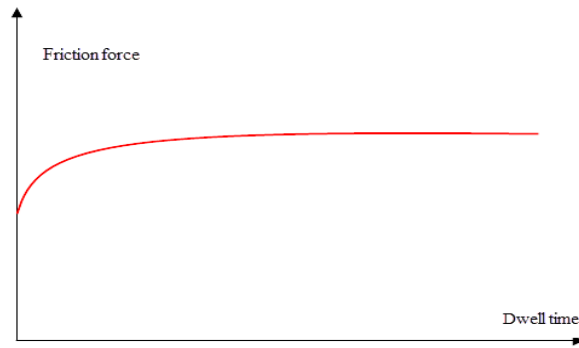


Figure 2.13 Friction as a function of dwell-time

Besides the rest time, the friction changes over time due to temperature, lubricants, wear and deformations of the surface material etc.

CHAPTER 3

FRICITION COMPENSATION METHODS

The increasing demands for quality and precision made many research works and large number of publication related to the friction compensation task. The main aim of these studies was to eliminate or minimize frictional effects so that to attenuate discontinuous motions due to friction. The success of friction compensators depends mainly on the quality of the friction model used and the suitability of the analysis technique employed.

In this Chapter, some notable friction compensation techniques dealing with control problems such as steady state errors, limit cycles, and instabilities are given. A complete survey on the friction compensation techniques and discussion on the applicability can be found in the study by Armstrong et al [6].

Although a wide range of friction compensation techniques were proposed in literature, they can be grouped in three main categories according to their approach to the friction problem [16]:

- Friction problem avoidance
- Non-model-based friction compensation techniques
- Model-based friction compensation techniques

3.1 Friction Problem Avoidance

The friction problem avoidance refers to the modifications of a system or design for control to minimize the disturbances due to friction. It is the first strategy to defeat the friction problem. Many studies showed that the amplitude of the stick-slip can be reduced by decreasing the mass, increasing the damping or increasing the stiffness of the mechanical system [6]. Inertia and stiffness are determined mainly by the geometry and composition of mechanism's bulk material. The placement and the selection of the servo systems units like actuators, sensors, and bearing affect the system inertia, damping, and stiffness. The transmission elements used in a servo system can also affect the stiffness of the system to make it more compliant. So, in order to prevent decreasing the stiffness of the system, it is necessary to reduce number of transmission elements or at least to use the components with high stiffness.

Damping is generally determined by selected lubricants and the sliding surfaces. Therefore, the servo machines are lubricated systematically related to service life and performance. The

lubrication is normally specified to maximize the machine life and so the friction modification is not always the priority of the lubrication engineer.

The mechanical structure of a servo system can limit the performance of the system by mechanical resonances and structural vibrations. The resonances can be excited during motion and reduce bandwidth and stability margins of the systems. The influence of structural vibration and resonances on positioning and tracking performance of systems can be reduced by well-balanced and integrated mechanical design.

The system modification does not guarantee the passive elimination of stick-slip but it produces a system with better performance and easier control. However, the friction avoidance techniques may be costly. For example, to eliminate stick-slip motion, some special materials are used on the machine tool guideways. These materials have a high Coulomb friction and low static friction, resulting in consumption of more power. Most effective friction compensation methods can provide higher performance with lower cost.

3.2 Non-model-based Friction Compensation

Model-free compensation methods refer to the approaches that do not require a structured non-linear friction model. These approaches are suitable for control application with friction in presence of varying and uncontrollable factors such as wear, temperature, humidity, and lubricants conditions. These techniques can prevent not only frictional effects but other nonlinear disturbances. Yet, these techniques are leaning to have additional drawbacks such as extra power consumption in steady state since they are indirect compensation scheme.

There are many non-model-based techniques proposed in literature; namely linear feedback controller, dither, impulsive control, disturbance observer, joint torque control, dual mode controller and learning controller.

3.2.1 Linear Feedback Controller

Proportional-integral (PI), proportional-derivative (PD) and proportional-integral-derivative (PID) controllers are widely used in industrial applications. The regulated system might be stable under PD controller, but it may experience stick-slip motions at low velocities [6]. It is known that increasing the damping or the stiffness of a system can eliminate stick-slip motions. In terms of control, this can be achieved by increasing the PD gains. An increasing derivative gain (D) increases damping of the system and an increasing proportional gain (P) increases the stiffness of the system, preventing stick-slip motions. This can be understood by the fact that by inclusion of frictional memory (friction lag) it is possible to explain the transition from stick-slip to steady state sliding by using high PD gains. However, maximum gains of PD controller are limited by loop stability considerations, sensor noise, and structural resonances.

While a stiff PD controller can be used to obtain stable tracking, the integral control of position is frequently used to reduce steady-state errors. However, the integral action increases the possibility of limit cycling around desired position. To prevent limit cycling, one standard method is to employ a deadband at the input of integral block [17]. However, this introduces its own steady-state errors and deadband also causes an additional nonlinearity.

Another problem with the integral control is that it can be ineffective and even deleterious at velocity reversals. Integral windup from prior motion can actually inhibit break-away. In order to prevent this effect, the integral is typically reset at velocity reversals [16]. While this prevents windup problem, the ensuing integral action produces minimal effect when required the most to overcome friction force at stick case. Another modification is multiplying the integrator by sign of the desired velocity, which is used in overcompensation case but it introduces high gain nonlinearity. The use of nonlinear PID is the further extension, where the gains are time-varying, mostly as a function of the errors / states of the system [18].

3.2.2 Dither

Dither is a high frequency signal introduced to the systems to smooth nonlinearities so that the system can be controlled easier. It is frequently used to prevent friction problems. The idea behind dither is that an extra force is applied to the system such that total applied force to the system gets larger than the static friction force (break-away) at velocity reversals. With that, it is tried to prevent the stiction problem.

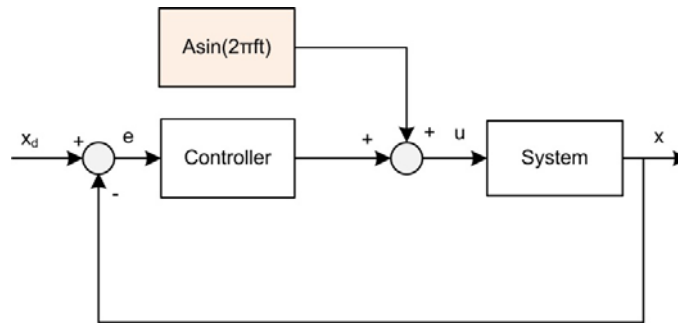


Figure 3.1 Representation of dither method

In control applications, the dither is added to the command input (Figure 3.1). This results in vibrations that are tangential to the sliding contact such that it modifies the effect of the friction by averaging the nonlinearity. The amplitude A and frequency f of the dither signal have to be determined experimentally. According to Canudas de Wit [19], the frequency should be chosen at least three times larger than systems' bandwidth such that its effect is

filtered out before reaching the output of the system. Also, the amplitude should overcome the static friction level.

In order to reduce the effect of the friction, the dither method is widely used in hydraulic servo actuators or pneumatic system [20]. However, the dither is not suggested for direct drive mechanical systems because it can cause some undesirable consequences such as:

- The frequency of the signal can excite one of the natural frequencies of the system.
- The vibrations introduced by the signal of the dither may cause the fatigue and wear problems.
- The extra power will be consumed.

3.2.3 Joint Torque Control

Joint torque control is a sensor-based technique which encloses the actuator-transmission subsystem in feedback loop to make it behave more nearly as an ideal torque sensor [21]. Joint torque control is applied as a means of compensating for actuator and transmission friction. General scheme representing joint torque control is shown in Figure 3.2. Here, an inner torque loop functions to make the applied torque T_a follow the commanded torque T_c . Hence, its implementation needs force or torque sensing as near as practical to the output element of the system so that nearly all of the actuator and transmission friction will be enclosed in the joint torque feedback. This requirement is not evident and is the main disadvantage of this method. The sensor and actuator are non-collocated, separated by the compliance of the transducer. This gives rise to the standard challenges of non-collocated sensing, including additional and possibly lightly damped modes in the servo loops [22].

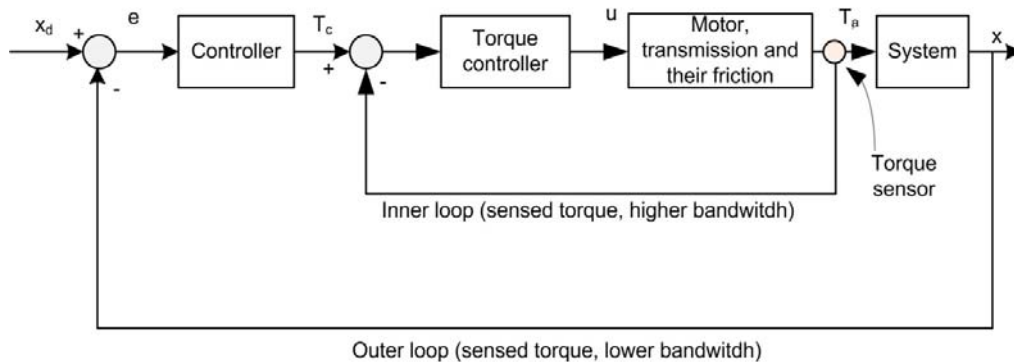


Figure 3.2 Representation of the joint torque control

3.2.4 Dual Mode Control

Some researchers consider the system as two different dynamic systems due to the fact that the friction has two different friction regimes (pre-sliding and sliding). They suggest using

two different control strategies for each of the systems (Figure 3.3). This technique is called dual mode or a variable structural controller [23]. S_1 and S_2 activate the corresponding controller depending on the active region of friction.

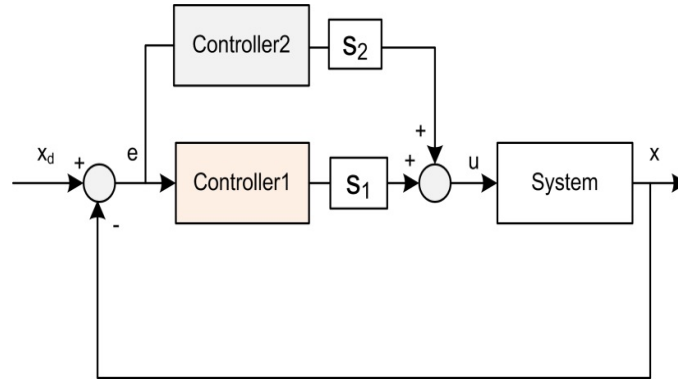


Figure 3.3 Representation of dual mode control

Some high precision applications such as diamond turning of optical elements use this method for nanometer positioning. Two different actuators are used for two different stage mechanisms. However, this technique needs two switch functions: switching between two linear controllers and two friction regimes. When the system is in pre-sliding/sliding regime may not be clear. Also, reinitializing the state of each controller after a switch has occurred is another problem [22]. Hence, the difficulty remains between the switching.

3.2.5 Disturbance Observer

Disturbance observer (DOB) is a model-free technique used to deal with external disturbances and or to compensate model mismatch [22]. The basic idea behind the disturbance observer is that by measuring system motion x together with applied load F_a and knowing the system dynamic model one can estimate the external friction force F_d using an observer [24], as shown in Figure 3.4. Here, the effect of real friction forces F_d is minimized by applying an estimated friction force F'_d which is the output of the disturbance observer.

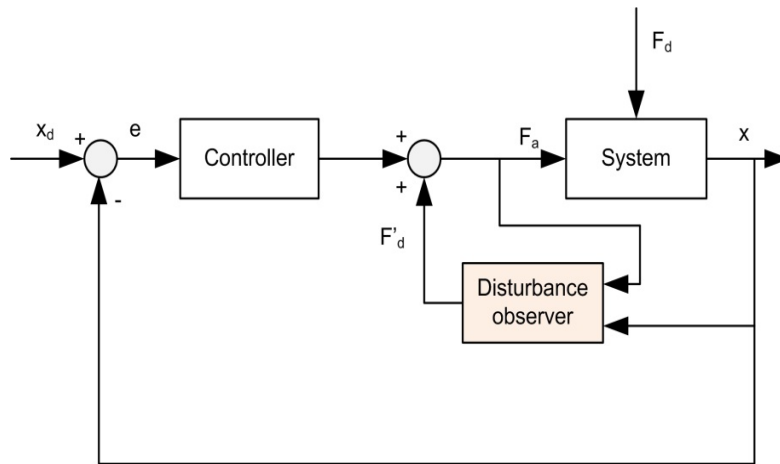


Figure 3.4 Representation of the disturbance observer structure

Parameter uncertainties are decreased by the disturbance observer compared with fixed parameter friction model. Also, tracking performance is increased well due the fact that the disturbance observer not only compensates the friction disturbance but also the other external disturbances. However, the disturbance observer has a limited disturbance rejection bandwidth hence for faster reference trajectories the position error may increases [25]. Also, these methods are apt to have the additional defects such the unstable self-oscillations or extra power consumption at the steady state because they use an indirect compensation scheme.

3.3 Model-based Friction Compensation

Model-based friction compensation methods attempt to capture the nonlinear friction behavior by modeling friction with reasonable complexity. The basic idea is that if well-modeled nonlinear friction model is available, it is possible to compensate the actual friction by applying a force command equal and opposite to the real friction (Figure 3.5). There are some requirements for a successful application of the friction model-based compensation [22]:

- An accurate friction model
- Adequate actuator bandwidth
- Stiff coupling between the actuator and friction element (load)

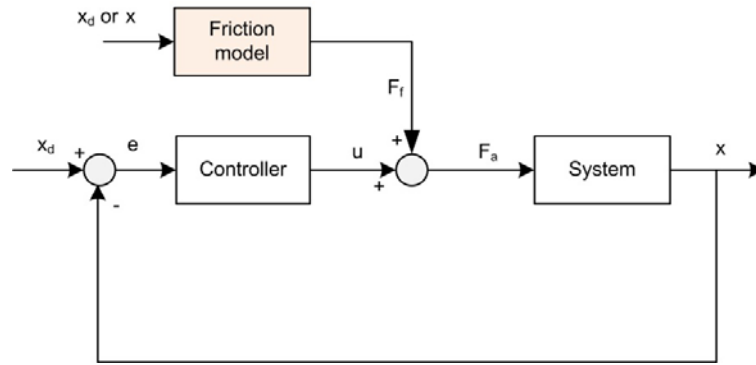


Figure 3.5 Representation of model-based friction compensation

An effective friction compensation requires high quality velocity measurements. The measured, estimated, or desired velocity can be used as input to the friction model. Using measured or estimated velocity to the friction model closes a feedback loop (feedback compensation). In case of using desired velocity as the input to the friction model, the friction compensation is called feedforward compensation. To reduce the influence of the noise coming from velocity sensor and to reduce stability problems, the desired or reference velocity is used. Also, using feedforward compensation is more robust than the feedback control [22].

One of the major difficulties in performing friction compensation is the difficulty of modeling friction at low velocities. Many problems may occur as a result of friction compensation based on a discontinuous model. The discontinuity at zero velocity allows the friction to take infinity number of values, resulting in errors or instabilities in algorithm that all depend on the correct velocity to compensate friction. Hence continuous friction models such as Dahl model [28], the second Blimen-Sorine model [29], and LuGre model [27] will compensate friction better than the discontinuous models. These models are called state variable models and they are better adapted to model friction at low velocities.

Using model-based friction compensation raises also the problem with the identification of model parameters. The model parameters can be identified either off-line or on-line. In off-line identification, the designer has more freedom to specify the motions and to conduct experiments according to the data required. In case of online identification, the data used for the model will be dictated by the operation of machine so the friction model will be strongly coupled and it is more difficult to identify friction parameters correctly. Online identification is called adaptive control if identified parameters are used in the friction model.

3.3.1 Adaptive Controller

The main problem with fixed parameters friction models is that the friction may change as a function of the normal forces in contact, temperature variations, position, etc. In order to adapt such changes, online identification procedures have attracted significant importance by the research community. Adaptive mechanisms observe and adjust automatically some controller parameters in real-time process. However, due to their nonlinear and time-varying character, adaptive controllers are very complex.

The challenges to adaptive control of a machine with friction are not like the general challenges of adaptive controller [22]:

- The stability is obtained under assumptions that the plant parameters are constant and disturbance is restricted. Yet, those restrictive assumptions about the controlled systems may not work in practical case.
- Adaptive controller can only provide a solution when the structure of the plant dynamics and the disturbances are available.
- The adaptive controller needs a persistent (indeed, sufficient) excitation for parameter estimation, which may also cause stability problems.
- The adaptation is typically suitable for slow time-varying parameters thus fast changing dynamics like dynamic friction can hardly be caught by an adaptive mechanism due to calculation of time delay. Also, inaccurate parameters may cause the degradation of the closed-loop performance.

Most of friction models are nonlinear in parameters so nonlinear identification techniques are suitable for the identification process. However, in case of adaptive controller, only for models linear in the parameters robust identification techniques available, such as recursive least square algorithm so only limited set of parameters or the parameters of a simplified model will be adapted online [22].

3.3.2 Static Friction Models

3.3.2.1 Classical Friction Models

During the early days of scientific study of friction, the observed friction phenomena have led to models of Coulomb, viscous, and static friction and all possible combinations. They are often called as classical friction models. The static models depend statically, not dynamically, on the applied load and the velocity. The simplest static friction model is Coulomb friction, in which the friction force is represented with a signum function and expressed as:

$$F_f = F_C \operatorname{sgn}(v) = \mu F_N \operatorname{sgn}(v) \quad (3.1)$$

where F_c is the friction force F_N the normal load and μ the friction coefficient and v is the velocity.

Due to its simplicity, Coulomb friction model is frequently used. It can be further improved by adding viscous friction (Figure 3.6a). However, Coulomb friction model does not specify the friction force at zero velocity. It may be zero or it can take any value in the interval between $-F_C$ and F_C . Hence, it cannot capture the stiction because the friction force at rest is higher than Coulomb friction. In order to capture this to the Coulomb friction model, the friction force at zero velocity is specified:

$$F_f = \begin{cases} F_a & \text{if } v = 0 \text{ and } |F_a| < F_S \\ F_S \text{sgn}(F_a) & \text{if } v \neq 0 \text{ and } |F_a| \geq F_S \end{cases} \quad (3.2)$$

where F_a is applied external force. Here, the stiction is a function of only applied load and not velocity.

The classical friction models can be combined in different ways (Figure 3.6). These models components are either linear or constant in velocity. Stribeck [6] observed that the friction force does not decrease discontinuously as in Figure 3.6 b, but that the velocity dependence is continuous as in Figure 3.6c. This is called Stribeck friction. A general description of static friction models is:

$$F_f = \begin{cases} s(v) + \sigma_2 v & \text{if } v \neq 0 \\ F_a & \text{if } v = 0 \text{ and } |F_a| < F_S \\ F_S \text{sgn}(F_a) & \text{otherwise} \end{cases} \quad (3.3)$$

where σ_2 is the viscous friction coefficient and $s(v)$ is the Stribeck curve. Different parameters have been proposed in literature [30], but the parameters depend on the specific application. One most common form that has been suggested is:

$$s(v) = \left(F_c + (F_s - F_c) e^{-\left| \frac{v}{v_s} \right|^\delta} \right) \text{sgn}(v) \quad (3.4)$$

with v_s is Stribeck velocity and δ the Stribeck shape factor.

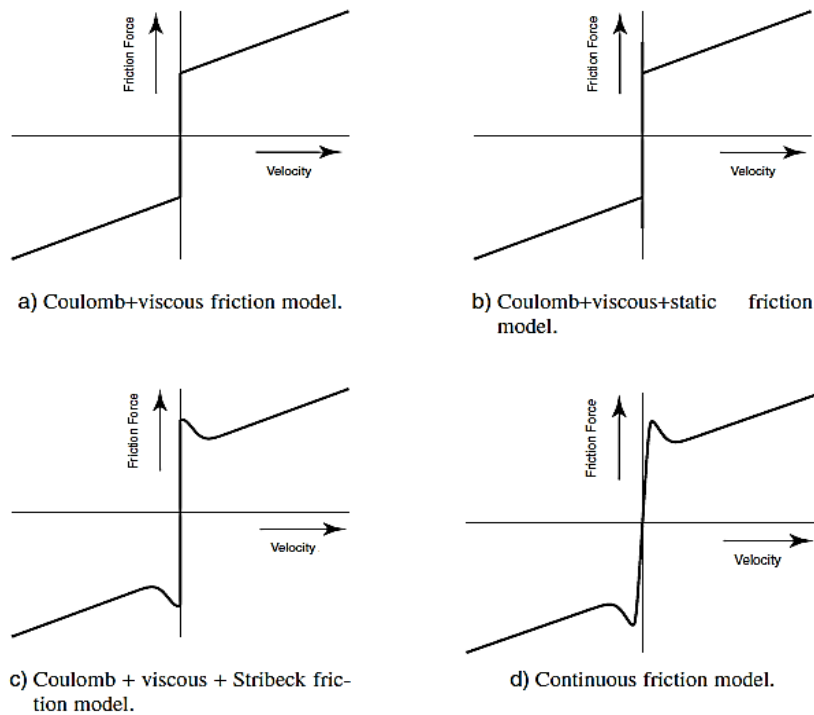


Figure 3.6 Various combinations of static friction model [17].

The main limitations of using a classical friction model are the problem zero crossing of velocity, the non-uniqueness of the solution for the system [31], and numerical problems if such model is used in simulations. For example, numerically integrating a system model that includes discontinuities may cause numerical chatter. One approach to prevent discontinuity is approximating or smoothing the friction-velocity map by a curve with finite slope [8] as in Figure 3.6d. However, in this case, the body will accelerate even if the external forces on the body is less than the peak static friction force F_S . Moreover, a very steep slope around zero velocity can cause very short integration time steps, slowing down simulation.

3.3.2.2 Karnopp Friction Model

To find a remedy to the problem of detecting when the velocity is zero, Karnopp proposed an alternative model [32]. To overcome the problem of locating zero velocity with high precision, he defined a small neighborhood of zero velocity (Figure 3.7). The model defines a zero velocity interval $|v| < DV$. Inside this block, the velocity may change and be non-zero but output of the block maintained at zero by dead-zone. Inside this band around velocity friction is calculated to be either the value required to keep the system at zero velocity or to be equal the break-away force. The one with smaller magnitude is used.

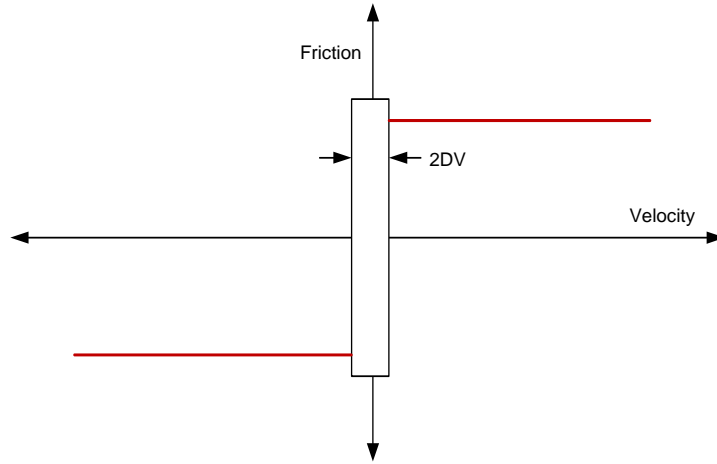


Figure 3.7 The Karnopp friction model

The main advantage of the Karnopp model is its efficiency in simulation. However, the model is strongly coupled with the rest of the system. The external force is an input to the model and this force is not always explicitly given. Hence, the success in simulation fails in practical applications.

3.3.2.3 Armstrong Friction Model

To account some observed dynamical behavior of the friction, a classical friction model was modified by Armstrong [6]. The model defines two separate equations to govern the sticking and sliding modes of the friction. During stiction, to capture some pre-sliding displacement behavior, the friction is modeled as a stiff spring when sticking:

$$F_f = \sigma_0 x \quad (3.5)$$

The sliding mode is defined by

$$F = \left(F_c + F_s(\gamma, t_d) \frac{1}{1 + \left(\frac{v(t - \tau_L)}{V_s} \right)^2} \right) \text{sgn}(v) + \sigma_2 v \quad (3.6)$$

where

$$F_s(\gamma, t_d) = \left(F_{s,a} + \left(F_{s,\infty} - F_{s,a} \frac{t_d}{t_d + \gamma} \right) \right) \quad (3.7)$$

describes the varying friction level at break-away. The level of the static friction force F_s varies with time at zero velocity t_2 (dwell time). The force $F_{s,a}$ is the magnitude of the Stribeck friction at the end of the previous sliding period; γ is an empirical parameter. The time delay τ_d accounts for desired frictional memory. This model tries to capture the dynamics of friction by introducing time dependency or a time delay. Since the model consists of two separate sub-models, one for sticking and one for sliding, a logical statement determines the switching. Also, the model states have to be initialized appropriately every time a switch occurs. As a result the model needs to make use of a switching function which is physically not justified. Therefore, the model is quite complicated to apply in practical applications.

3.3.3 Dynamic Friction Models

One of the major disadvantages of the static friction models is their limited capability, which will cause inaccurate friction models for certain regions of the interest, such as pre-sliding displacement in the stiction regime or frictional lag in sliding regime. The static models have to be extended to dynamic models in order to capture more friction phenomena and to overcome problems mentioned previously.

3.3.3.1 Dahl Friction Model

Dahl developed a model [28] to simulate systems with ball bearing friction and this model has been widely used as simulation model in aerospace industry. The starting point for Dahl's model is the stress-strain curve in classical solid mechanics (Figure 3.8). When subject to stress, the friction force increases gradually until rupture occurs. To describe pre-sliding displacement, i.e., elastic and plastic deformations of the asperity junctions before macroscopic sliding, Dahl thought of exploiting the stress-strain curve of two surfaces under contact. The stress-strain curve can be transformed into a force-displacement curve, which is considered to be the solution of a differential equation in the form of

$$\frac{dF_f}{dx} = \sigma_0 \left(1 - \frac{F_f}{F_c} \operatorname{sgn}(v) \right) \quad (3.8)$$

where F_c is Coulomb friction and σ_0 is the stiffness of the asperity junctions.

In this model, it can be noticed that the friction is only a function of displacement and the sign of the velocity, implying that the friction force depends only on the position. This, so called rate independence, is an important property of the model, making possible to use the theory of hysteresis operators.

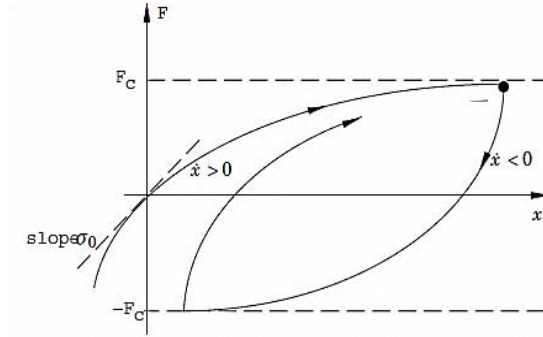


Figure 3.8 Dahl curve [28]

To convert the model into time domain, Dahl observed that

$$\frac{dF_f}{dt} = \frac{dF_f}{dx} \frac{dx}{dt} = \frac{dF_f}{dx} v = \sigma_0 \left(1 - \frac{F_f}{F_c} \text{sgn}(v) \right) v \quad (3.9)$$

This is a generalization of ordinary Coulomb friction model. By introducing \$F = \sigma z\$ the model can be rewritten to the following single state friction model

$$\frac{dz}{dt} = v - \frac{\sigma_0 |v|}{F_c} z \quad (3.10)$$

$$F_f = \sigma_0 z \quad (3.11)$$

The Dahl model is a simple dynamic friction model without any switching function so it is useful in simulation of the friction. However, the Dahl model neither captures the Stribeck effect, which is a rate dependent phenomenon, nor does it capture the stick-slip motion.

3.3.3.2 Bliman and Sorine Model

A further extension of the Dahl model was developed by Blimen and Sorine [29, [31]. Their model is based on the experimental investigations by Rabinowicz [15]. The complexity of the models is given by the dimension of the state space. The first order model is equal to the Dahl model and the second order actually consists of two first-order models:

$$\frac{dz}{dt} = v - |v| \frac{\sigma_0 z}{F_c} \quad (3.12)$$

$$\frac{dz'}{dt} = v - |v| \frac{\sigma_0' z'}{F_s - F_c} \quad (3.13)$$

$$F_f = \sigma_0 z - \sigma_0' z' \quad (3.14)$$

This model can be viewed as a parallel connection of a fast and a slow Dahl model. The fast model has a higher steady state friction than the slow model. The force from the slow model $\sigma_0' z'$ is subtracted from the fast model $\sigma_0 z$, resulting in a total friction force F . Bliman and Sorine showed that as σ_0 goes infinity, the model behaves as a classical static friction model with Coulomb and static friction forces. It should be noted that the Stribeck effect, claimed by the authors, is not the same as observed by Stribeck [6]. Also, this model does not give stiction, nor does it give a friction peak at a specific break-away distance [26].

3.3.3.3 LuGre Model

A model that is in line with the considerations of Dahl was developed at the universities of Lund and Grenoble by Canudas de Wit et al [27] is called LuGre friction model. The Dahl model captures many friction properties but does not capture the Stribeck effect and hence cannot predict the stick-slip motion. The LuGre model which is the extension of Dahl model captures the Stribeck effect and thus describes the stick-slip motion. The model also captures the friction lag in sliding regime and the hysteresis curve in pre-sliding regime. It is also able to estimate the break-away force at transition from pre-sliding to sliding regime. The friction between surfaces is visualized as forces produced by bending bristles/asperities behaving like springs. It is based on the average deflection of bristles. The model has the following form

$$\frac{dz}{dt} = v - \sigma_0 \frac{|v|}{s(v)} z \quad (3.15)$$

$$F_f = \sigma_0 z + \sigma_1 \frac{dz}{dt} + \sigma_2 v \quad (3.16)$$

where v is the velocity between two surfaces in contact, z is the internal friction state, and F is the predicted friction force. The state z which is analogous to the strain in the Dahl model can be interpreted as the average bristle deflection. The LuGre model reproduces spring-like behavior for small displacements, where σ_0 is the bristle stiffness and σ_1 is the bristle (micro) damping and σ_2 is the viscous damping coefficient, (Figure 3.9).

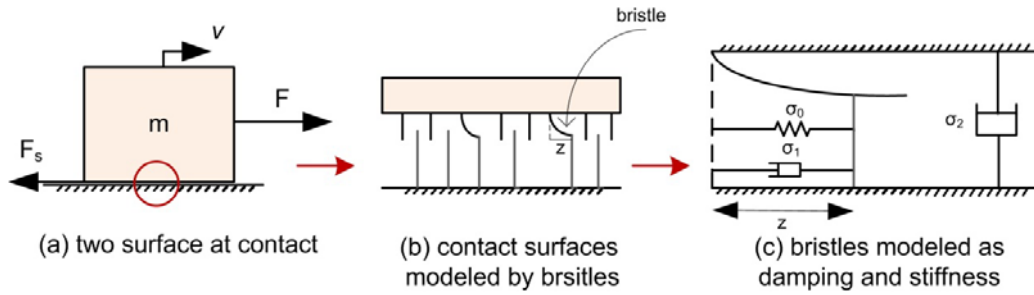


Figure 3.9 Physical explanation of the LuGre model

For constant velocity, the steady-state friction F_{ss} is given by

$$F_{ss} = s(v)\text{sgn}(v) + \sigma_2 v \quad (3.17)$$

where $s(v)$ captures Coulomb friction and the Stribeck effect. A reasonable choice of $s(v)$ for a good approximation of the Stribeck effect is given as

$$s(v) = F_c + (F_s - F_c)e^{-\frac{|v|}{v_s}^\delta} \quad (3.18)$$

where F_s is the stiction friction, F_c is the Coulomb friction, v_s is the Stribeck velocity and δ is the Stribeck curve shape factor. The value $\delta = 1$ is suggested in [33] while [34] finds values in the range 0.5 to 1 and [30] uses the values $\delta = 2$ for LuGre friction model.

The LuGre friction model is a very popular model for friction compensation [27], simulation [36] and estimation [26] studies. It shows a rich behavior in terms of observed friction phenomena and is able to model stiction, the Stribeck effect, frictional lag, or hysteresis, and stick-slip transition. However, some of practically observed hysteresis related phenomena cannot be predicted accurately by the LuGre model as shown by Olsson et al [35] and Swevers et al [25].

3.3.3.4 Leuven Model

The Leuven model was developed by Swevers et al [37, [38] at Katholieke University of Leuven. This model is based on the experimental findings that the friction force in pre-sliding regime is a hysteresis function of the position with non-local memory. The Leuven model tries to modify the LuGre friction model in order to fit the experimental findings in the pre-sliding regime to the LuGre friction model such that more precise tracking can be obtained. The equations of the Leuven model are

$$\frac{dz}{dt} = v \left(1 - \operatorname{sgn} \left(\frac{F_h(z)}{s(v)} \right) \left| \frac{F_h(z)}{s(v)} \right|^{\delta_l} \right) \quad (3.19)$$

$$F_f = F_h(z) + \sigma_1 \frac{dz}{dt} + \sigma_2 v \quad (3.20)$$

where σ_1 and σ_2 have the same meaning as for the LuGre friction model, δ_l is the Leuven model shape factor determining the transformation between the state variable z and position of the moving mass, $s(v)$ represents the Stribeck effect. As in case of the LuGre friction model, it converges to the Stribeck friction $s(v)$ for steady-state case at constant velocity input. $F_h(z)$ represents the behavior of hysteresis with nonlocal memory as a function of internal state variable z . The hysteresis force is a nonlinear function with a nonlocal memory [22]. This means that:

- A new branch of hysteresis curve is initiated at velocity reversal.
- The shape of the hysteresis curves is determined by the past extreme values of the F_h , i.e., the shape is independent of the particular manner of the variation of z between the extreme points.
- The value of F_h after any time t_0 depends not only on the value of F_h , but also on the past extreme values of F .

The hysteresis function $F_h(z)$ can be implemented by using Maxwell-slip approximation [38]. It consists of N elasto-plastic elements in parallel. Each element i has one common input z and one output F_i and each element is characterized by its own maximum elementary Coulomb force W_i , an elementary stiffness value k_i and a state variable ζ_i (Figure 3.10). The state variable ζ_i describes the position of element i . The elements have no mass, yielding a static relationship between the force F_i and the relative displacement ($z - \zeta_i$) for each element. The relationship can be described as

$$F_i = \begin{cases} \begin{cases} F_i = k_i(z - \zeta_i) \\ \zeta_i = \text{constant} \end{cases} & \text{if } |z - \zeta_i| < \frac{w_i}{k_i} \\ \begin{cases} F_i = \operatorname{sgn}(z - \zeta_i)W_i \\ \zeta_i = z - \operatorname{sgn}(z - \zeta_i) \frac{w_i}{k_i} \end{cases} & \text{if } |z - \zeta_i| \geq \frac{w_i}{k_i} \end{cases} \quad (3.21)$$

The total hysteresis force is equal to the sum of hysteresis forces of each element as

$$F_h(z) = \sum F_i(z) \quad (3.22)$$

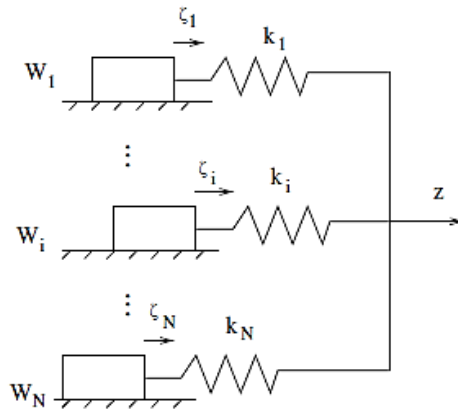


Figure 3.10 Representation of Maxwell-slip friction model using N elementary models [37]

The output of each element is given graphically in Figure 3.11. The maximum force of an element W_i and linear hysteretic behavior of an element are represented. Since the spring constant and the maximum force of each element in the Maxwell-slip model are different from each other, a nonlinear hysteresis curve is obtained by using then N elements.

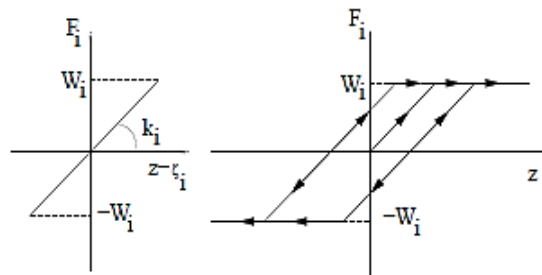


Figure 3.11 The characteristics of one element Maxwell-slip model [37]

The Leuven model simulates friction behavior in pre-sliding regime accurately. However, in order to calculate the hysteresis force different internal states are used [22]. The LuGre model has one internal state but the Leuven model is multiple states friction model. The internal states cannot be physically measured. Hence, the model is complex and may not be practical in real applications. Also, the model has more parameters to be identified than the LuGre model, resulting in more uncertainties in terms of parameters.

3.3.3.5 Generalized Maxwell-slip (GMS) friction model

The Generalized Maxwell-slip (GMS) friction model was developed by Lampaert et al [39]. It is an extension of the Maxwell-slip implementation for a hysteresis function used in the Leuven model that is why it is called Maxwell-slip friction model. It is based on a physically motivated generic friction model mentioned in Chapter 2. The developed model,

as a parallel connection of different single state friction models, all have the same input namely the velocity. The friction force is given as the summation of the outputs of N elementary state models in addition to an extra viscous term, if viscous friction present at the interface. The model is mathematically described as

$$F_f(t) = \sum F_i(t) + \sigma_2 v \quad (3.23)$$

Each single state friction model has a logic state which indicates if the element sticks or slips. The dynamics of each elementary model is determined by the following rules:

If the elementary model sticks, the state equation is given by

$$\frac{dF_i}{dt} = k_i v \quad (3.24)$$

and the model remains sticking until $F_i > \alpha_i s(v) = W_i$

If the elementary model slips, then state equation is given by

$$\frac{dF_i}{dt} = \text{sgn}(v) C \left(\alpha_i - \frac{F_i}{s(v)} \right) \quad (3.25)$$

and the model remains slipping until the velocity goes through zero.

The parameter σ_2 and the Stribeck curve $s(v)$ are the same as for the LuGre and Leuven model. The attraction parameter C determines the attraction of the total friction force towards the Stribeck curve in the sliding regime. Each elementary model i has its own stiffness k_i and elementary fractional parameter α_i which determines the maximum force of each elementary block in sticking region.

The GMS friction model is based explicitly on the three friction properties.

- The Stribeck curve for constant velocities in sliding regime
- The hysteresis function with nonlocal memory in the pre-sliding regime
- The friction lag in sliding regime

These three properties are captured by LuGre, Leuven, and GMS friction models. However, it is claimed in [39, [22] that the GMS model represents the second property more accurately than the Leuven and LuGre friction models. The main disadvantage of the GMS friction model is that it requires two different switching functions to pass through friction regions. This may be problematic in practical applications because the sensor noise can be sufficient to force a transition between one structure to another. Moreover, when a transition from sliding to sticking is detected, it can be necessary to back up the simulation to the point of

transition and restart it in the new structure [40]. This complexity is always undesirable and may be unsuitable for real-time implementations.

3.4 Conclusions

In this Chapter, various friction compensations techniques proposed in the literature are given. Table 3.1 represents a summary of these friction models from simple static models to complex dynamic ones. In this table, the friction models are compared in terms of capturing different types of friction behaviors. ‘+’ shows that the property is captured by the model and ‘o’ shows that the model approximates the property. In terms of application, ‘-’ shows the negative property of the model and K corresponds to the number of elementary Maxwell-slip models used in the Leuven and the GMS friction models.

The friction model performances are compared according to the different studies found in literature. How well the model captures the friction behavior depends on the identification procedure, actuator bandwidth, stiff structure between actuator and friction element etc. In order to use a friction model in control applications, it should be as simple as possible to be practical, but complex enough to capture friction properties. Also, the number of parameters should be as small as possible and easy to identify. The existing models which meet the requirements are generally the dynamic friction models. The classical friction models are simple but they cannot capture most friction behaviors such as stick-slip, varying break-away force and friction lag. Hence, for a precise control and better tracking, a dynamic friction model is required to be used.

Table 3.1 Comparison of the friction behaviors for different friction models

	Classical	Karnopp	Armstrong	Dahl	Bli-Sorine	LuGre	Leuven	GMS
Static property								
Coulomb friction	+	+	+	+	+	+	+	+
viscous friction	+	+	+			+	+	+
static friction	+	+	+	+	+	+	+	+
Stribeck effect	+	+	+		o	+	+	+
Dynamic property								
friction lag						+	+	+
break-away					o	+	+	+
stick-slip			o			+	+	+
pre-sliding				o	o	o	+	+
Application								
# of parameters	4	4	7	3	4	6	9+2K	6+2K
model complexity	+	+	-	+	-		-	-
switch function			-					-

The Dahl-type friction models offer a good balance between ease of implementation and fidelity to the details of friction with guaranteed boundedness and convergence [40]. The LuGre model offers a smooth transition of motion from pre-sliding to sliding regime and vice versa without switching functions. The criticism for the LuGre model is that it does not simulate hysteresis behavior well in pre-sliding regime [[3, [22, [51]. The Leuven model is proposed which models pre-sliding accurately. However, the Leuven model is more complex than the standard parameterization of the LuGre model due to the use of a hybrid hysteresis model and therefore more difficult to be used for control design and analysis [17]. Similarly, Maxwell-slip model captures hysteresis behavior more accurately in pre-sliding regime, but switches between functions could cause some problems about how to determine when the object is in the pre-sliding regime or in the sliding regime. Moreover, the number of parameters used for Leuven and GMS model are more than the LuGre model, resulting in more uncertainties in terms of parameters and difficulty in terms of identification and implementation.

The LuGre model introduces an extra state variable z which is physically immeasurable. Hence, the identification of the dynamic parameters may be problematic, but the LuGre model contains only a few parameters compared to the other dynamic friction models, thus it can be matched to experimental data easier. Hence, throughout this thesis the LuGre friction model will be used as a dynamic model-based friction compensation method.

CHAPTER 4

FRICITION IDENTIFICATION

In order to determine friction characteristics of the test system and to determine friction model parameters, various kinds of experiments are performed on a real experiment setup in sliding and presliding regimes. Then, according to the test results, the parameters of LuGre and general static friction models are estimated.

4.1 Experimental Setup

Figure 4.1 shows an example of setup that is used to identify the friction model and to analyze experimentally the compensation techniques. The test system is a gyro-stabilized remotely controlled gun system. It automatically tracks the target and fires via stabilized turret. It is basically a rotating arm system. The arm (the gun) mounted on a turret (or gimbal) which rotates about azimuth and elevation axes. Two permanent magnet AC brushless servo motors are used to move each axes. An analog signal resolver is mounted on the shaft of servo motor in order to measure the angular displacement and velocity of the servo motor. The angular displacement information is used to drive the servo motor via PWM (pulse width modulation) technique. Also, the angular velocity is used for the system servo control purposes. The test system adopts gear train structure to generate a high output torque. The transmission elements between the servo motor and the turret are a low backlash planetary gearbox and ring-pinion gear element. The gearbox with 1:10 reduction and low backlash is used in front of the servo motor in order to increase torque output of the motor. Similarly, a ring-pinion gear is used between the gearbox and the turret to further increase the torque output, see Figure 4.2. To decrease the backlash in the gear train structure, an anti-backlash gear mechanism is employed (Figure 4.2). In this mechanism, the driving gear (pinion) is pressed against the mating gear by applying a preload to the driving gear. The angular displacement of the system is measured by an incremental encoder with 16 bit resolutions. Similarly, the angular velocity of the system (the turret) is measured by using two axis fiber optic gyroscope with a 23 bit resolutions.



Figure 4.1 An example of setup (Photo Courtesy of ASEL SAN Inc.)

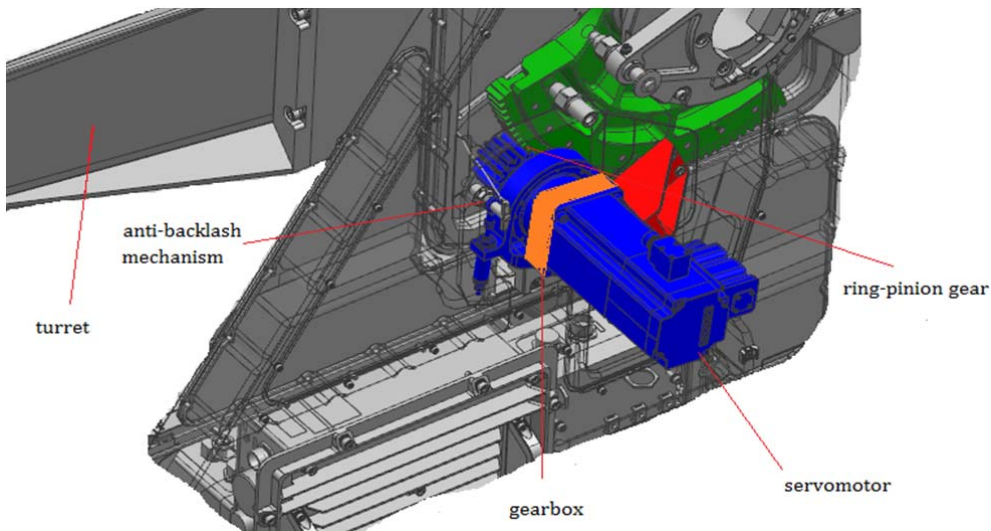


Figure 4.2 Typical construction of test set-up in 3D wireframe

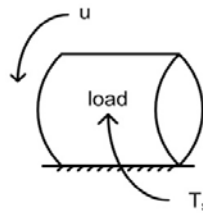
The control and signal processing of the system are accomplished with a customized servo controller, which includes onboard A/D and D/A converters and a slave digital signal processor (DSP). It is used to drive servo motors by a pulse modulation source inverter which translates the input signal expressed in a voltage, into three phase signals with a fundamental frequency. The signals from feedback devices are read and processed by this servo controller. An external model developed in the MATLAB environment is used to

facilitate real-time graphing, data logging by RS-422 serial port. Also, a graphical user interface is developed to adjust control gains without recompiling program. Data acquisition and control implementation are performed at 1.0 kHz sampling frequency.

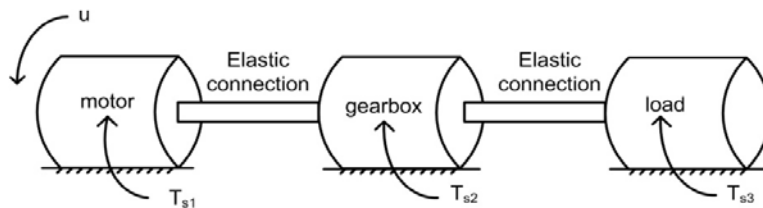
4.2 The System Analysis

4.2.1 Non-located Friction

As mentioned previously, the test system is a geared-electromechanical system, i.e. there are transmission elements between the servo motor and the load. Therefore, the actuation and the friction are non-located, meaning that the friction torque and the actuation torque do not act at the same location. The load is flexibly connected to the servo motor through a gearbox which is also subject to the friction, (Figure 4.3). Here, u is the control input signal and T_s is the friction torque. Hence, the friction seems to be sandwiched in between the motor (input side) and the load (output side). The control input has to pass through the transmission elements (gearbox) to compensate the frictional effects.



(a) Actuation and load are at the same side (collocated friction)



(b) Actuation and load are at the different side (non-located friction)

Figure 4.3 Representation of collocated and non-located friction

The friction source in the system may be divided into three parts; namely, inside the motor, in the gearbox, and at the load side. In order to get an insight about the value of these friction torques, the motor, the gearbox and the load are demounted for themselves and their friction torques are measured separately via a torque sensor (Figure 4.4).

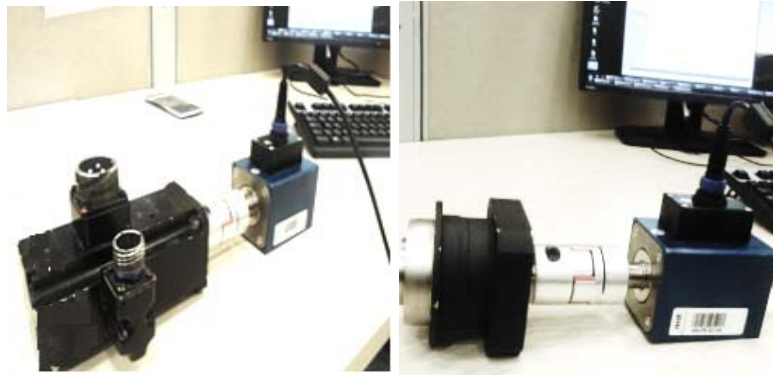


Figure 4.4 Friction measurement of the motor and gearbox

Table 4.1 lists the friction test results of the motor and gearbox at the motor. The values are the measured friction torques at the onset of motion i.e., they are the static or the breakaway friction torques. The results indicate that the friction value of the motor and gearbox are nearly the same. The similar tests are repeated for the load side friction. In these tests, the motor and the gearbox are demounted from the load (the turret) so that the measured friction torque value is equal to the friction torque in the bearing of the load (the load side friction). In Table 4.1, friction torque values at the load side are given. In order to compare the friction torques in the system components, the friction torque values of the motor and the gearbox projected to the load side by multiplying their friction values with the reduction ratio. It is seen that the friction at the load side is dominant (more than 70% of the total friction value) when compared to the friction value at the motor and at the gearbox. Hence, at the onset of the motion of the system, the friction at motor and gearbox are to be broken (overcome) firstly and the friction at the load side is to be broken lastly.

Table 4.1 Friction test results of the load side

№ of test	Motor, T_{s1} (Nm)	Gearbox, T_{s2} (Nm)	Load, T_{s3} (Nm)
1	5.60	5.60	23.53
2	5.60	5.60	22.75
3	5.60	5.60	23.66
4	4.20	4.20	22.10
5	4.20	5.60	20.28
6	4.20	4.20	20.80
7	4.20	4.20	20.41
8	4.20	4.20	18.98
9	4.20	4.20	22.10
10	4.20	4.20	19.19
mean	4.60	4.60	21.60
standard deviation	0.64	0.64	1.44

4.2.2 The flexibility

The mechanical transmission elements in the system introduce the flexibility between the motor and the load, resulting in structural resonance and reducing the bandwidth of the system. Since the control input effort has to be transferred through a flexible connection to compensate the frictional effects, the effective friction compensation may be limited by the transmission dynamics. In order to evaluate the effect of the elastic components on the system servo characteristics, some open loop experiments are performed. During these tests, an input current signal is applied to the system and the velocity response of the system is measured. The current given to the system is multiplied by motor torque constant and reduction ratio to determine the torque given to the system. Here, frequency sweep tests are performed to obtain frequency response of the system by varying the signal frequency from 0.5 to 100 Hz with increments of 0.5 Hz and each lasting 16 cycles for each excitation. Then, according to the input-output relationship obtained, the frequency response of the system is obtained by using FFT (Fast Fourier Transform) techniques via MATLAB computation tools.

Figure 4.5 shows the open loop frequency response obtained the test set-up. It is seen that the open loop system has first elastic mode near 11 Hz (Figure 4.5). On the other hand during the stabilization purposes, the disturbance torques coming from the base movements are at almost up to 2-3 Hz which much smaller than the first resonance frequency of the test set-up. The desired input frequencies are lower than 2 Hz during the stabilization of the system. Hence, it is possible to assume the system to have rigid connection at least up to its first resonance frequency as represented schematically in Figure 4.6. Therefore, the friction identification tests will be conducted as if the friction torques acting on the components of the system is lumped on the load side. The friction lumped on the load side will be identified and then according to the identified friction, the friction model parameters will be estimated. The lumped friction is the sum of all friction torques coming from the motor, gearbox and the load, which will be verified in the next section.

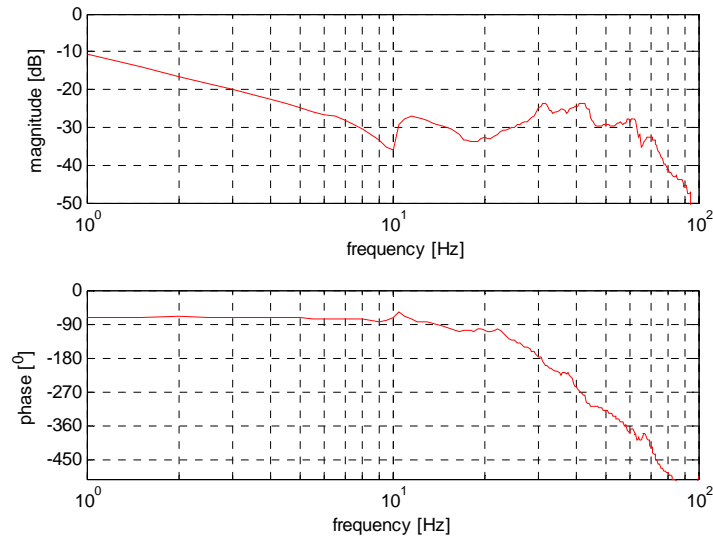


Figure 4.5 Open loop frequency response of the system

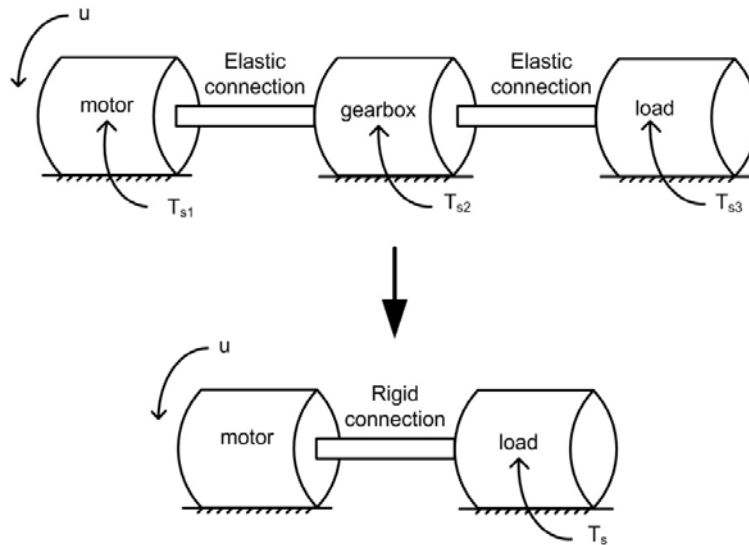


Figure 4.6 Schematic representation of rigid body assumption

4.2.3 Tuning Controller Parameters

The test platform consists of the two orthogonal stabilized axes which are azimuth and elevation. The control scheme of each individual axes consists of a PI velocity feedback controller. The controller of the test set-up was designed in terms of stability, minimization of disturbance effects, rapid and smooth tracking of a set point, elimination of steady-state

error, robustness to change in process conditions etc. Since the main aim of this work to compensate the frictional effects, the detail of the design of the system controller is not stated here.

The performances characteristics of the control system are specified in terms of the transient response to a step reference tracking. The system linear model is prepared in MATLAB Simulink environment and PI velocity controller is tuned via MATLAB Simulink Control Design PID Tuner. Simulink block diagram of the linear system is given in Appendix.

Figure 4.7 shows step response of the system with tuned controller. The reference input is normalized about 1° . The design requirements are selected as a settling time less than 400 ms, a rise time less than 40 ms, and zero steady-state error to the step reference input. In order to achieve these requirements, the controller gains are used as 3 for proportional and 30 for integral actions in the system controller algorithm.

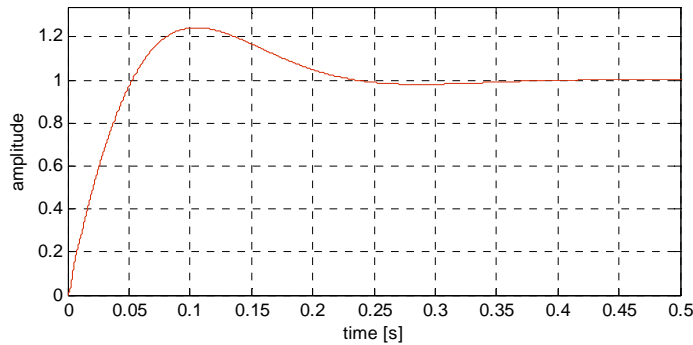


Figure 4.7 Step response of the linear system with tuned controller

4.3 The Identification of the Friction Model Parameters

Two different friction regimes are distinguished for the friction: the presliding and sliding regime. In sliding region, the friction depends mostly on the relative velocity at interface of two mechanical components. Hence, in this region, the friction is modeled as the static mapping between the relative velocity of the two contacting surfaces and the friction torque. With the static model in the sliding region, only the limited friction characteristics can be captured. However, the friction can also exhibit internal dynamics such as presliding, stick-slip, and frictional hysteresis [27]. These behaviors of the friction can be modeled in the presliding regime. In presliding regime, there are the asperity-junctions contacts at the interface of the sliding surfaces. As a tangential load is applied, these junctions deform elastically or plastically. Therefore, the friction depends mostly on the displacement of the sliding surfaces. Hence, the friction is modeled as a function of the displacement in this region.

Since the friction is divided into two distinct regions, various experiments are conducted which are specific at in each region to identify the friction model parameters in the system. That is,

- The steady-state characteristics of friction torque as a function of velocity (sliding phase)
- The dynamic characteristics of the friction torque as a function of position (presliding phase)

The static friction parameters are identified in sliding phase and the dynamic friction parameters are identified in the presliding phase by performing appropriate experiments in each regime.

4.3.1 Sliding Phase Experiments

The friction torque in sliding phase is determined by constant velocity experiments. During a reference constant velocity, the torque applied to the system is equal to the friction torque since acceleration is no present and the system is balanced (the system mass center is coincident with rotation axes). The current given to the system is measured by a current transducer and Then, in order to obtain the torque applied to the system, the current is multiplied by the motor torque constant and reduction ratio. Also, the system velocity is measured by a gyroscope.

In order to get a measurement at one point of the steady state velocity-friction torque characteristics, the velocity of the system has to be kept constant for a considerable time. The experiments have to be performed in closed loop under PI control. By using this constant velocity data, a friction-velocity map (friction torque as a function of the rotational velocity) is obtained.

In this work, the experiments are carried out for 80 different velocities ranging from 0.05 deg/s (0.001 rad/s) to 65 deg/s (1.14 rad/s) for both negative and positive directions. At each velocity, the system is moved from the same initial position to a final position. To reduce the effect of the dwell time on the friction, the system is warmed up by moving it in negative and positive directions before starting the tests since the friction is sensitive to the temperature [16, 45]. To obtain a good approximation for the Stribeck curve, a large number of points are collected at low velocities. An example constant velocity experiment is shown in Figure 4.8.

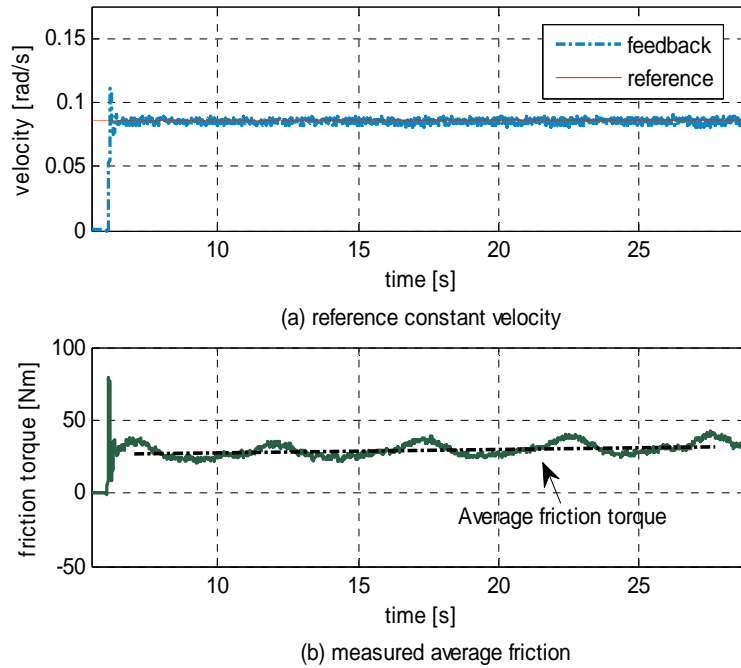


Figure 4.8 Determining of one point on friction-velocity map

To verify repeatability of the test data, the constant velocity experiments at certain velocities are repeated. Six set of the constant velocity experiments are carried out, two set of which are shown in Figure 4.9 for both negative and positive directions. From Figure 4.9, it can be concluded that the measurements shows qualitatively the same friction characteristics. Friction torque decreases for increasing velocities up to a certain point of the velocity (the Stribeck effect) and then it increases for increasing velocities (the viscous effect). The geometry-induced preload and the mechanical imperfections in the system components are known to be responsible for some asymmetric behaviors between negative and positive directions in the velocity maps.

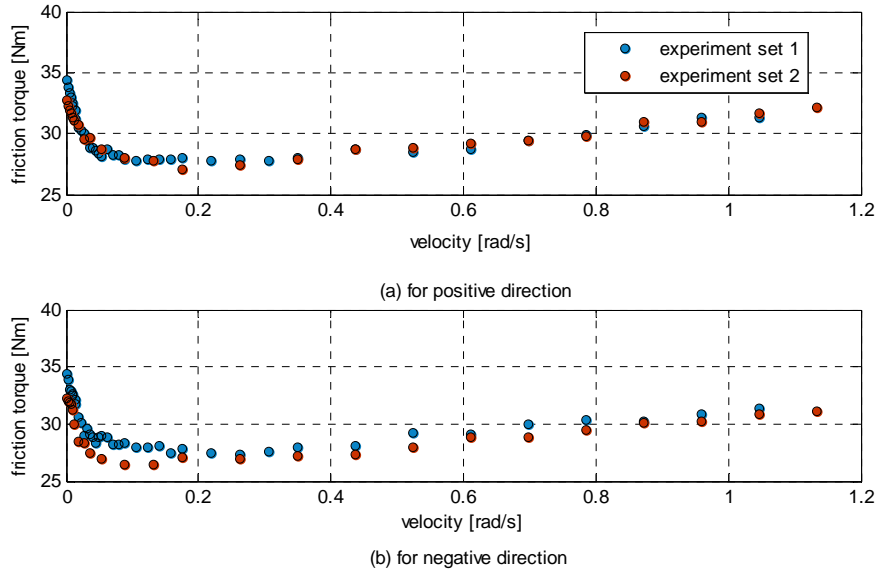


Figure 4.9 Friction-velocity map for two different set of the experiment

4.3.2 Estimation of static friction parameters

The steady-state characteristics of the friction torque are observed in the sliding phase. In this phase, the friction is modeled as a static mapping between the relative velocity of the two contacting surfaces and the friction torque. The static friction parameters are estimated by using the friction-velocity map.

Assuming that the rotating arm system is balanced i.e., the mass center coincides with its rotation axis, applying torque equilibrium in the steady state case, the generalized model for one axis (traverse axis for this work) can be given as

$$\mathbf{u} = \mathbf{J}\ddot{\mathbf{q}} + \mathbf{T}(\dot{\mathbf{q}}, \mathbf{z}) \quad (4.1)$$

$$\mathbf{T}(\dot{\mathbf{q}}, \mathbf{z}) = \sigma_0 \mathbf{z} + \sigma_1 \frac{d\mathbf{z}}{dt} + \sigma_2 \dot{\mathbf{q}} \quad (4.2)$$

$$\frac{d\mathbf{z}}{dt} = \dot{\mathbf{q}} - \sigma_0 \frac{|\dot{\mathbf{q}}|}{s(\dot{\mathbf{q}})} \mathbf{z} \quad (4.3)$$

$$s(\dot{\mathbf{q}}) = T_c + (T_s - T_c) e^{-|\frac{\dot{\mathbf{q}}}{\dot{\mathbf{q}}_s}|^\delta} \quad (4.4)$$

where J is the effective inertia of the motor-transmission-rotating arm combination, q is the angular displacement and u is the control input signal (the input torque to the system). The term $\sigma_2 \dot{q}$ is the velocity dependent damping torque. The friction model takes into consideration the Stribeck effect through the function $s(\dot{q})$. The velocity \dot{q}_S is the sliding speed coefficient that determines the Stribeck curve and $s(\dot{q})$ such that $T_c \leq s(\dot{q}) \leq T_s$.

Under steady state velocities, the bristle deflection z will be constant and $\frac{dz}{dt}$ becomes zero. Using equation (4.3), z_{ss} can be written as:

$$z_{ss} = \frac{s(\dot{q})}{\sigma_0} \text{sgn}(\dot{q}) \quad (4.5)$$

By substituting Equation 4.5 and 4.4 into Equation 4.2, the steady state friction as shown in Equation 4.6 is obtained:

$$T_{ss}(\dot{q}) = \left(T_c + (T_s - T_c) e^{-\left| \frac{\dot{q}}{\dot{q}_S} \right|^\delta} \right) \text{sgn}(\dot{q}) + \sigma_2 \dot{q} \quad (4.6)$$

In Figure 4.10, a typical static LuGre friction model is shown. Here, $s(\dot{q})$ represents the Stribeck and $\sigma_2 \dot{q}$ represents the viscous friction torque. The viscous and Stribeck friction can be chosen such that $T_{ss}(\dot{q})$ matches the measured steady state friction. Definitions of all LuGre friction model parameters are given in Table 4.2.

Table 4.2.

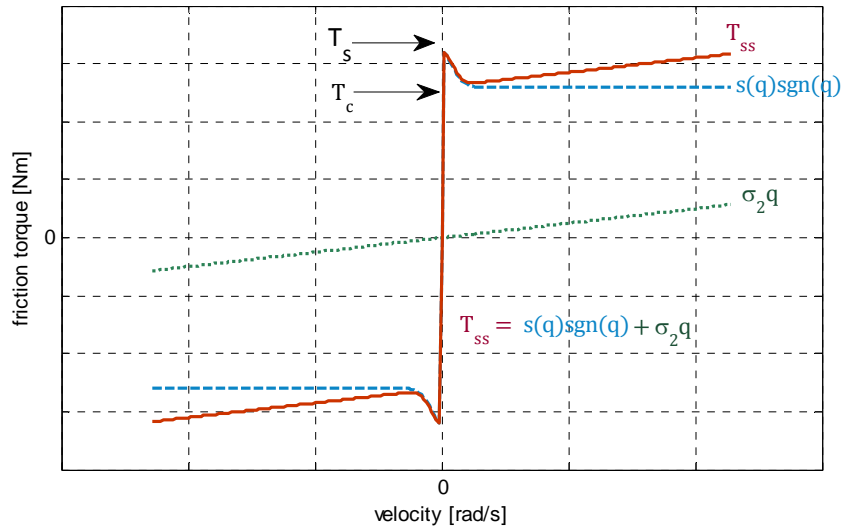


Figure 4.10 A typical representation of static LuGre model

Table 4.2 Definition of parameters of LuGre model

Definition	Symbol
Bristle stiffness	σ_0
Bristle damping	σ_1
Average bristle deformation	z
Viscous friction coefficient	σ_2
Coulomb friction force	T_c
Static friction force	T_s
Stribeck velocity	\dot{q}_s
Stribeck shape factor	δ

The parameters T_c , T_s , σ_2 , and \dot{q}_s can be determined from the friction-velocity map. In order to identify static friction parameters, the data obtained in experiments is analyzed with the similar procedure that was described in [42]. The LuGre model static parameters $\psi = [T_s \ T_c \ \dot{q}_s \ \sigma_2]$ are obtained by using nonlinear optimization techniques (by applying the MATLAB function `lsqcurvefit.m`) such that the quadratic cost function I is minimized:

$$\min_{T_s, T_c, \dot{q}_s, \sigma_2} I = \sum_{i=1}^n [\tilde{T}_{ss}(\dot{q}_i) - T_{ss}(\dot{q}_i)]^2 \quad (4.7)$$

where $\tilde{T}_{ss}(\dot{q}_i)$ equals to the experimental averaged friction torque during constant velocity \dot{q}_i , n is the number of data points and $T_{ss}(\dot{q}_i)$ is represents the model output given in Equation 4.6. The identified LuGre model friction parameters are given in Table 4.3. The Stribeck shape factor δ for LuGre model is used as 2 [27], but for application of the static friction model, it is also identified. The steady-state friction model output (line) and the data points (dots) are shown in Figure 4.11.

Table 4.3 Estimated static parameters of the LuGre model

Parameter	Unit	Positive velocity	Negative velocity	Nominal value
σ_2	Nm.s/rad	3.87	4.27	4.07
T_c	Nm	25.3	26.7	26
T_s	Nm	32.7	35.1	33.9
\dot{q}_s	rad/s	0.0271	0.0291	0.0281
δ	-	0.96	0.85	0.91

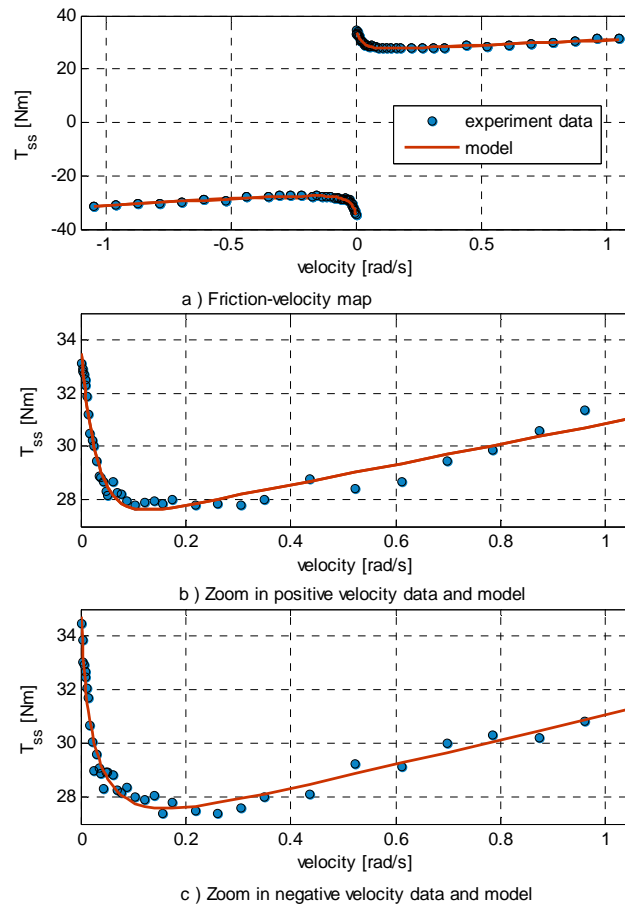


Figure 4.11 Friction torque-velocity map and fitted static LuGre friction model

In section 4.2, the averages of the friction torques measured for the motor, for the gearbox and for the load are measured as 4.6 Nm, 4.6 Nm and 21.6 Nm, respectively. The sum of all these friction torques is nearly 31 Nm, which is close to the identified static friction torque $T_s = 32.7$ Nm as given in Table 4.4. Therefore, the previous assumption that all the friction is lumped on the load side during identification of the friction tests is verified.

To verify the repetitiveness of the estimated model parameters, six set of the constant velocity experiments are carried out in negative and positive direction of the system. The experiments are performed on different days. Hence, in order to avoid dwell time effect, the system is warmed up before collecting the test data.

The experimental results are tabulated in Table 4.4. The repetitiveness of the experiments is achieved with less than %5 standard deviation from mean. The maximum deviation in the model parameters is observed in viscous friction coefficient σ_2 .

Table 4.4 Comparison of estimated static parameters of the LuGre model for different experiments

Parameter	set 1,2		set 3,4		set 5,6		mean	std
	Neg.	Pos.	Neg.	Pos.	Neg.	Pos.		
σ_2	3.85	4.26	3.78	4.21	3.87	4.27	4.03	4.7
T_c	27.2	26.7	25.8	26.4	25.3	26.7	26.4	2.4
T_s	31.3	33.8	32.4	35.3	32.7	35.2	33.4	4.2
\dot{q}_s	0.0281	0.0299	0.0275	0.0288	0.0271	0.0291	0.0284	3.4

4.3.3 Presliding Phase Experiments and Estimation of Dynamic Friction Parameters

The frictional surfaces are modeled as the elastic bristles in the LuGre model. The bristles are randomly distributed over the contacting surfaces. When an external tangential force is applied to these bristles, they deform elastically and/or plastically like a nonlinear spring as seen in Figure 4.12.

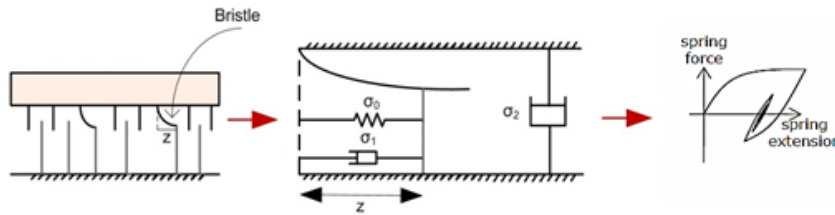


Figure 4.12 Representation of modeling of contact surfaces in LuGre

Among six parameters of the LuGre model, two remains to be identified (σ_0 and σ_1). These parameters represent damping and stiffness characteristics of the bristles in micro scale, respectively, see Figure 4.12. Hence, the identification of the friction model parameters has to be accomplished in the presliding region. Compared with the identification of the static parameters, the dynamic parameters are more difficult to identify since apart from the nonlinearity in the model, the parameter z is immeasurable, which describes the internal state of the friction. In literature, some optimization algorithms like Particle Swarm Optimization and Genetic Algorithms [44] are presented for the identification of the friction model parameters. Hensen [17] and [51] proposed a frequency domain approach to identify the dynamic friction parameters. Yet, the shape of the frequency response function depends on the type and level of the excitation signal in the presliding regime. Hence, in order to

have a good excitation of the whole presliding regime, the choice of the excitation amplitude is crucial. In this work, time domain identification proposed in [[36, [43, [45, [46]] will be used for dynamic friction parameter estimation.

The presliding regime is specified by small junction deformation where the internal friction state $|z| \ll s(v)$. With this condition, Equation (4.4) reduces to $\dot{z} = \dot{q}$ which after integration leads to $z = q + q_0$ where q_0 is an integration constant related to the displacement for relaxed junctions. Therefore, the rotating arm dynamics within small displacements are described by:

$$u = J\ddot{q} + (\sigma_1 + \sigma_2)\dot{q} + \sigma_0(q + q_0) \quad (4.7)$$

This system is linear when it is written in the deviation variables $\tilde{q} = q + q_0$. Then, the relation between u and z can be written as:

$$u = J\ddot{\tilde{q}} + (\sigma_1 + \sigma_2)\dot{\tilde{q}} + \sigma_0\tilde{q} \quad (4.8)$$

In Laplace domain:

$$\frac{z(s)}{u(s)} = \frac{1}{Js^2 + (\sigma_1 + \sigma_2)s + \sigma_0} \quad (4.9)$$

where s represents the Laplace variable. This form is a second order LTI (Linear Time Invariant) system about the equilibrium point for small displacements. Therefore, it can be rewritten as the following second order system [46]:

$$\frac{z(s)}{u(s)} = \frac{K}{s^2 + 2\zeta\omega_n s + \omega_n^2} \quad (4.10)$$

Comparing Equations 4.9 and 4.10, one can write σ_0 and σ_1 as:

$$\sigma_0 = \omega_n^2 J \quad (4.11)$$

$$\sigma_1 = 2\zeta\omega_n J - \sigma_2 = 2\zeta J \sqrt{\frac{\sigma_0}{J}} - \sigma_2 \quad (4.12)$$

where ζ is damping ratio and ω_n the system natural frequency in the presliding regime.

Assuming the presliding behavior of the system as a mass-spring like behavior, the initial slope of the friction-position curve indicates the stiffness of the bristles. Hence, an approximated estimation of σ_0 can be obtained by measuring applied torque and micro

presliding displacement. Hereto, a small magnitude, slowly varying torque input u is applied to the system in the open loop. Assuming that the excitation torque remains smaller than the breakaway torque level, the system exhibits presliding micro-displacements. In this case, it can be assumed that $\ddot{q} = 0$, $\dot{q} = 0$ and \dot{z} is constant. Then, from Equation (4.3) and (4.8), the following equation may be obtained:

$$\Delta u = \sigma_0 \Delta(q + q_0) = \sigma_0 \Delta \tilde{q} = \sigma_0 \Delta z \quad (4.13)$$

The breakaway experiments can be used in order to estimate bristle stiffness σ_0 . In the breakaway experiment, a slowly increasing ramp torque input is applied to the system and the system response is measured, (Figure 4.13a and Figure 4.13b). The break-way torque (T_s) is defined as the maximum friction torque at onset of sliding and it can be estimated by applying a very slow ramp input to the system which is initially at rest in an open loop [41]. Yet, the starting point of motion is not well defined because the motion is already observed before sliding begins, (Figure 4.13c). Hence, when the velocity of the system reaches a defined value, i.e., when a considerable motion is observed, it may be assumed that the transition from presliding to sliding occurs and the torque input given to the system may be considered as a breakaway torque value.

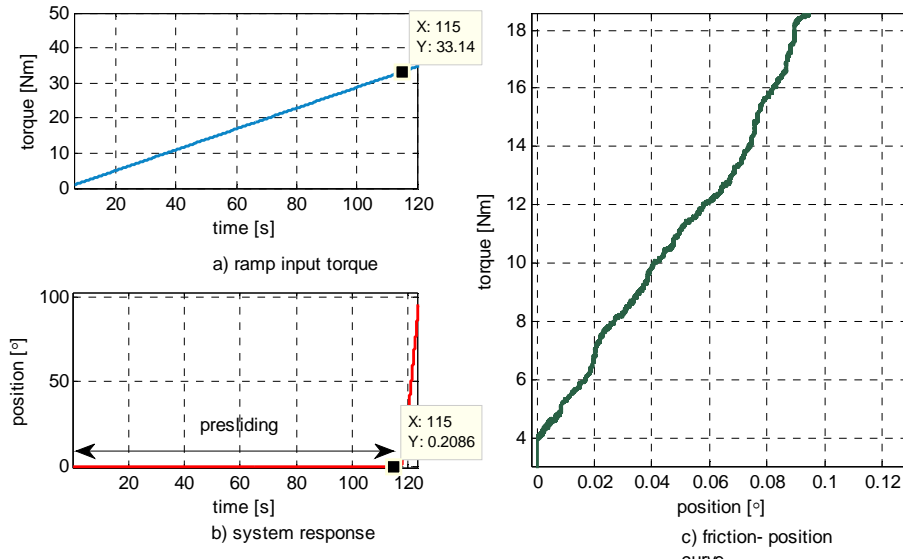


Figure 4.13 Estimation of bristle damping constant in presliding regime

As stated previously, in presliding region, a small displacements between the contacting surfaces of the system take place before stiction is overcome, i.e. before the friction torque reaches its maximum value (breakaway torque), indicating that a nonzero input torque applied to the system results in a nonzero displacement of the system (Figure 4.13).

The estimated bristle stiffness value is obtained by measuring the initial slope of friction-position curve before the system passes through the sliding regime. After identifying the bristle stiffness σ_0 , the bristle damping σ_1 can be estimated by using Equation 4.14. Here, the system inertia J is identified as 35 kgm^2 and viscous friction coefficient σ_2 is identified in the constant velocity experiments in the previous section. Hence, the system damping ratio is the only remaining parameter to be determined to identify the bristle damping σ_1 . Here, σ_1 is determined such that the system has damping ratio between 0.8 and 1 [45].

The estimated dynamic friction parameters are given for various positions of the system in Table 4.5. As in case of the static parameter identification, different results are obtained at various position of the system. These parameters are to be used for initial estimation but some tuning may require during practical applications.

Table 4.5 Estimated dynamic friction parameters

\neq meas.	σ_0 (Nm/rad)	σ_1 (Nm.s/rad)
1	14251	1125
2	15784	1185
3	14865	1149
4	15697	1181
5	15672	1180
6	14301	1127
7	14885	1150
8	16254	1202
9	16334	1205
10	14798	1147
mean	15284	1165

4.4 Identified Friction Model

The static and LuGre friction model with identified parameters versus velocity is represented in Figure 4.14. In order to observe the behavior of the friction compensation models near zero velocities, a sine shape velocity signal is given to the friction models. The behavior of the curve may vary according to the shape, the frequency and the amplitude of the given input signal.

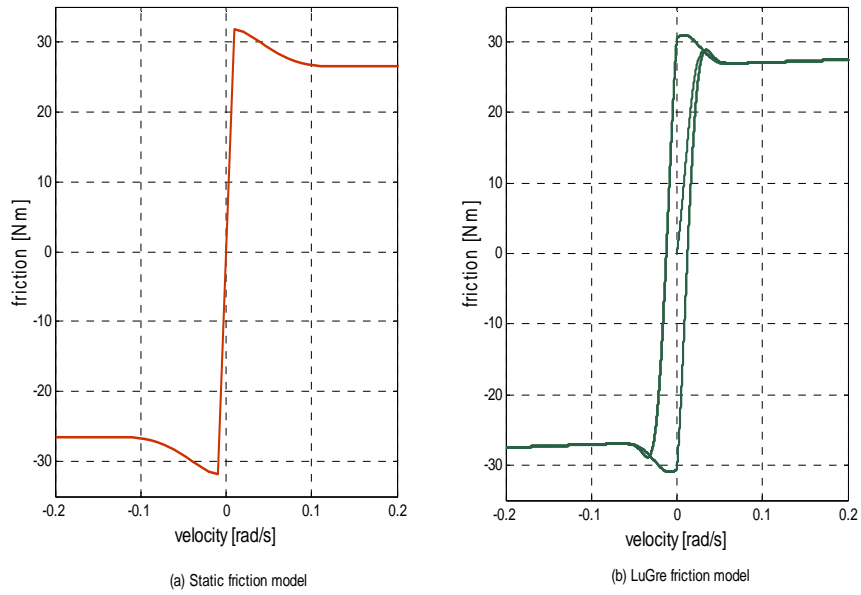


Figure 4.14 Identified friction model curves

MATLAB Simulink block diagram representation of the LuGre model is given in Appendix.

CHAPTER 5

FRICITION COMPENSATION

As represented in Chapter 3, many research works and large number of publication related to the friction compensation task were proposed in literature [6, [22, [3]. The main aim of these studies was to minimize frictional effects so that discontinuous motions due to friction can be eliminated. The success of the compensation methods depends mainly on the quality of the friction model used and the convenience of the analysis technique employed.

Friction compensation techniques in literature can be categorized as model-based and model-free compensation methods. This Chapter focuses on the application of two friction compensation techniques: a friction model based compensation and a disturbance observer which does not depend on a structured non-linear friction model. The stabilization performance is determined and compared for disturbance observer, the general static and LuGre friction model by conducting the simulations and practical experiments.

5.1 Gyro Stabilized Motion Platform

The test set-up used for the experimental validations is shown in Figure 4.1. This platform refers to the system designed such that its line of fire (LOF) or the aimpoint remains stationary with respect to the reference frame when the base is rotated by utilizing a gyro feedback device. Several sources of torque disturbances such as friction unbalance and coupling can produce excessive motion or oscillations in the components being stabilized. Also, during the stabilization, the control of the stabilized platform may require to respond to command inputs as well. The gyro rate is utilized as the feedback signal in closed loop of the system to counteract the destabilizing disturbance torques and to control the system so that it can respond to a given command inputs.

However, in real applications, the platform is mounted on a land or a naval vehicle. Figure 5.1 gives idea as an example in which the platform is aimed to stabilize across the random movements of the sea.

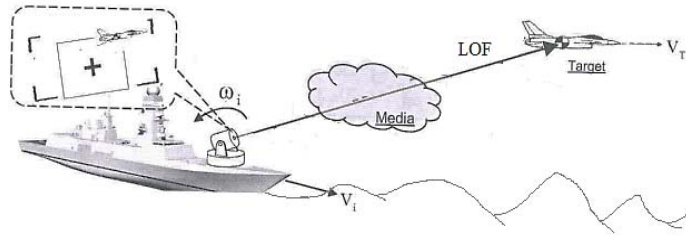


Figure 5.1 A typical gyro stabilized motion platform application

In this study, in order to simulate a vehicle subjected disturbances which may be subject to during its voyage or a ship which is subjected to the random sea waves, a mechanism which has six degrees of freedom named as Stewart platform is used, (Figure 5.2). This platform is capable of moving in three linear directions and three angular directions singly or in any combination of those. It has six legs with six servo motors, resulting to respond to the command inputs in controllable manner. Also, it has two bases: one is fixed to the ground and the other is movable one, on which the stabilized object is mounted. The legs between the fixed and movable base has controllable means for extending its length.

The Stewart platform is arranged in accordance with a pre-determined program involving linear and angular movements or a combination of both so that the various signals can be given to the platform in accordance with the required inputs to control the moveable base in the desired directions. Besides the common signals like sine and step, it is possible to apply real data inputs obtained from a practical application of a vehicle or a ship to the Stewart platform. So, it is possible to apply real destabilizing disturbances to the tested system by using the Stewart platform.



Figure 5.2 The Gyro stabilized platform mounted on a Stewart platform (Photo Courtesy of ASELSAN Inc.)

5.2 Model-based Friction Compensation

The friction can severely limit the performance of an electromechanical servo or tracking systems in terms of tracking errors and the stick-slip motions. Particularly, stick-slip is an undesirable behavior because it causes an oscillatory and persistent motion, in which the contacting bodies stick and slip with respect to each other.

The stabilization performance of the test set-up can be highly degraded due to the stick-slip behavior of the friction because during tracking a movable or stationary target, the system may be subjected to the low frequency motions and some velocity reversals, meaning that the system spends most of its time in stick-slip condition. Being a dynamic friction model, the LuGre captures most frictional effects including friction induced stick-slip behaviors. In order to suppress such oscillatory motion and increase the stabilization performance, the LuGre friction model given in Equation 4.2 with identified parameters listed in Table 4.4 and Table 4.5 is applied to the system control algorithm.

The general scheme of model-based friction compensation in the system control structure is shown in Figure 5.3. The test platform consists of two orthogonal stabilized axes which are azimuth and elevation. The control scheme of each individual axis consists of the same velocity (primary loop) and current (secondary loop) feedback controllers resulting in a nested loop configuration. While the gyro velocity feedback is used for the stabilization loops, the resolver and encoder which are relative-motion transducer are used for other servo control purposes. The resolver is coupled with the shaft of the servo motor (the input side) and measures the motion of the motor relative to the hull, whereas the encoder is mounted on the turret (on the load side) and measures the motion of the load relative to the hull.

The stabilization loop consists of a PI velocity controller, a PI current controller, a current sensor, motor impedance, rate gyro and stabilized object (the plant). Input to the friction model is the relative velocity between the system and the base. The base motion is simulated by the Stewart platform. The motion of the servo motor relative to the base (moveable base of the Stewart platform) is measured by a resolver. In order to compensate the friction of the servo motor and gearbox, the resolver feedback signal is utilized. Similarly, the motion of the load (the turret) relative to the base is measured by an encoder. In order to compensate the friction at the load side, measurement signal of the encoder is used. According to relative movements of the interacting surfaces of the gimbal and the base, the estimated friction torque of the load side T'_{f1} and motor side T'_{f2} are generated to compensate real friction torque of the load side T_{f1} and the motor side T_{f2} as shown on the block diagram in Figure 5.3. Note that the kinematic inputs from the base affects the system as the physical or real friction as shown on the block diagram given in Figure 5.3.

Table 5.1 Definitions of the parameters and the symbols used in block diagram shown in Figure 5.3

Parameter	Symbol
Rate command	ω_i
Base (hull) motion	ω_b
Current command	I_i
PI velocity controller	G_{cv}
PI current controller	G_{cc}
Motor armature inductance	L
Motor armature resistance	R
Motor torque constant	K_t
Motor back EMF constant	K_e
Voltage across motor winding	V_m
Back EMF voltage	V_b
Effective load inertia	J
Gear ratio	N

5.2.1 Simulation Results

The friction compensation performance is validated numerically in MATLAB/Simulink environment by using the block diagram of the stabilization loop shown in Figure 5.4. The simulink block diagram of the system stabilization loop with addition of the model-based friction model used in the simulation analysis is given in Appendix A. Performance of the static and the LuGre friction models are calculated numerically by giving a sinusoidal acceleration command to the Steward Platform with frequency of 0.24 Hz and amplitude of 18 deg/s² or 0.3142 rad/s² as a kinematic disturbance. The amplitude and frequency of the disturbance are chosen according to the real disturbance data taken from a ship in which the test set-up is mounted. With a sine shaped disturbance, it is possible to observe high number of velocity reversals and slow movements where the stick-slip behavior due to friction is most evident. The stabilization loop is commanded with 0 rad/s velocity input, which also means that it is pointing out a stationary target and tries to keep its position relative to the target unchanged despite the kinematic disturbances coming from the base.

In Figure 5.4, the relative velocity between the gimbal and the base (the hull) is given. The stick-slip behavior of the gimbal shown in Figure 5.4 is given for without friction compensation, with using the static and the LuGre friction model cases. A considerable amount of stick is observed in uncompensated case as depicted in zoomed plots at the right

in Figure 5.4. The LuGre friction model almost completely compensates stick-slip behavior due to the fact that LuGre friction model is also used to simulate the real friction.

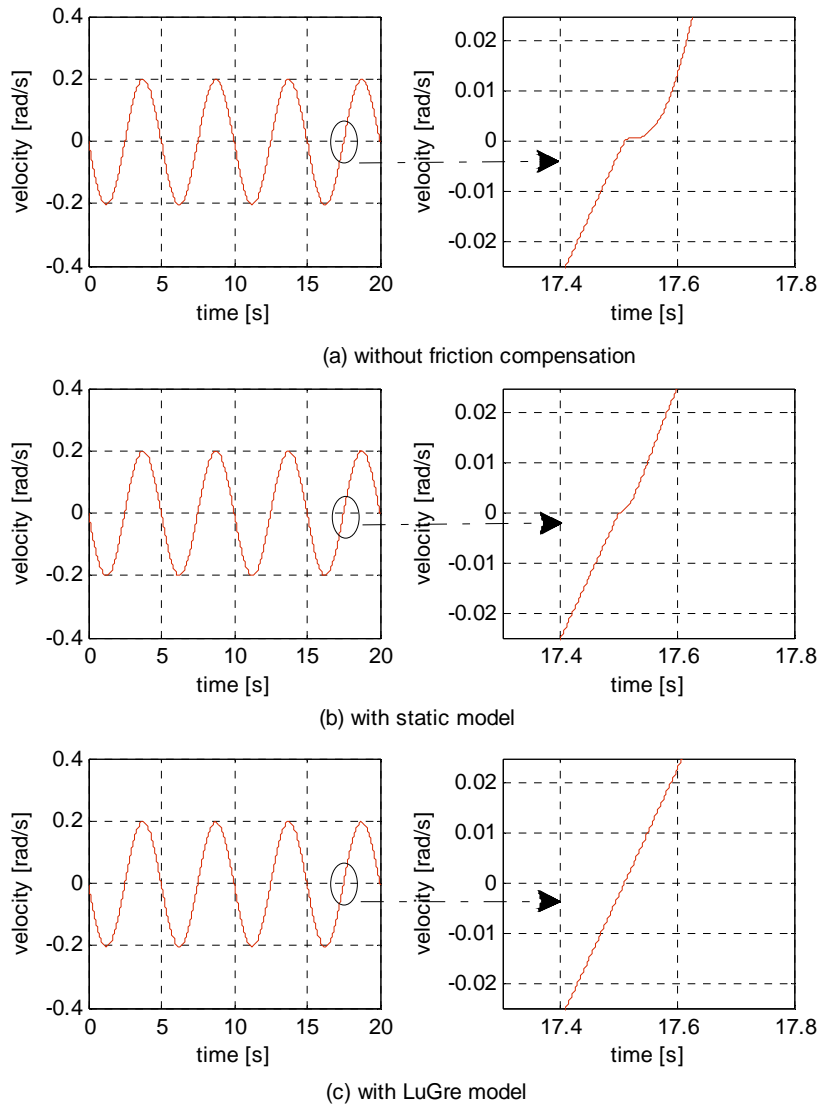


Figure 5.4 The velocity of the system relative to hull for application compensation methods

Table 5.2 summarizes the simulation results for the effectiveness of three friction compensation methods. The position error or fluctuations from the aimpoint is named as the stabilization error. The stabilization performance criterion is given as the standard deviation

of the stabilization error from its mean value. One can see that the stabilization error is reduced from 0.4844 mrad (without any friction compensation) to 0.0004 mrad (friction compensation by LuGre).

Table 5.2 Simulation analysis of stabilization performance for different compensation techniques

Friction Compensation Method	Stabilization Error (mrad, 1σ)
Without friction compensation	0.4844
With static model compensation	0.0660
With LuGre model compensation	0.0004

5.2.2 Experimental Studies

In this section, results of experiments of adding the static and the LuGre friction models are presented. The effect of adding friction compensation technique on the servo characteristics of the system is observed. Then, the stabilization performance is measured, robustness of compensation techniques and sensitivity analysis of model parameters are given in details.

5.2.2.1 Servo Characteristics of the System with Friction Model

A detailed analytical analysis of the LuGre friction model is given in [27]. If the friction is underestimated, it dissipates energy or if the friction is overestimated it induces an unstable behavior [36]. The detailed analysis of the model is not given here. Instead, in order to show how the stability and closed loop response of the system are affected by adding a friction compensation model to the system control algorithm; a frequency response analysis is conducted experimentally.

The friction compensation model makes use of the system's relative velocity with respect to the hull as input and then produces a feedforward signal to compensate the actual frictional torques. In order to see the effect of the LuGre friction model on the system's servo characteristics, the LuGre friction model is added to the system's control algorithm as shown in Figure 5.3. With this control algorithm, the open and closed loop frequency responses of the system are measured. During these tests, an input current signal is applied to the servo motor and the velocity response of the system is produced. The measured current input given to the motor is multiplied by motor torque constant and gear ratio to determine the torque applied to the system.

Frequency sweep tests are performed to obtain frequency response of the system by varying the excitation frequency from 0.5 to 100 Hz with increments of 0.5 Hz and lasting to cover 16 cycles at each frequency. According to the input-output relationship obtained, the

frequency response of the system is generated by using FFT (Fast Fourier Transform) technique. For these tests, it is ensured that the amplitude of input torque signal given to the system is larger than the breakaway torque level to release the system from stick its condition.

The closed loop frequency response of the system is determined according to the conducted tests with and without using the friction compensation model as shown in Figure 5.5. The system closed loop bandwidth frequency without adding the friction compensation model is 7.4 Hz and with friction model is 7.5 Hz by considering -3dB gain drop.

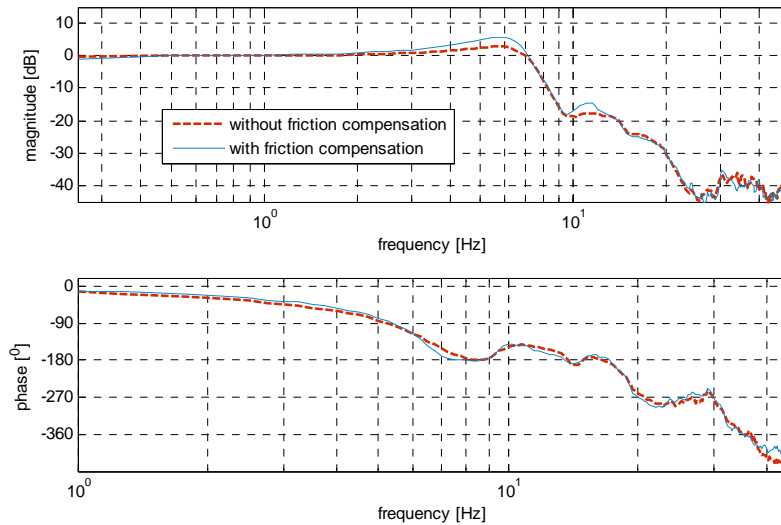


Figure 5.5 Experimental closed loop frequency response of system with and without friction compensation

Also, the open loop frequency response of the system is obtained and represented in Figure 5.6. The gain and phase margins with and without applying friction compensation model are given in Table 5.3. It is calculated that the gain and the phase margin with adding friction compensation changes from 30.5 dB and 70° to 29.6 dB and 71°, respectively. The system stability is still preserved by friction compensation compared to the original system control algorithm without any friction compensation model. Therefore, the friction model has little effect on the closed and open loop frequency responses and so on the stability and servo characteristics of the system.

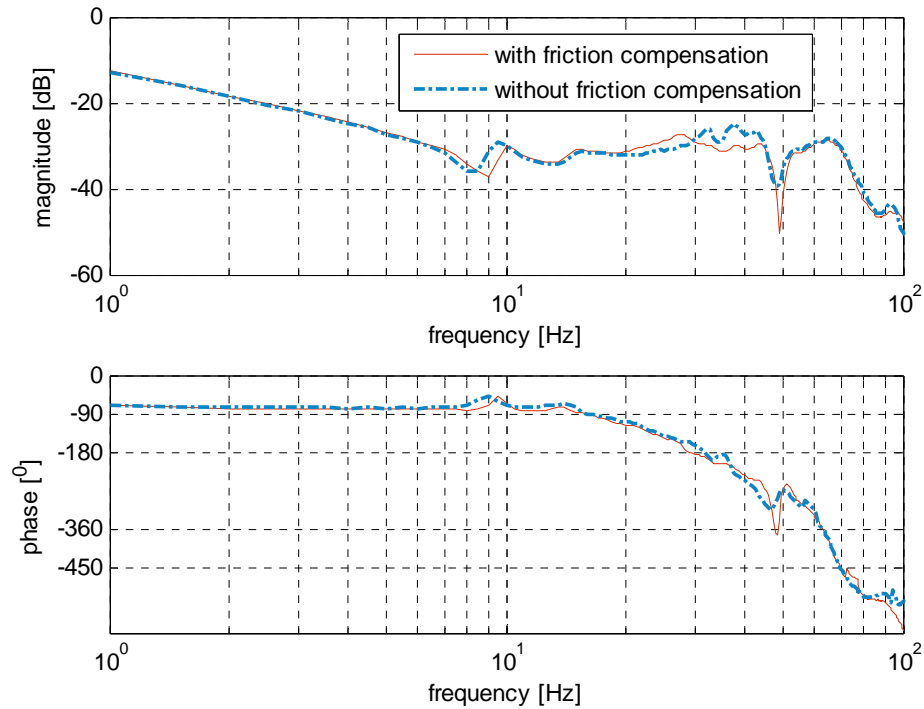


Figure 5.6 Experimental open loop frequency response of system with and without friction compensation

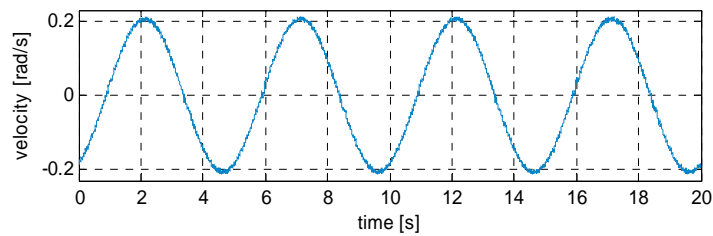
Table 5.3 System servo characteristics with and without friction model

Value	without friction compensation	With friction compensation
Bandwidth [Hz]	7.4	7.5
Gain margin [dB]	30.5	29.6
Phase margin [°]	70	71

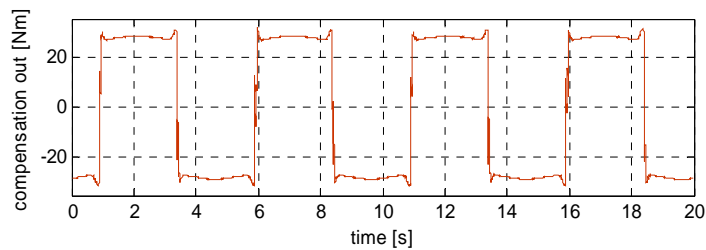
5.2.2.2 The Stabilization Performance with Friction Compensation

In order to validate the effectiveness of the model-based compensation techniques for the stabilization purposes, a sinusoidal acceleration disturbance with a frequency of 0.24 Hz and amplitude of 18 deg/s^2 or 0.3142 rad/s^2 is given to the Stewart platform represented in Figure 5.2. The frequency and amplitude of this disturbance is chosen according to real disturbance data measured on a ship subjected to certain sea movements. Besides that, with a sinus shaped disturbance, it is possible to observe high number of velocity reversal and slow movements where the friction induced stick-slip is most evident.

In these experiments, the LuGre friction model and static friction model are included to the system control algorithm and their friction compensation capabilities are evaluated and compared without any friction compensation and within each other. While being stabilized, the turret is to be pointed to a stationary target point so the rate command input or reference velocity to the system is zero. It is desired to keep the position of the turret relative to the ground unchanged no matter what disturbances come externally. The turret changes its position relative to the base in order to come across the external disturbances and hence to keep its reference (or inertial) position unchanged. The velocity of the gimbal relative to the base for acceleration disturbance and the torque output of the LuGre compensation model using the relative velocity input are given in Figure 5.7.



(a) The velocity of gimbal relative to the base



(b) The torque output of LuGre

Figure 5.7 The Gimbal velocity relative to the base and corresponding compensation output

It is observed that the gimbal is in stick at velocity reversals, resulting in a stabilization error. Therefore, the performance of the friction model is mostly determined by how to eliminate or decrease these stick-slip motions. In Figure 5.8, the stick behavior of the gimbal is indicated for three cases: uncompensated, using static and LuGre friction compensation methods. It can be seen that a significant reduction of time in the stick region observed in case of using the LuGre friction model compared without using any compensation technique.

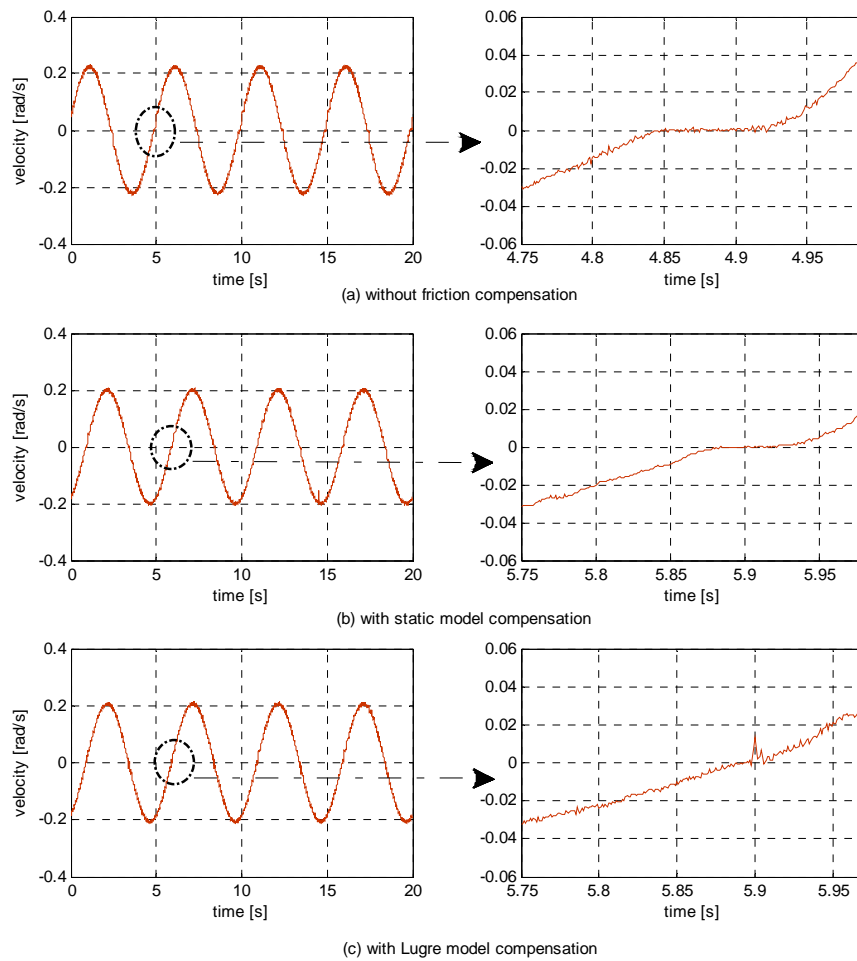


Figure 5.8 The system velocity relative to hull for application of different friction compensation methods

Figure 5.9, the stabilization error for no compensation, using the static and the LuGre model friction compensation cases are given. It is observed that the position error is mostly affected at velocity reversal since at this condition the stick occurs and as the system stays in the stick, the error increases since the LOF of the system deviates from the aimpoint or target. Since the stick case is mostly eliminated by using the LuGre compensation technique, the stabilization error is decreased significantly. (The amplitude of the error is indicated by circle in Figure 5.9).

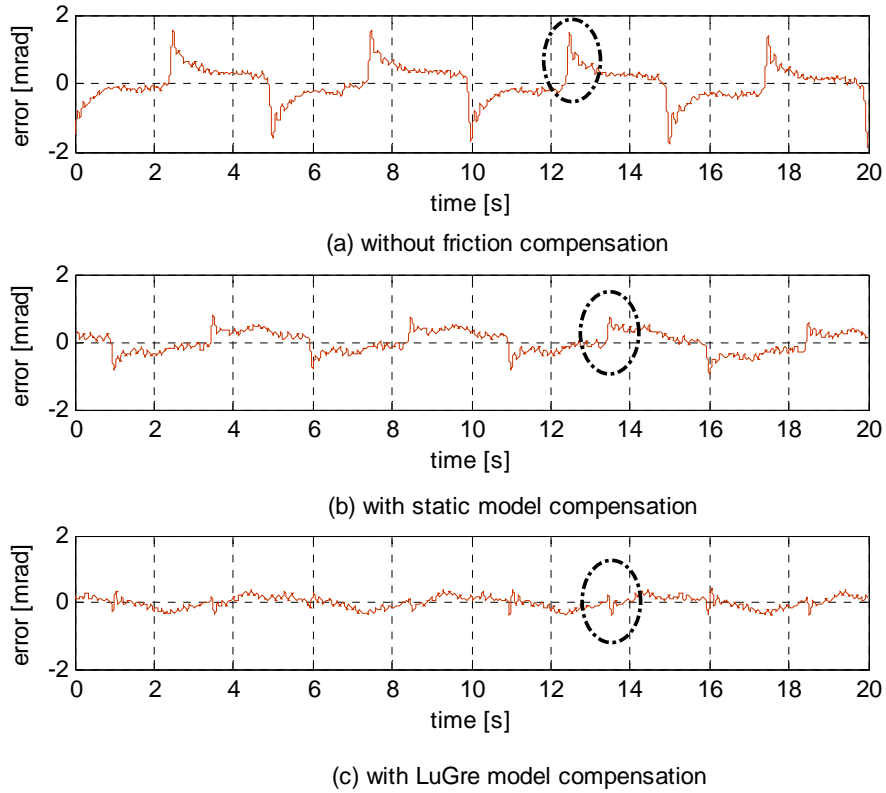


Figure 5.9 Position error for application of different friction compensation methods

Table 5.4 summarizes the tests results for the performance of different friction compensation methods. The gyro signal is integrated to obtain the position error of the turret or the deviation from the aimpoint. The standard deviation of position error is given as the stabilization performance criterion. In Table 5.4, the stabilization error is given as the standard deviation from its mean value. One can see that the stabilization error is reduced from 0.59 mrad (no friction compensation case) to 0.17 mrad (LuGre friction compensation case). The stabilization error is reduced with more than 3 times by adding LuGre model friction compensation model.

Table 5.4 Stabilization performance of friction compensation methods

Friction Compensation Method	Stabilization Error (mrad, 1σ)
Without compensation	0.59
With static model compensation	0.33
With LuGre model	0.17

5.2.2.3 Robustness of Friction Compensation Techniques

The experimental studies show that the LuGre model estimates real friction behavior quite well and significant improvement in stabilization performance is obtained by using the LuGre model over using static friction model and no compensation cases. In order to observe the stabilization performance of the system with variations in disturbances, some additional tests are conducted on the same test set-up.

In order to apply various disturbances to the system, the disturbance frequency is changed from 0.1 Hz to 2 Hz and the stabilization error is determined. The amplitude of the disturbance is 36 deg/s^2 (0.6234 rad/s^2), which is kept unchanged as the frequency of the disturbance changes. The disturbances coming from the sea waves are in low frequencies while the disturbances coming from the land vehicles are in high frequencies that is why the disturbance frequencies are varied from low to high values.

To give an example, Figure 5.10 shows the stabilization error for the disturbance input with 2 Hz frequency for without any friction compensation, with the static friction compensation and with the LuGre friction compensation. Again, a significant reduction in stabilization error is observed in case of using the LuGre friction model compared the static friction model compensation and without any compensation cases.

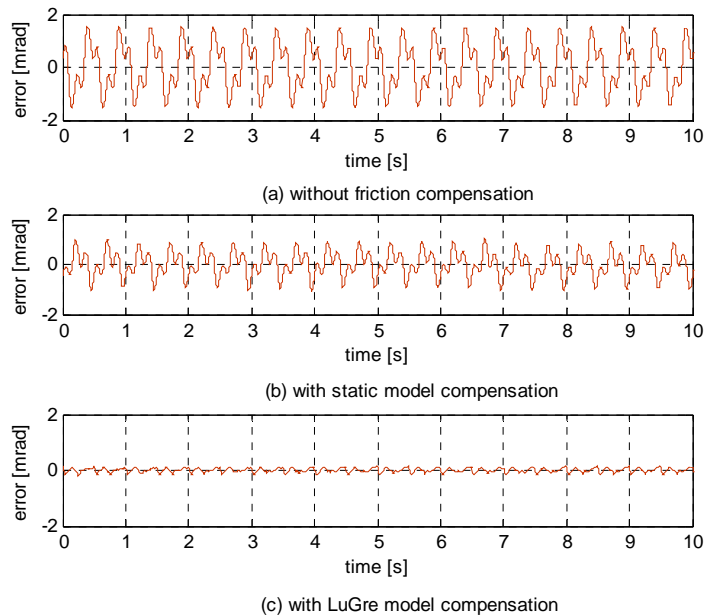


Figure 5.10 Position error for 2 Hz disturbance frequency

Table 5.5 lists the standard deviation of stabilization error for the disturbance input with various frequencies. As the frequency of the disturbance input increases, the stabilization error increases so the stabilization performance decreases without friction compensation and static friction compensation. However, the small deviations in the stabilization error are determined in case of using the LuGre friction model as the frequency of the disturbance is increased.

Table 5.5 Stabilization performance of friction compensation methods for different disturbance frequencies

Stabilization Error [mrad, 1σ]				
Frequency (Hz)	without friction	With LuGre model		
	compensation	With static model		
0.1	0.31	0.19	0.11	
0.2	0.50	0.27	0.13	
0.4	0.67	0.34	0.15	
0.8	0.70	0.43	0.15	
1.0	0.77	0.47	0.17	
1.5	0.89	0.49	0.18	
2.0	0.91	0.59	0.19	

The parameter uncertainties are indispensable for model-based friction compensation techniques due to the presence of varying and uncontrollable factors such as slow or sudden changes in normal force variation, wear, humidity and temperature. In order to observe ability of the LuGre friction model to resist change without adapting its initial stable configuration in case of friction torque variation, the average friction torque of the system is increased from 33 Nm to 50 Nm. In normal case, the anti-backlash mechanism is preloaded such that the backlash pinion-ring gear is minimized, see Figure 5.11. For this test, the anti-backlash gear mechanism is preloaded more than from its normal operation condition so that the preload for initial tension of the spring in the mechanism and so the average friction torque increases. With that condition, the sinusoidal acceleration disturbance input with a frequency of 0.24 Hz and amplitude of 18 deg/s^2 or 0.3142 rad/s^2 is applied to the system by Stewart platform.

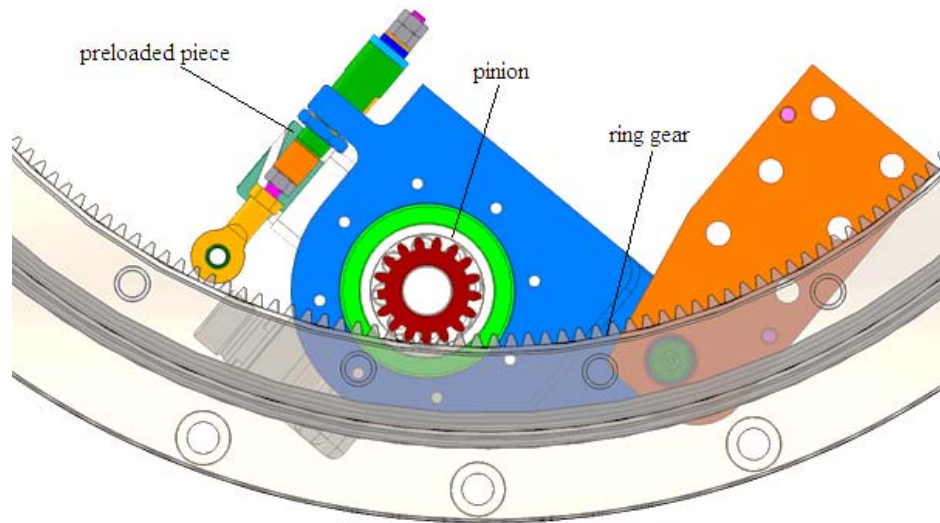


Figure 5.11 Spring preloaded anti-backlash mechanism 3D wireframe

With increasing the friction torque and without changing the identified friction model parameters, the stabilization performance is measured. Table 5.6 shows the standard deviations of stabilization error for three different compensation techniques. It is investigated that the stabilization error is increased with increasing average friction value but the change in error between two conditions is small in case of using LuGre friction model compared with other cases.

Table 5.6 Stabilization performance of friction compensation methods in case of increasing the average friction torque

Average friction (Nm)	Stabilization Error [mrad, 1σ]		
	without compensation	With Static model	With LuGre model
33	0.59	0.33	0.17
50	0.68	0.45	0.22

With increasing average friction torque value condition, the experiments are conducted for different disturbance frequencies. Table 5.7 lists the standard deviation of stabilization error for different frequencies of the disturbance input. Again, the stabilization error increases with increasing frequencies for no compensation and static friction compensation method. Yet, there is no considerable change in the stabilization error in case of using LuGre friction model as the frequency of the disturbance is increased. The success of the LuGre compensation technique is due to the fact that it is a dynamic model and so it can capture the most frictional effects and handle different frequency disturbances at different conditions.

Table 5.7 Stabilization performance of friction compensation methods with increased normal force and different disturbance frequencies

Stabilization Error (mrad, 1σ)			
Frequency (Hz)	without compensation model	With static model	With LuGre model
0.1	0.42	0.26	0.13
0.2	0.55	0.47	0.17
0.4	0.67	0.60	0.23
0.8	0.75	0.63	0.24
1.0	0.80	0.67	0.27
1.5	0.83	0.70	0.28
2.0	0.95	0.77	0.30

5.2.2.4 Sensitivity Analysis of LuGre Friction Model for Stabilization Performance

The success of the model-based friction compensations methods depends mostly on the accuracy of their parameters. But, the identified parameters on the real system are always uncertain to some extent due to changes in operating conditions, errors in measurements devices, and identifications techniques. Hence, this fact attracts one to investigate the degree to which a change in input parameter affects the friction compensation model output and the performance of the technique. For this purpose, some analyses in terms sensitivity of the model parameters are carried out on the experimental test setup.

There exist several local and global sensitivity analysis techniques in literature [5]. The local analysis examines the change in output values based on the changes in one input factor while the global analysis observes the change in output values when all the parameters values change. Since the friction model is nonlinear and complex, a local sensitivity analysis is preferred in this study. This technique is also called one-way or parameters varying method in which the influence of the variation in the input parameters is observed on the output of the model [5].

The LuGre friction model has six parameters, two of which are dynamic and remaining are static parameters. Each parameter is increased and decreased to some value from its mean and its impact on the output of the model is examined while keeping all other parameters fixed. During the experiments, the changes in parameters value are carefully changed so that the tested system remains stable. In Figure 5.12 and Figure 5.13, all parameters are varied to observe their influence on the overall friction model output. It can be seen that the parameters σ_0 , and σ_1 affect the dynamic behavior of the friction. Also, this investigation (Figure 5.13) indicates that the parameters F_C and F_S can potentially play a more significant role in affecting the output of the friction model, i.e. the model output is more sensitive to these parameters when compared to other model parameters.

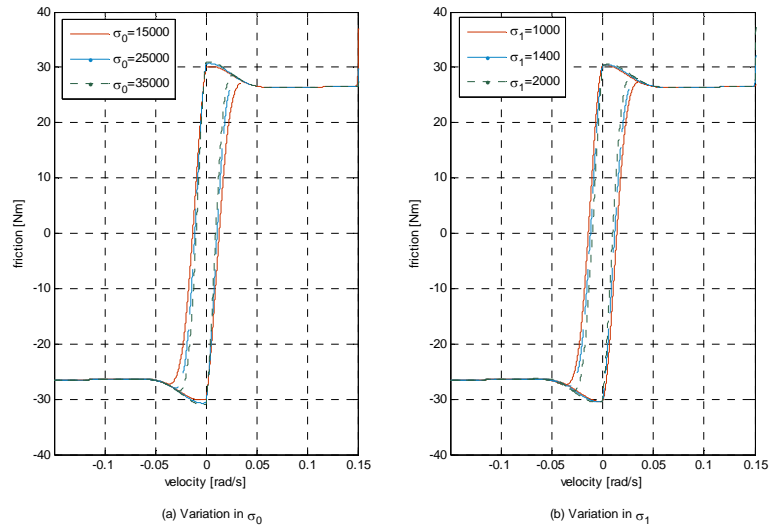


Figure 5.12 LuGre friction model output for variations in its dynamic parameters

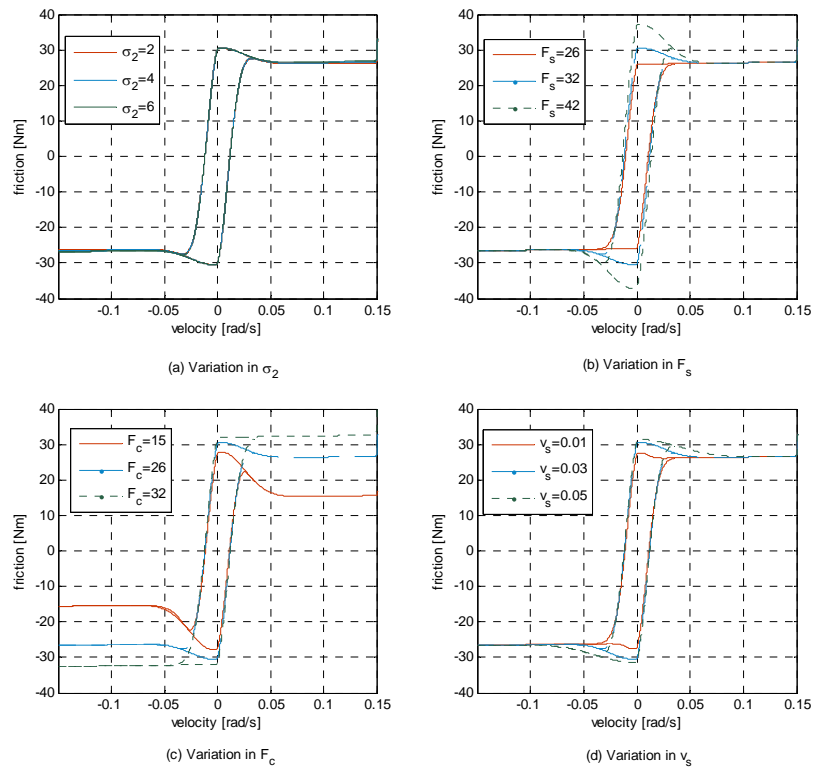


Figure 5.13 LuGre friction model output for variations in its static parameters

The experimental tests are conducted to see the effect of the model parameters variation on the stabilization performance of the system. In order to obtain one point of the stabilization error versus the parameters value map, for each parameter value, the tests are repeated three times and then the mean value of the stabilization error versus the parameter value is obtained. The performance index is taken as the change in stabilization error when the error exceeds the value of 0.2 mrad. The stabilization error versus all parameters variations are plotted in Figure 5.14.

In Figure 5.14(a), the change in stabilization error by changing bristle stiffness coefficient σ_0 is represented. It can be seen that the variation in σ_0 value is significant if its value is changed more than 40%, deviating the stabilization error from 0.17 to over 0.2 mrad.

Figure 5.14(b) indicates the effect of variation in bristle damping coefficient σ_1 . It is observed that the variation up to 50% has little importance on stabilization error, meaning σ_1 is less sensitive when it is compared to σ_0 .

Figure 5.14(c) shows variation in viscous constant σ_2 . It is seen that the influence of this parameters is negligible on the stabilization error by varying its value up to 65%.

Figure 5.14(d) indicates the effect of variation in static friction value F_s . It is observed that the variation up to 25% deviate the stabilization error from 0.2 mrad value.

Figure 5.14(e) shows variation in Coulomb friction value F_c . It is seen that % 20 variations in this parameters affects the stabilization error, meaning that is most important parameter with static friction in terms of stabilization error.

Lastly, in Figure 5.14(f), the variation in Stribeck velocity v_s is represented. The change in this parameter value up to 30% starts to influence the stabilization error.

In summary, assessing the sensitivity of the friction model to parameter changes the following list is valid in increasing order: σ_2 , σ_1 , σ_0 , v_s , F_s , F_c . From the test results, it is obvious that the parameters F_c and F_s have a greater potential for the introduction of the stabilization error due to inaccuracies in the estimation of model parameters. Hence, this fact is to be taken into account during identification procedures.

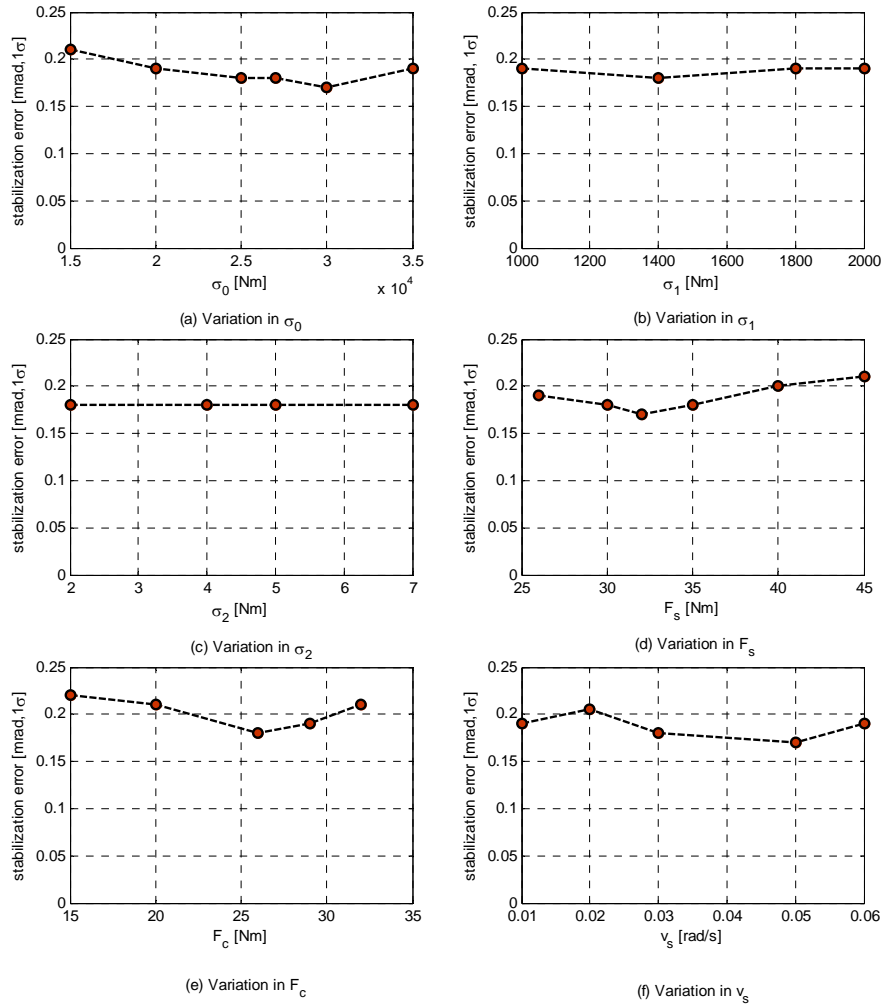


Figure 5.14 Stabilization accuracy for LuGre model parameters variations

5.3 Model-Free Friction Compensation

In the previous section, the experimental results confirm that the LuGre friction compensation model is the best in eliminating the effects of friction and is effective to improve the stabilization accuracy. Furthermore, the ability of the LuGre friction model is justified experimentally across the change of disturbances. This is due to the fact that the LuGre is a continuous dynamic model and hence it captures most dynamic nonlinear frictional effects such as Stribeck, stick-slip and pre-sliding behavior. The challenge in using the LuGre friction model is in estimating its parameters that enter the model nonlinearly, as

well as in estimating all six parameters of the friction model simultaneously. Also, the parameter uncertainty is another drawback of using model-based friction.

In Chapter 3, it is shown that in addition to model-based friction estimation, there are non-model-based compensation methods to estimate nonlinear friction. In those methods, the plant modeling may be necessary although a well-structured friction model is not required. Non-model-based friction compensation methods address friction characterization in the presence of variable and uncontrollable factors such as wear, temperature, humidity, lubricant condition, and sudden or slow normal force variation. Besides that, in addition to friction compensation, model-free methods are emphasized to accommodate multiple sources of nonlinearities or other disturbances such as unbalance, coupling, wind and cable forces/torques etc.

Several model-free compensation methods were proposed as covered in Chapter 3. This study discusses a state estimator, configured as a reduced-order disturbance observer, which was previously shown to be an effective in friction compensation and improve disturbance rejection performance [47]. A general structure of a disturbance observer is shown in Figure 5.15. The basic idea behind the disturbance observer is to sum all the internal and external disturbances acting on the system as a single disturbance term, estimate it and produce a feedforward signal to eliminate its effect. By using the system response and applied load to the system and knowing the system dynamic model, it estimates the friction and all other disturbances acting on the system.

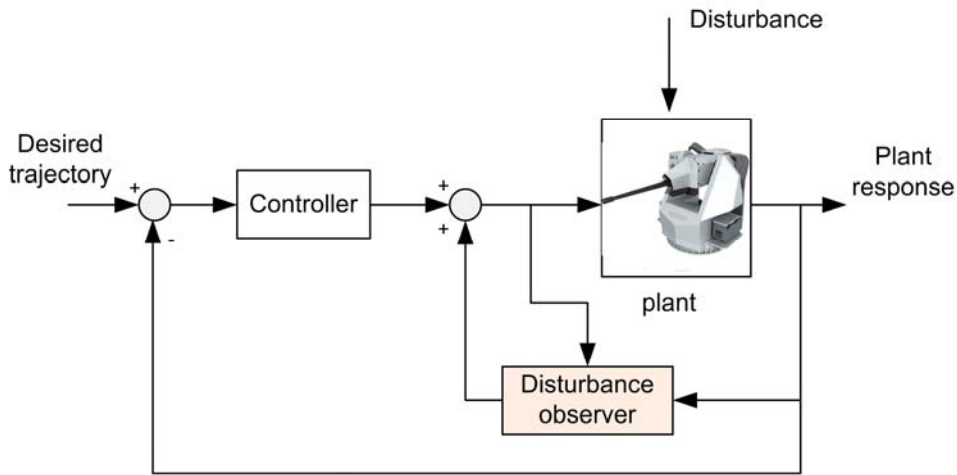


Figure 5.15 Disturbance observer architecture

The disturbance observer was shown to be generally effective and robust in many applications if they are properly designed. Various kind of linear and nonlinear configurations have been proposed in literature, [24], [25], [47], [48], [49], and [50]. Although many of these methods have been confirmed to be effective, a primary barrier to

their acceptance is that they consist of a detailed multi-state model and require determination of several gain terms [25]. For example, theoretical treatments are based on that a complete system plant model is available but this is not practical when detailed structural response of a system is taken into account, which require unlimited number of states and gains. Furthermore, finding a suitable set of gains is somewhat complicated and hence it requires extensive experience and experimental intuition. Also, considerable manipulations are required in determining tradeoffs in order to obtain practical and effective design.

In this work, instead of trying to obtain an accurate multi-state model of the plant, a minimum single-state model is identified and used in the observer, a general structure of which is introduced by Luenberger [47] and further refined in [48]. By using this approach, the whole algorithm is quite simple to be implemented and there is just one gain that can be easily adjusted. In the following paragraphs, the single-state disturbance observer is introduced and its characteristics which are given in detail in [48] are represented. In order to assess how the single-state disturbance observer performs in an actual case, its effectiveness and characteristics is examined on the test set-up by practical application.

5.3.1 Single-State Disturbance Observer

The structure of a single-state disturbance observer can be constructed as in Figure 5.16. The definition of symbols and parameters are given in Table 5.1. The observer takes motor torque T_m and the gyro rate ω as the input signals. The motor torque is determined from $T_m = K_t i_m$ where the K_t is the motor torque constant and i_m the current applied to the motor. K_0 is the gain of the observer.

The observer is configured as closed loop and it attempts to drive the error between the measured gyro rate and estimated rate ω' to zero. The error is applied to the output of controller through the gain K_0 , which is equal to estimated disturbance torque T_f' . This estimated torque is used to counteract the actual disturbance $T_f = T_{f1} + T_{f2}$ by summing the estimated disturbance with the torque signals acting on the system. Practically, it is obtained by giving the estimated current input to the motor. Here, K_0 is only one adjustable parameter related to the observer.

Also, using Newton's second law for the effective inertia J with applied motor torque T_m and disturbance torque T_f , the following equations can be derived.

$$T_f = NT_{f1} + T_{f2} \quad (5.2)$$

$$T_m + T_f = J\dot{\omega} \rightarrow T_m + T_f = J\omega s \rightarrow T_f = J\omega s - T_m \quad (5.3)$$

Comparing Equation 5.1 with Equation 5.3, one can observe that the first term of Equation [5.1] is a first order low pass filter and second term is the disturbance measurement. Hence, it is clear that the disturbance observer produces a filtered measurement of the disturbance as pointed out in [48]. The observer takes differentiation of the output of the gyro hence the performance of the disturbance is affected by the noise at the output of the gyro signal. In other words, a design tradeoff between the bandwidth of the observer and any noise at output of the gyro may be required.

5.3.2 Single-State Disturbance Observer Characteristics

In order to obtain the more fundamental characteristics of the single-state disturbance observer, gyro and motor dynamics are ignored. Detailed derivations are given in [47] and [48]. The effects of the observer on the closed loop system characteristics are verified experimentally by frequency response tests later.

In order to see the disturbance rejection characteristics with single-state disturbance observer, the transfer function between disturbance torque T_f and rate output ω can be derived as follow:

$$\frac{\omega}{T_f} = \left(\frac{\frac{1}{J}}{s + \frac{G_{CV}}{J}} \right) \left(\frac{s}{s + \frac{K_0}{J}} \right) \quad (5.4)$$

The first factor in Equation 5.4 is the disturbance rejection transfer function without observer while the second factor represents the effect of disturbance observer. One can see that the disturbance observer improves the disturbance characteristics up to corner frequency K_0/j without changing the stability or servo loop characteristics of the system [48].

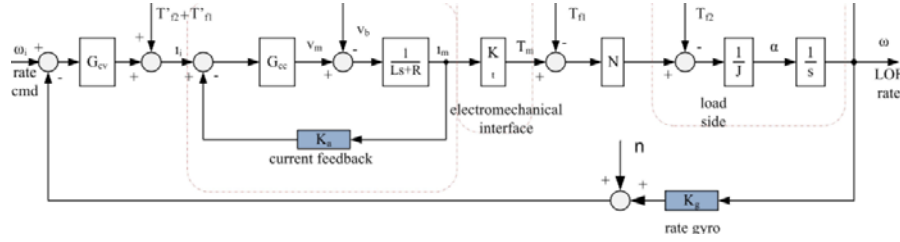


Figure 5.17 Block diagram view of adding some noise n on the gyro output

In order to rebuild an estimate of the disturbance torques, the observer differentiates the gyro signal hence it is required to investigate how noise in the gyro signal influence inertial velocity ω . In doing so, the transfers function between the noise function n describing the gyro noise and inertial velocity ω (Figure 5.17) can be constructed as follows.

$$\frac{\omega}{n} = - \left(\frac{\frac{G_{cv}}{J}}{s + \frac{G_{cv}}{J}} \right) - \left(\frac{\frac{K_0}{J}}{s + \frac{K_0}{J}} \right) \left(\frac{s}{s + \frac{G_{cv}}{J}} \right) \quad (5.5)$$

Equation 5.5 is recognized as the noise coupling transfer function. The first factor represents the condition when no observer present and the second factor indicates the noise coupling at LOF due to the observer. Therefore, it may be concluded that the observer may increase the gyro noise coupling at the LOF rate. Hence, a tradeoff between the disturbance rejection performance and noise coupling is to be taken into account during implementation whereas the combination of them gives an optimum case.

5.3.3 Simulation Results

The friction compensation performance of the single-state disturbance observer is validated numerically with MATLAB/Simulink by using the simulation model shown in Figure 5.16. MATLAB Simulink block diagram of the single state disturbance observer structure for the stabilization loop for the simulation is given in Appendix A. The disturbance rejection performance of the single-state observer is measured and compared numerically by given a sinusoidal acceleration input with frequency 0.24 Hz and 18 deg/s² or 0.3142 rad/s² as a kinematic disturbance.

In Figure 5.18, the stick behavior of the gimbal is given for no friction compensation, using disturbance observer, static and LuGre friction model. It can be seen that a considerable stick-slip case is observed without any compensation case. The disturbance observer almost completely compensates stick-slip behavior of the friction.

Table 5.8 summarizes the simulation results for the performance of different friction compensation methods. The position error or stabilization error (fluctuations from stationary

point) is given as stabilization performance criteria. The disturbance observer mostly eliminates the frictional effects and reduces the stabilization error to around zero value.

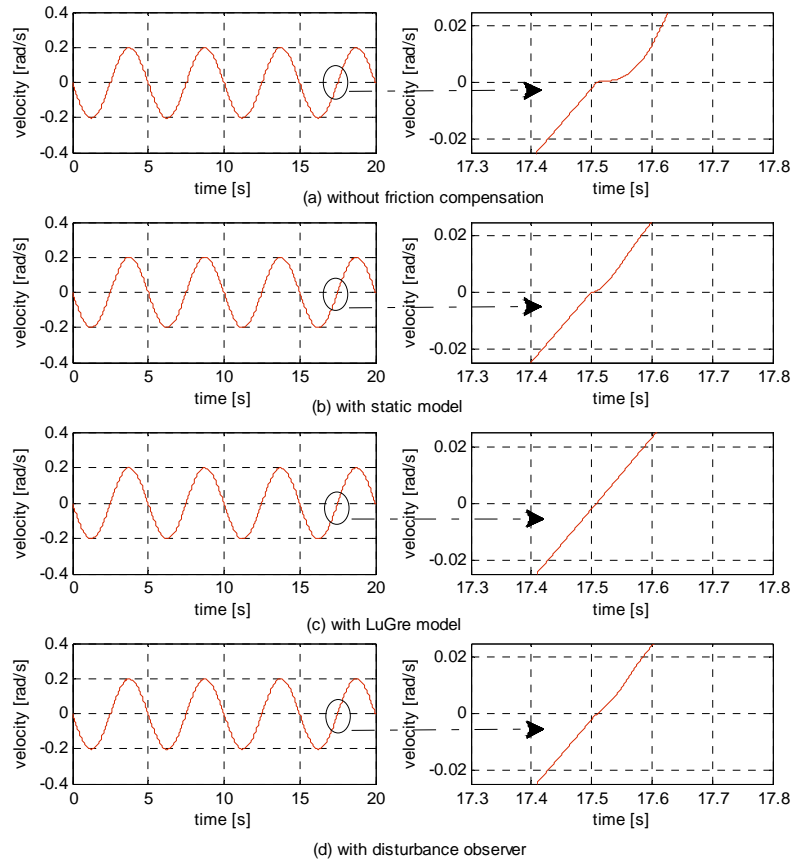


Figure 5.18 The system's velocity relative to hull for application compensation techniques.

Table 5.8 Simulation analysis of stabilization performance for compensation techniques

Friction Compensation Method	Stabilization Error (mrad, 1σ)
Without friction compensation	0.4844
With static model compensation	0.0660
With LuGre model compensation	0.0004
With disturbance observer	0.0008

It is measured that as the gain of the observer K_0 is increased, the friction effect is decreased and so the stabilization performance is improved. The observer gain K_0 serves as a correction signal to converge the error between the estimated rate and the measured gyro rate to zero. For multi-state models, the desired value of the observer gains may be obtained using different method by converting the system equations into state-space form [12]. In [48], the observer gain K_0 is varied such that the observer bandwidth is about twice the bandwidth of the original system, beyond which it is stated that the observer interacts with the control system. Therefore, by using Equation 5.4, the value of gain observer K_0 might be determined. Moreover, for the single-state observer, there is only one gain and it can be easily adjusted via simulation [48]. In order to attenuate the unknowns involved in the system, the gain of observer should be taken relatively large but if the measured state is contaminated by some noises and disturbances then the observer gain should be chosen relatively small [12]. In Equation 5.5, it was shown that the observer causes to increase the gyro noise coupling at the LOF. Furthermore, due to the structure of Luenberger observers, they are so susceptible to sensor noise that the primary upper limits of observer gains is sensor noise not stability concerns [13]. Hence, as stated before, some tradeoff between the disturbance rejection performance and noise coupling is to be taken into account during implementation of the observer.

5.3.4 Experimental Studies

In this section, the disturbance observer is added to the real system control algorithm and its performance is validated by practical tests. The effect of adding compensation technique on the system servo characteristics is observed, the improvement in stabilization performance is obtained, and robustness of the observer is analyzed.

5.3.4.1 System Characteristics with Disturbance Observer

It was shown in [48] that the observer does not have any impact on the stability nor servo loop characteristics of the system theoretically. However, the system has some un-modeled dynamics such as the structural response, servo motor and gyro dynamics, feedback devices, and noise coupling effects. Hence, it is expected that the observer will change the system stability and other characteristics to certain extent.

In order to see the effect of the disturbance observer on system characteristics, it is implemented in the control algorithm of the tested system as shown in Figure 5.16. With this control algorithm, the frequency response of the system is obtained by exciting the system with a sinusoidal signal torque input by varying frequency from 0.5 to 100 Hz with an increment of 0.5 Hz. The closed loop frequency response of the system is measured with and without adding the observer as shown in Figure 5.19. The system bandwidth in case of no observer present is 7.5 Hz and with observer it is 7.3 Hz. Also, the open loop frequency

response is shown in Figure 5.20. The gain and phase margins with and without applying the disturbance observer is given in

Table 5.9. It is measured that phase and gain margin with adding disturbance observer changes from 30.5 dB and 70° to 29.4 dB and 72° . The system stability is still preserved with implementing the observer compared to the original system without the observer. Hence, it can be concluded that the observer has little effect on the closed and open loop frequency responses and so on the stability and servo characteristics of the system.

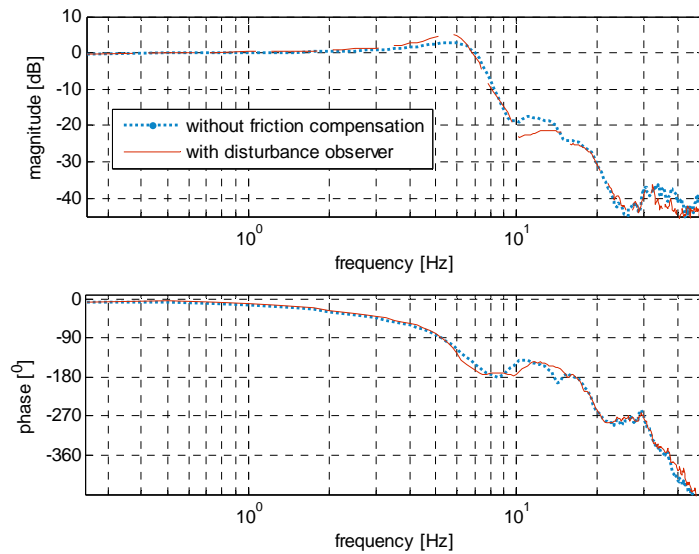


Figure 5.19 Experimental closed loop frequency response with and without DOB

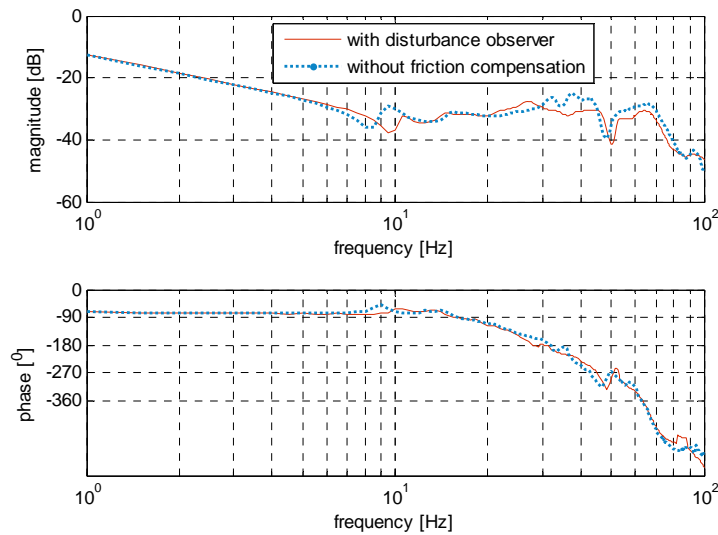


Figure 5.20 Experimental open loop frequency response with and without DOB

Table 5.9 System servo characteristics with and without adding disturbance observer

Value	Without friction compensation	With disturbance observer
Bandwidth [Hz]	7.5	7.3
Gain margin [dB]	30.5	29.4
Phase margin [$^{\circ}$]	70	72

5.3.4.2 The Stabilization Performance with Disturbance Observer

In this section, the results of stabilization performance are presented. In these experiments, the turret is pointed to a stationary point so the rate command input or reference velocity to the system is zero and the stabilization performance is measured under sinusoidal disturbances with different frequencies. In order to evaluate the performance of disturbance observer in improvement in stabilization numerically, the standard deviation of angular position (the stabilization error), is calculated. Moreover, LuGre and static model based friction compensation methods are also applied and the results are given for comparison.

The model-based compensation techniques take the relative velocity as input while the input to the disturbance observer is the inertial velocity measured by the rate gyro. Figure 5.21 represents the gyro rate output and the output of the disturbance observer to compensate frictional effects. When compared with Figure 5.7, one can see that the output torque of disturbance observer and LuGre friction model are different. This is due to the fact that the LuGre attempts to compensate only the frictional torques whereas the disturbance observer is designed to eliminate all the disturbances.

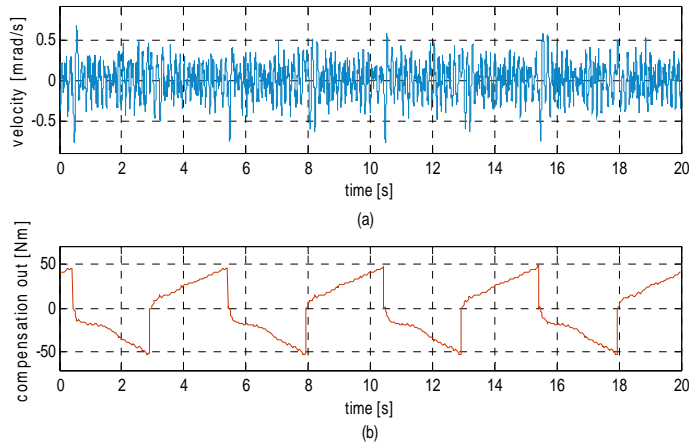


Figure 5.21 (a) the rate output and (b) the output of the disturbance observer

In Figure 5.22, the gimbal velocity relative to the base is illustrated. In this specific experiment, sinusoidal acceleration input with a frequency of 0.24 Hz and amplitude of 18 deg/s^2 is given to Stewart platform to simulate the disturbances. For the same experiment, stabilization errors are also given in Figure 5.23. As it can be clearly observed from these figures, stiction occurs at low velocity regions or velocity reversals due to friction. In order to show the performance of the presented single-state observer, performance of the system with LuGre and static model based friction compensation method are also given. As illustrated in these figures, single-state disturbance observer based compensation approach mostly prevents stiction in velocity reversals. Also, in Figure 5.23, in case of using disturbance observer, the position error is kept around zero whereas in case of using LuGre compensation, a cyclic behavior of the position error is observed around zero. This success of the disturbance observer is due to the fact that it not only compensates the friction but also counteracts other disturbances.

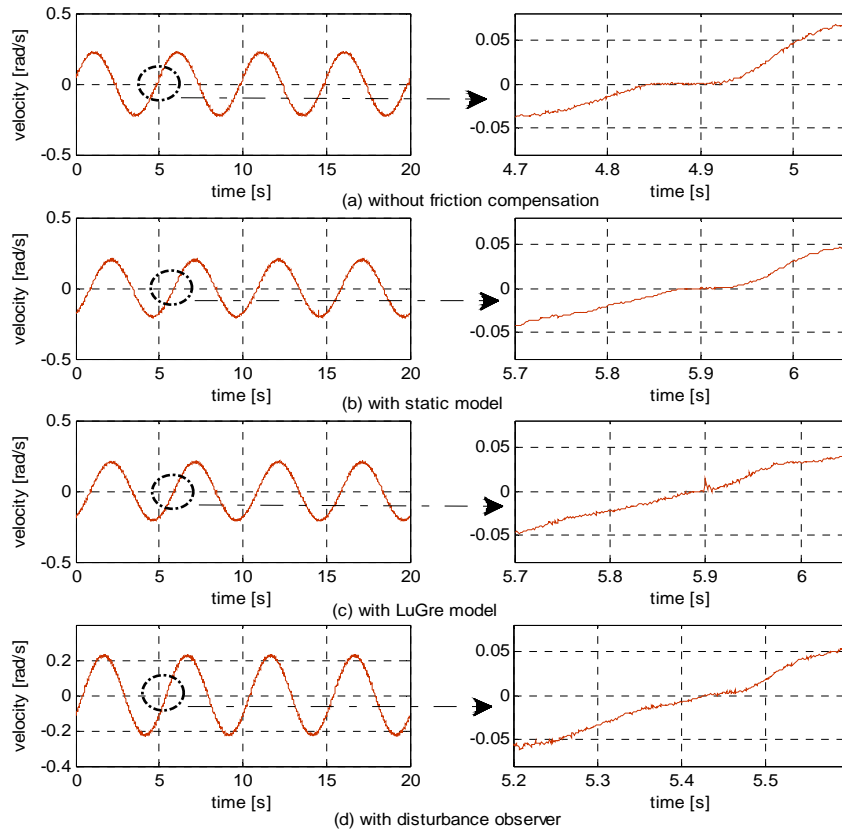


Figure 5.22 The system velocity relative to hull for application of compensation methods

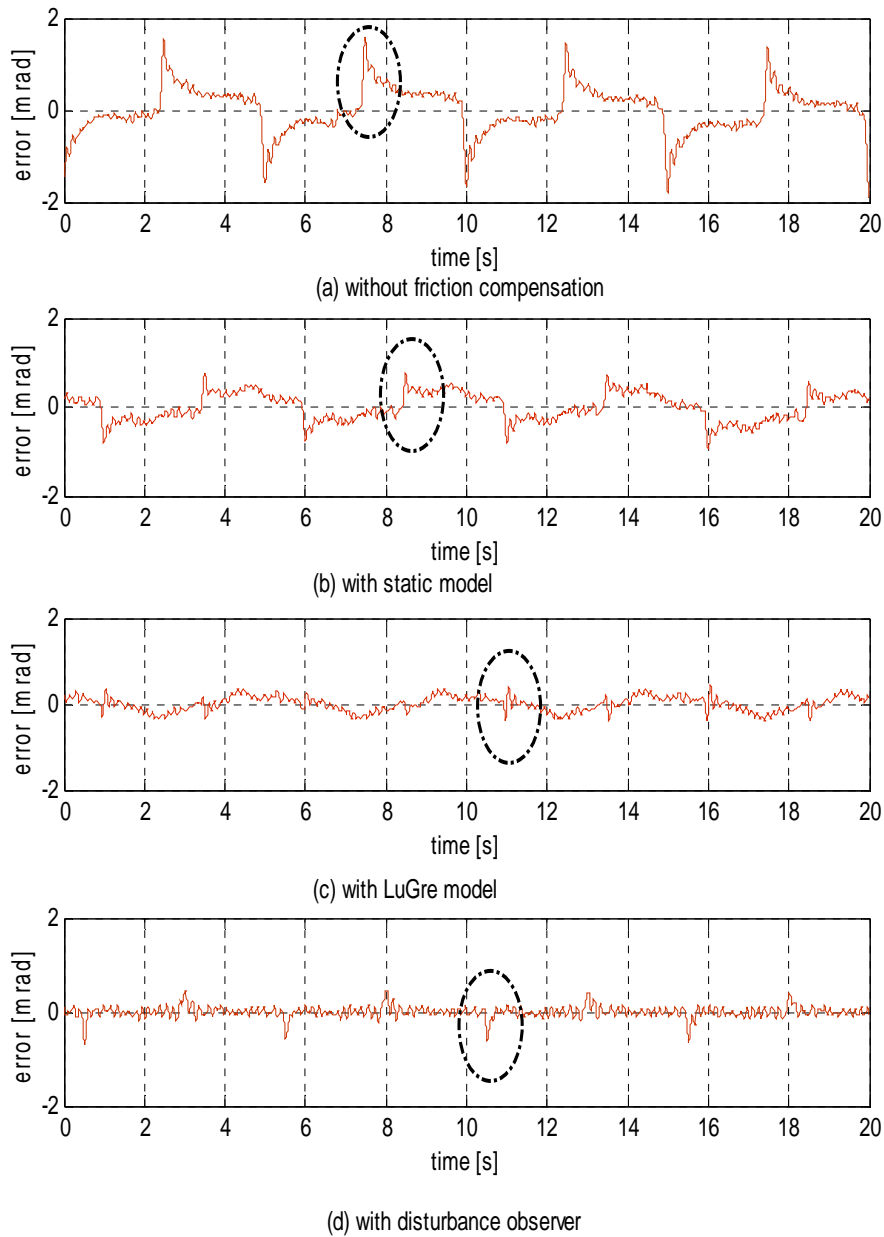


Figure 5.23 Position error for application of compensation methods

In order to evaluate the stabilization performance numerically, the standard deviation of angular position, i.e. integral of angular velocity obtained from gyro rate is calculated. Table

5.10 summarizes the results of stabilization performance for different friction compensation methods. One can see that the stabilization error is reduced from 0.59 mrad (no friction compensation) to 0.15 mrad (using single-state disturbance observer). Again, the stabilization error is reduced with more than 3 times via adding the disturbance observer to the system control algorithm.

Table 5.10 Stabilization performance for different compensation methods

Friction Compensation Method	Stabilization Error (mrad, 1σ)
without compensation	0.59
With static model	0.33
With LuGre model	0.17
With disturbance observer	0.15

5.3.4.3 The Robustness of Disturbance Observer

It is observed that the best stabilization performance is obtained by using the single-state disturbance observer. In this section, in order to examine the ability of the single-state disturbance model to resist change without adapting its initial stable configuration, its effectiveness is experimentally validated by some kind of tests. The same tests are performed for the model-based friction compensation model and their effectiveness are evaluated and compared with each other.

Table 5.11 lists the standard deviation of stabilization error for the disturbance inputs with different frequencies. It is observed that as the frequency of disturbance increases, the stabilization error increases in case of using disturbance observer. Hence, the effectiveness disturbance observer decreases as the frequency of disturbance frequency increases.

To give an example, Figure 5.24 indicates the stabilization error with application of the disturbance observer under the disturbance frequency with 2 Hz. It is observed that the effectiveness of the disturbance observer is mostly degraded at this frequency.

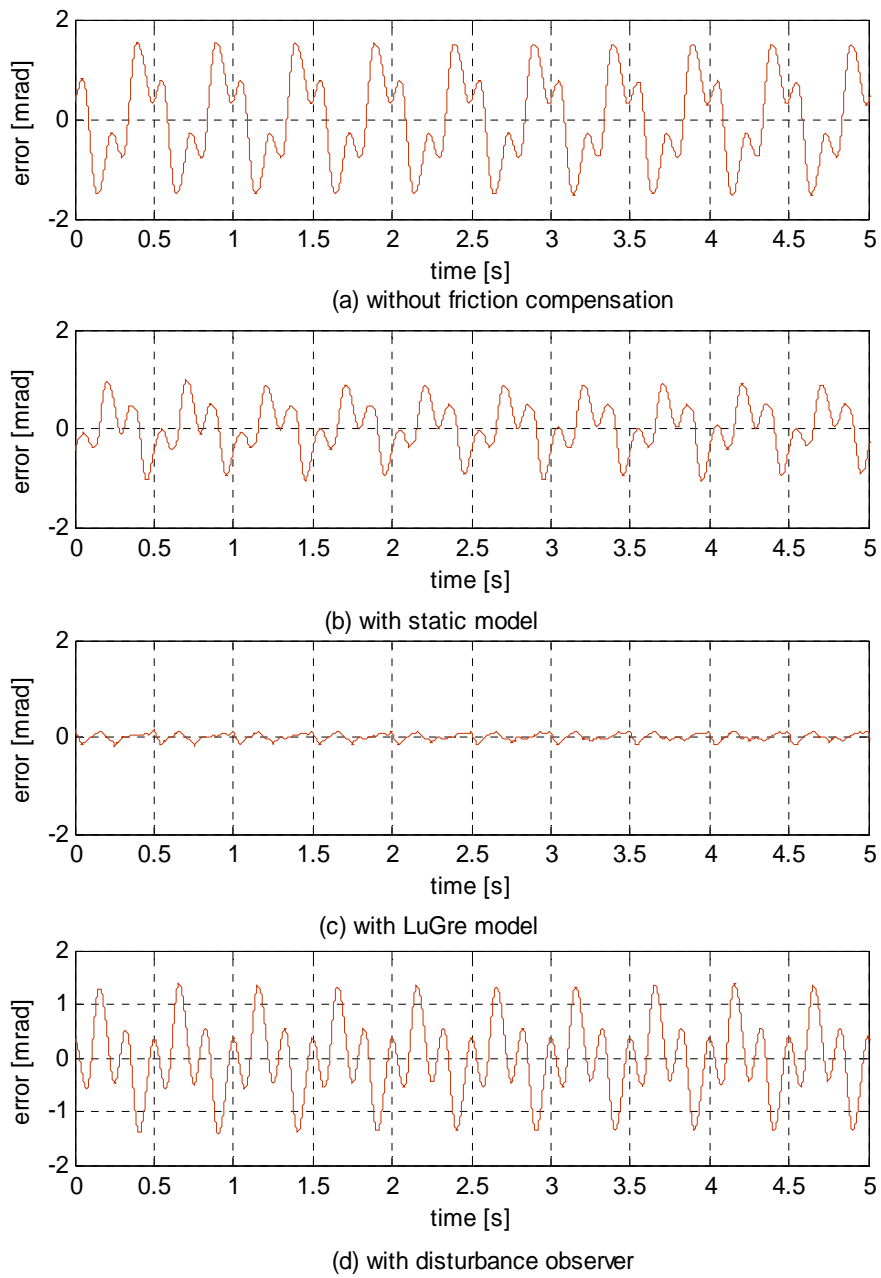


Figure 5.24 Position error for 2 Hz disturbance frequency for compensation techniques

Table 5.11 Stabilization performance for different disturbance frequencies

Frequency (Hz)	Stabilization Error (mrad, 1σ)			
	Without compensation	With static	With LuGre	With DOB
0.1	0.31	0.19	0.11	0.11
0.2	0.50	0.27	0.13	0.14
0.4	0.67	0.34	0.15	0.24
0.8	0.70	0.43	0.15	0.33
1.0	0.77	0.47	0.17	0.37
1.5	0.89	0.49	0.18	0.59
2.0	0.91	0.59	0.19	0.67

Friction force at the system is increased arbitrarily by squeezing anti-backlash gear mechanism more than its initial preload value. As stated previously, the ant-backlash mechanism is preloaded such that the backlash and the friction forces are optimized. In these tests, in order to observe the robustness of the disturbance observer, the mechanism is preloaded such that the average friction is increased from 33 Nm to 50 Nm. With that condition, the sinusoidal acceleration disturbance input with a frequency of 0.24 Hz and amplitude of 0.3142 rad/s^2 is given to the system by Stewart platform and the stabilization error is measured. Table 5.12 shows the test results. It is measured that the stabilization error is increased more than 2 times, meaning that the performance of the observer is reduced with the same factor.

Table 5.12 Stabilization performance for variations in normal force

Average friction (Nm)	Stabilization Error (mrad, 1σ)			
	Without compensation	With static	With LuGre	With DOB
33	0.49	0.31	0.18	0.15
50	0.63	0.43	0.22	0.31

With increasing average friction value by squeezing anti-backlash mechanism, the experiments are conducted for different disturbance frequencies. Again, the performance of the disturbance rejection is degraded as the disturbance frequency increases as shown in

Table 5.13 Stabilization performance for variations in normal force at different disturbance frequencies

Frequency (Hz)	Stabilization Error [mrad, 1σ]			
	Without compensation	With static	With LuGre	With DOB
0.1	0.42	0.26	0.13	0.21
0.2	0.55	0.47	0.17	0.27
0.4	0.67	0.60	0.23	0.42
0.8	0.75	0.63	0.24	0.52
1.0	0.80	0.67	0.27	0.64

1.5	0.83	0.70	0.28	0.68
2.0	0.95	0.77	0.30	0.72

During tests, it is measured that as the gain of the observer K_0 is increased, the friction effect is decreased and so the stabilization performance is improved. Yet, one is not free to increase the value of gain K_0 since in order to obtain an estimate of the disturbance torques, the observer differentiates the gyro signal (see, Equation 5.1) hence as the frequency increases, the noise coupling with high frequency components affects the performance of the disturbance observer further. Moreover, beyond a certain values of gain K_0 , the system falls in unstable condition. The frequency of the disturbances is up to 2 Hz. Hence, the observer corner frequency is chosen to be 2 Hz. from Equation 5.5, the gain of the disturbance observer was $\frac{K_0}{j} = 2 \cdot 2\pi \frac{\text{rad}}{\text{s}} \rightarrow K_0 = 440$, beyond which no improvement in the stabilization is expected since the rejection ability of the observer is limited up to the its corner frequency [48]. Therefore, the stabilization performance decreases as the frequency of disturbance increases.

5.4 Conclusion

The stabilized system with friction was tackled by both model-based and model-free compensation techniques. The performance of compensation techniques was measured and compared in terms of the stabilization performance and their robustness.

For each test, the same proportional-integral controller is used for all different compensation techniques. The controller parameters are the same for all the experiments in order to compare the different friction compensation methods appropriately.

The best stabilization performance is obtained in case of using the disturbance observer provided that the disturbance is not too brusque. It is observed that the disturbance observer can handle only the disturbances with low frequencies. The effectiveness of the disturbance observer is related with its corner or cut-off frequency. As its corner frequency increases, its disturbance rejection capacity is also increases since the friction torques at velocity reversal have high frequency content. However, the corner frequency of the disturbance observer is restricted by the system dynamics and the noise coupling at LOF rate.

The use of model-based friction compensation improves the stabilization performance quite well. Especially, using dynamic friction model eliminates the stick-slip behaviors and reduces the stabilization error. This this due to the fact that the LuGre models the presliding regimes and has a good transition to the sliding regime. On the other hand, the static friction model cannot capture the presliding behavior and has a discontinuity at velocity reversal hence it is not effective at low movements or at velocity reversal conditions.

CHAPTER 6

CONCLUSION

In this work, in order to get a satisfactory stabilization performance of a gyro-stabilized system under the effect of friction, the modeling, identification, and compensation of friction phenomenon are studied. In this Chapter, the work is summarized, the concluding remarks based on the simulation and the experimental analysis are given, and lastly some suggestions regarding to studies on this work are stated.

6.1 Summary

In order to get an insight in mechanism of the friction and friction characteristics, some basics of tribology and physically-based friction models at microscopic level are presented. Various types of friction characteristics studied by different researchers are described. Notable friction compensation techniques which are suitable for compensating the frictional effects are investigated. Although a wide range of friction compensation techniques were proposed in literature, they can be classified in two groups as model-based and model-free. The compensations methods under these groups are compared in terms of their capability to capture friction behaviors and their simplicity to be applicable. Among these methods, the LuGre as a dynamic friction model and a general Stribeck as a static friction model are chosen to be used in this study. Also, a single-state disturbance observer is used as a model-free friction compensation method.

A detailed procedure to identify friction compensation model parameters is represented. The tests are conducted in presliding and sliding (or gross sliding) regions to estimate dynamic and static friction parameters, respectively. The friction torques of the system components is obtained and friction characteristics of the system are investigated.

A detailed block diagram of stabilization loop with friction compensation method of gyro-stabilized platform is constructed in detail and the effectiveness of the friction compensation techniques are studied numerically in MATLAB Simulink environment.

Friction compensation methods are added to the real system control algorithm and their effectiveness are validated by the tests conducted on a gyro-stabilized system mounted on a six axes Stewart platform. The effects of adding compensation techniques on the system servo characteristics are observed via frequency response tests; the improvement in stabilization performance is measured, and robustness of the compensation methods are examined. Effects of friction model parameters on the overall model are also discussed.

6.2 Conclusions

A simulation analysis is performed on a constructed block diagram of the system stabilization loop with adding frictional disturbances. According to the simulation results the system with dynamic LuGre friction compensation mostly eliminates the intermittent motion due to stick-slip and gives smoother and better results than the general static friction model. Actually, these results are expected because the LuGre model is also used to represents the actual friction in the system model.

The single-state disturbance observer gives similar results as the LuGre model in terms of the reduction in stick-slip motions and improvement in the system stabilization performance. Besides that, the LuGre models friction-induced stick-slip behavior quite well hence it can be used in performing simulation analysis of a control system to represent real friction effects.

Table 6.1 Simulation and experiment results of improvement in stabilization performance for different compensation methods

Compensation method	Stabilization Error (mrad, 1σ)	
	Simulation	Experimental
Without friction compensation	0.4844	0.59
With static model compensation	0.066	0.33
With LuGre model compensation	0.0004	0.17
With disturbance observer	0.0008	0.15

Some experimental studies are conducted on a real gyro-stabilized platform. The performance of the friction compensation methods are measured and compared with each other and with no compensation case in terms of the enhancement in the system stabilization accuracy (Table 6.1). Based on the experimental tests, the following results may be inferred

- During the stabilization, the system is subject to the low movements or velocity reversals. Hence, the system spends most of its time in stick-slip behavior, degrading the stabilization performance. It is observed that the LuGre friction model mostly eliminates discontinuous motion due to stick-slip condition. The stabilization error is reduced with more than 3 times by adding LuGre model friction compensation model compared to no compensation case. This is due to the fact that the LuGre models presliding regime well and has a good transition from presliding to sliding regime.

- The importance of modeling the presliding regime is verified via using a static model. The LuGre model improves the system stabilization performance %50 more than the general static friction model. This is due to the fact that the static model cannot capture the presliding behavior and the discontinuity of the static model at velocity reversal.
- The sensitivity analysis of the LuGre model parameters indicates that the parameters F_C and F_S can potentially play a more significant role in effecting the output of the friction model and for the introduction of the stabilization error due to inaccuracies in the estimation of model parameters.
- It is relatively easy to use the single-state disturbance observer. The whole algorithm added to the controller is highly simple and only one gain needs to be adjusted. Moreover, there are no time consuming identification experiments and the problem of parameter variation due to uncontrollable factors such as wear, humidity, and temperature as in case of model-based friction compensation models. Despite its simplicity, this technique gives more or less the same improvement in the stabilization performance as the LuGre friction model at low frequencies.
- The disturbance rejection performance of the single-state disturbance observer is related to its dynamics and it is effective only at low frequencies. As the cut-off frequency of observer increases, the stabilization performance improves since the friction torque contains high frequency contents at velocity reversal. Yet, the cut-off frequency of the observer is limited since the observer increases the gyro noise coupling and takes differentiation of the gyro output to produce a disturbance rejection signal. Therefore, an inherent trade off exists between the any noise at output of gyro and disturbance observer bandwidth

6.3 Recommendations for Future Works

The main shortcomings of the model-based friction compensation techniques are the identification problem and the low robustness to parameter variations. In this study, offline identification techniques are used. In order to decrease time consuming parameters identification tests and minimize the effect of the parameter variations, online parameter identification method (adaptive control) may be developed. Adaptive control has been applied to the LuGre but only limited parameters are identified online and it is assumed that the friction model is linear [36].

Effective friction compensation requires good velocity measurements. The desired or reference velocity may be used for servo control purposes. However, in case of stabilization, the measured relative velocity is to be used as input to friction model. Measured signals may result in the noise on the measurements, which may prevent to compensate friction precisely even if the friction model is perfect. Also, the use of measured velocity with noise may

degrade the robustness of the model. One can wonder if it is possible to eliminate the influence of the noise coming from the velocity measurement sensor to the friction model without reducing the effectiveness of friction compensation model.

Some improvements in the single-state disturbance observer may be possible such as adding an integral and/or derivative action in addition to the gain of the observer. Also, adding the gyro dynamics to the observer and/or using a system model in more details in the observer instead of using just inertia of the plant may be other enhancements in the single-state disturbance observer. However, such enhancements may cause the complexity and/or some sensitivities of the design, resulting in difficulties in applying to a real system. Hence, one should be aware of these facts when attempting to apply the disturbance observer with adding such enhancements.

REFERENCES

- [1] Bhushan, Bharat. *Modern Tribology Handbook, Two Volume Set*. CRC press, 2010.
- [2] Tabor, David. "Friction: the present state of our understanding." *Journal of lubrication technology*, 103 (1981): 169.
- [3] Baykara, Berkay. "Control of system under the effect of friction." *MS thesis, Middle East Technical University*, 2009.
- [4] Al-Bender, F., and K. De Moerlooze. "Characterization and modeling of friction and wear: an overview." *Sustainable Construction and Design 2.1* (2011): 19.
- [5] Mehmood, Adeel, et al. "Sensitivity analysis of LuGre friction model for pneumatic actuator control." *Vehicle Power and Propulsion Conference (VPPC)*, IEEE, 2010.
- [6] Armstrong-Hélouvry, Pierre Dupont, and Carlos Canudas De Wit. "A survey of models, analysis tools and compensation methods for the control of machines with friction." *Automatica* 30.7 (1994): 1083-1138.
- [7] Suh, Nam P. *Tribophysics*. Englewood Cliffs, NJ: Prentice-Hall, 1986.
- [8] Haessig Jr, David A., and Bernard Friedland. "Modeling and simulation of friction.", *Orlando, FL*. International Society for Optics and Photonics, 1991.
- [9] Al-Bender, Farid, Vincent Lampaert, and Jan Swevers. "A novel generic model at asperity level for dry friction force dynamics." *Tribology Letters* 16.1-2 (2004): 81-93.
- [10] Hilkert, J. M. "Inertially stabilized platform technology concepts and principles." *Control Systems, IEEE* 28.1 (2008): 26-46.
- [11] Parlitz, U., et al. "Identification of pre-sliding friction dynamics." *Chaos: An Interdisciplinary Journal of Nonlinear Science* 14.2 (2004): 420-430.
- [12] Ogata, Katsuhiko. *Modern control engineering*. Fourth Edition, Prentice Hall, 2002.
- [13] Ellis, George. *Observers in control systems: a practical guide*. Access Online via Elsevier, 2002.
- [14] Olsson, Henrik, et al. "Friction models and friction compensation." *European journal of control* 4.3 (1998): 176-195.

- [15] Rabinowicz, E. "The intrinsic variables affecting the stick-slip process." *Proceedings of the Physical Society* 71.4 (1958): 668.
- [16] Johansson, K., and Carlos Canudas-De-Wit. "Revisiting the LuGre friction model." *Control Systems, IEEE* 28.6 (2008): 101-114.
- [17] Hensen, Ronnie Herman Anna. "Controlled mechanical systems with friction." *Phd Thesis, Dortmund University*, (2002).
- [18] Armstrong, Brian, David Neevel, and Todd Kusik. "New results in NPID control: Tracking, integral control, friction compensation and experimental results." *Control Systems Technology, IEEE Transactions on* 9.2 (2001): 399-406.
- [19] Pervozvanski, Anatoli A., and Carlos Canudas-de-Wit. "Asymptotic analysis of the dither effect in systems with friction." *Automatica* 38.1 (2002): 105-113.
- [20] Bonchis, Adrian, et al. "Variable structure methods in hydraulic servo systems control." *Automatica* 37.4 (2001): 589-595.
- [21] Wu, Chi-haur. "Compliance control of a robot manipulator based on joint torque servo." *The International journal of robotics research* 4.3 (1985): 55-71.
- [22] Lampaert, Vincent. "Modelling and control of dry sliding friction in mechanical systems." *Phd Thesis, Katholieke University of Leuven*, (2003).
- [23] Huang, Shih-Jung, Jia-Yush Yen, and Shui-Shong Lu. "Dual mode control of a system with friction." *Control Systems Technology, IEEE Transactions on* 7.3 (1999): 306-314.
- [24] Ray, Laura R., Ashok Ramasubramanian, and Jennifer Townsend. "Adaptive friction compensation using extended Kalman-Bucy filter friction estimation." *Control Engineering Practice* 9.2 (2001): 169-179.
- [25] Lampaert, Vincent, Jan Swevers, and Farid Al-Bender. "Comparison of model and non-model based friction compensation techniques in the neighbourhood of pre-sliding friction." *American Control Conference, IEEE*, 2004.
- [26] Olsson, Henrik. "Control systems with friction." *Department of Automatic Control, Lund Institute of Technology* 1045 (1996).
- [27] Canudas de Wit, Carlos, et al. "A new model for control of systems with friction." *Automatic Control, IEEE Transactions on* 40.3 (1995): 419-425.

- [28] Dahl, P. R. *A solid friction model*. No. TOR-0158 (3107-18)-1. Aerospace Corp El Segundo Ca, 1968.
- [29] Bliman, P. A., and M. Sorine. "A system-theoretic approach of systems with hysteresis. Application to friction modelling and compensation." *Proceedings of the 2nd European control conference*, 1993.
- [30] Armstrong-Helouvry, Brian. *Control of machines with friction*. Vol. 128. Springer, 1991.
- [31] Bliman, P. A., and M. Sorine. "Easy-to-use realistic dry friction models for automatic control." *Proceedings of 3rd European Control Conference, Rome, Italy*. 1995.
- [32] Kamopp, D. "Computer simulation of slip-stick friction in mechanical dynamic systems." *Trans. ASME: J. Dyn. Syst., Measurement, Control*, (1985):100-103.
- [33] Tustin, A. "The effects of backlash and of speed-dependent friction on the stability of closed-cycle control systems." *Electrical Engineers-Part IIA: Automatic Regulators and Servo Mechanisms, Journal of the Institution of* 94.1 (1947): 143-151.
- [34] Bo, Li Chun, and D. Pavelescu. "The friction-speed relation and its influence on the critical velocity of stick-slip motion." *Wear* 82.3 (1982): 277-289.
- [35] Olsson, Henrik, et al. "Friction models and friction compensation." *European journal of control* 4.3 (1998): 176-195.
- [36] De Wit, C. Canudas, and Pablo Lischinsky. "Adaptive friction compensation with partially known dynamic friction model." *International journal of adaptive control and signal processing* 11.1 (1997): 65-80.
- [37] Swevers, Jan, et al. "An integrated friction model structure with improved presliding behavior for accurate friction compensation." *Automatic Control, IEEE Transactions on* 45.4 (2000): 675-686.
- [38] Vincent Lampaert, Jan Swevers, and Farid Al-Bender. "Modification of the Leuven integrated friction model structure." *Automatic Control, IEEE Transactions on* 47.4 (2002): 683-687.
- [39] Al-Bender, Farid, Vincent Lampaert, and Jan Swevers. "A novel generic model at asperity level for dry friction force dynamics." *Tribology Letters* 16.1-2 (2004): 81-93.
- [40] Hayward, Vincent, et al. "Discrete-time elasto-plastic friction estimation." *Control Systems Technology, IEEE Transactions on* 17.3 (2009): 688-696.

- [41] Armstrong, Brian. "Friction: Experimental determination, modeling and compensation." *Robotics and Automation, Proceedings., 1988 IEEE International Conference on*,1988.
- [42] Rivetta, Claudio H., and Sten Hansen. "Friction model of the 2.5-mts SDSS telescope." *Astronomical Telescopes & Instrumentation*. International Society for Optics and Photonics, 1998.
- [43] Wang, Xingjian, and Shaoping Wang. "High performance adaptive control of mechanical servo system with LuGre friction model: identification and compensation." *Journal of dynamic systems, measurement, and control* 134.1 (2012).
- [44] HAN, Jia-peng, and Yan-yang WANG. "Research on the Parameter Identification of LuGre Tire Model Based on Genetic Algorithms." *Mathematics in Practice and Theory* 18 (2007): 011.
- [45] Kumar, T. S., and R. N. Banavar. "Identification of friction in the 50/80 cm ARIES schmidt telescope using the LuGre model." *Proc. of The 18th IFAC World Congress*. Vol. 18. 2011.
- [46] Lischinsky, P., C. Canudas-de-Wit, and G. Morel. "Friction compensation for an industrial hydraulic robot." *Control Systems, IEEE* 19.1 (1999): 25-32.
- [47] Luenberger, D. A. V. I. D. "An introduction to observers." *Automatic Control, IEEE Transactions on* 16.6 (1971): 596-602.
- [48] Hilkert, J. M., and Brian Pautler. "A reduced-order disturbance observer applied to inertially stabilized line-of-sight control." *SPIE Defense, Security, and Sensing*. International Society for Optics and Photonics, 2011.
- [49] Zhang, Qing, Zhenfan Tan, and Ying Liang. "Gyro Stabilized System Based on Auto-Disturbance Rejection Controller." *Computing, Communication, Control, and Management, ISECS International Colloquium on*. Vol. 2. IEEE, 2008.
- [50] Jamaludin, Zamberi, Hendrik Van Brussel, and Jan Swevers. "Quadrant glitch compensation using friction model-based feedforward and an inverse-model-based disturbance observer." *Advanced Motion Control, AMC'08. 10th IEEE International Workshop on*. IEEE, 2008.
- [51] Altpeter, Friedhelm. *Friction modeling, identification and compensation*. Diss. École Polytechnique Fédérale De Lausanne, 1999.

APPENDIX

BLOCK DIAGRAMS OF MATLAB SIMULINK MODEL FOR SIMULATION

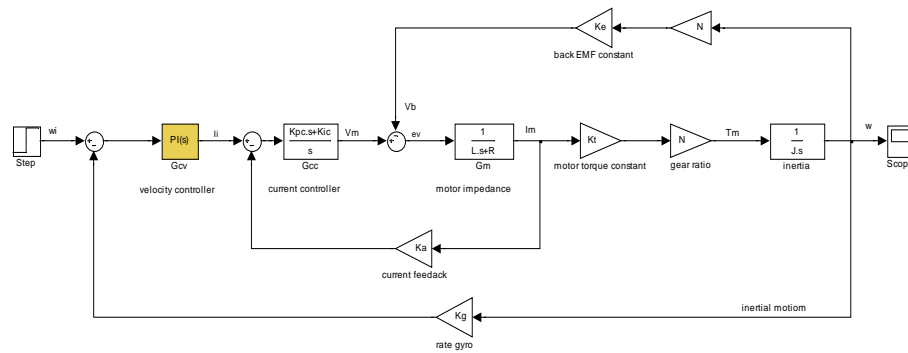


Figure A Simulink block diagram of the system control loop and its linear model

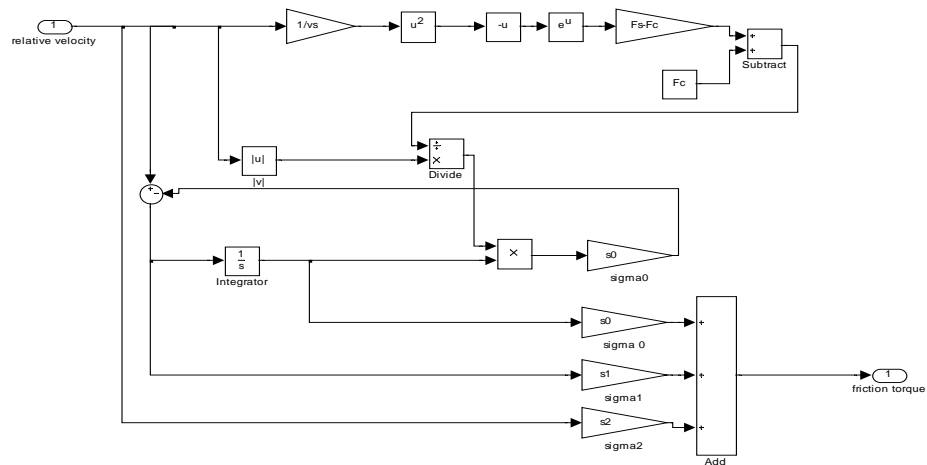


Figure B Simulink block diagram of LuGre friction model

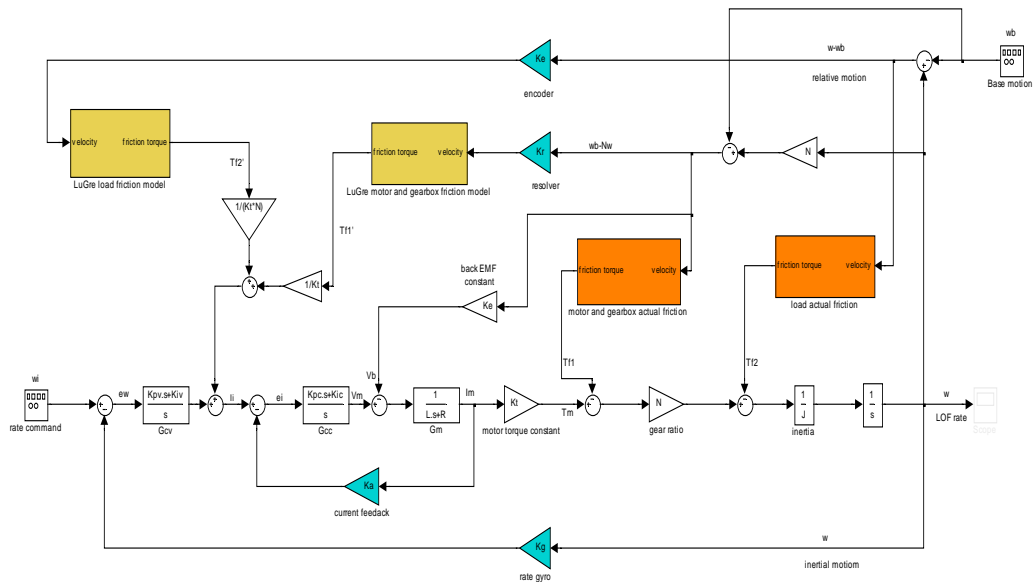


Figure C Simulink block diagram of the system stabilization loop with adding friction model

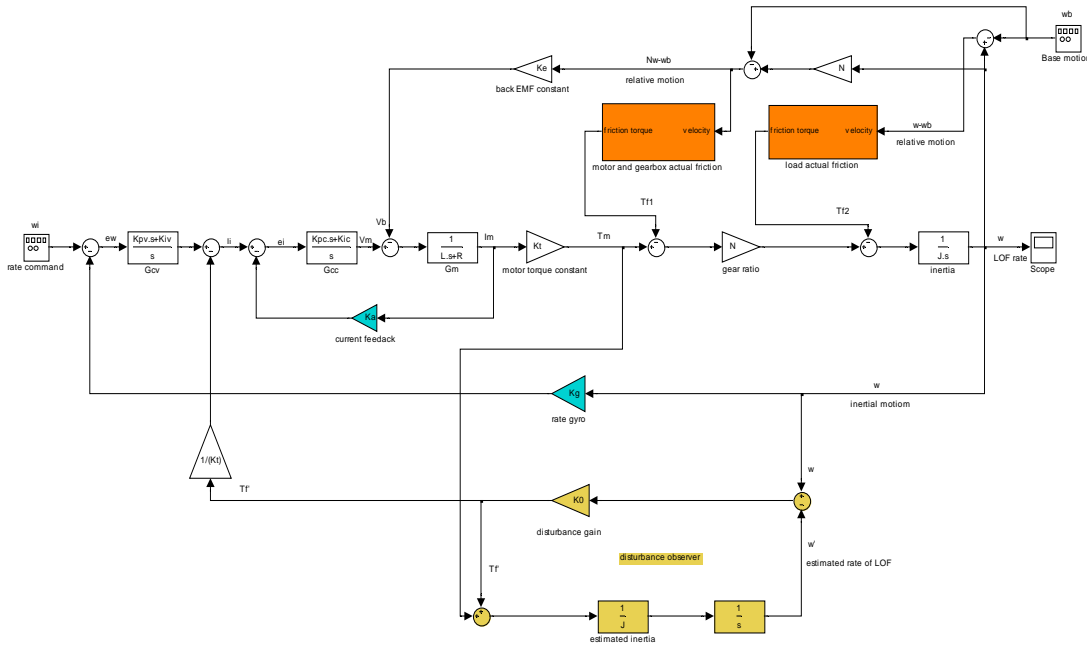


Figure D Simulink block diagram of the system stabilization loop with adding the single-state disturbance observer.

The system parameters used for simulation

```
J=35;           % effective system inertia, kgm^2
Kt=0.086;      % motor torque constant,Nm/Arms
Ke=0.071;      % motor back EMF constant,V.s/rad
L=0.238;       % motor terminal inductance, H
R=0.136;       % motor terminal resistance, Ohm
Kpv=3;         % velocity controller proportional gain, Arms.s/rad
Kiv=30;        % velocity controller integral gain, Arms/rad
Kpc=0.78;      % current controller proportional gain,V/Arms
Kic=1000;      % current controller integral gain, V/Arms
N=141.176;     % reduction ratio
c=180/pi;      % from deg to rad
Kg=1*c;        % gyro constant times rad to deg
Kr= 1;         % resolver constant;
Ke= 1;         % encoder constant;
Ka= 1;         % current meas. constant;

% Load side friction model parameters

Fs=32;         % static friction torque,Nm
Fc=26;         % coulomb friction torque,Nm
vs=0.03;       % Stribeck velocity,rad/s
s0=18000;      % bristle stiffness,Nm/rad
s1=800;        % bristle damping,Nm.s/rad
s2=4;         % viscous damping, Nm.s/rad

% Motor and gearbox friction model parameters

Fs1=0.04;      % static friction torque Nm
Fc1=0.03;      % coulomb friction torque Nm
vs1=0.03;      % Stribeck velocity rad/s
s01=1000;      % bristle stiffness Nm/rad
s11=0.5;       % bristle damping Nm.s/rad
s21=0.001;     % viscous damping, Nm.s/rad
K0=2000;       % disturbance gain, Arms.s/rad
```